Mechanism of Age-related Macular Degeneration:

The Role of HtrA1 and Related Molecules

NG, Tsz Kin

A Thesis Submitted in Partial Fulfillment

of the Requirement for the Degree of

Doctor of Philosophy

in

Ophthalmology and Visual Sciences

The Chinese University of Hong Kong

August 2010

Thesis/Assessment Committee

Professor Gary Hin-Fai YAM (Chair)

Professor Chi Pui PANG (Thesis Supervisor)

Professor Timothy Yuk Yau LAI (Committee Member)

Professor Kwong Wai CHOY (Committee Member)

Professor Benjamin Fuk Loi LI (External Examiner)

Abstract

Age-related macular degeneration (AMD) is a major retinal disease leading to severe visual impairment and even irreversible blindness in people aged 50 or above in the developed world. At present, it affects about 50 million people worldwide. Genetic studies play pivotal roles in understanding the pathogenesis of AMD, but only few studies have been reported. Previous genome-wide association studies pinpointed complement factor H (*CFH*) on 1q31 and high temperature requirement factor A1 (*HTRA1*) on 10q26 to be the AMD-associated genes even though the disease-causing genes in these loci are still unknown. This thesis describes the molecular analysis of *CFH* and *HTRA1* to affirm their association with exudative AMD.

A mutation screening analysis was conducted on *CFH* and *HTRA1* genes in 163 Chinese exudative AMD patients and 390 unrelated control subjects. Both *CFH* (rs800292; $p = 0.00056$) and *HTRA1* (rs11200638; $p = 1.74 \times 10^{-12}$) genes were associated with exudative AMD. Significant additive effect of *CFH* (rs800292) and *HTRA1* (rs11200638) was found (odds ratio = 23.3). In addition, a *HTRA1* variant (34delCinsTCCT) was identified to be significantly associated with exudative AMD ($p = 0.002$), of which the variant allele was more frequently found in control subjects (7.9%) than in AMD patients (1.2%). The protective effect of this variant on exudative AMD was confirmed by a haplotype analysis that the variant allele was located in the protective haplotype. Transfection of variant in human retinal pigment

epithelial (RPE) cell line, ARPE-19, was further shown to improve cell viability and reduce the apoptosis, when compared to wildtype protein. By bioinformatics analysis, the variant with a serine insertion at the 12th position is predicted to influence the signal peptide recognition. The transfection study revealed that the variant protein was more localized in the endoplasmic reticulum, which was unlike the wildtype protein in the Golgi apparatus, and the secretion of variant was retarded.

To establish the association of HtrA1 with AMD pathogenesis, the interaction of HtrA1 with other AMD-associated proteins was investigated. A screening study of human vitreous humor from 55 patients revealed for the first time that HtrA1 levels were positively related to vascular endothelial growth factor (VEGF) levels *in vivo*, especially in patients with retinal detachment (Pearson's correlation coefficient test; r = 0.835, $p = 2.14 \times 10^{-7}$), which is related to stress and inflammatory responses. The association of HtrA1 and VEGF with stress and inflammation was further validated as *HTRA1* and *VEGFA* expressions were simultaneously upregulated in primary human fetal RPE cells upon tunicamycin and DTT treatments. However, proteasome inhibitor, MG132, unexpectedly downregulated both gene expressions. Nevertheless, no direct interactive effect between HtrA1 and VEGF was observed *in vitro*. Finally, HtrA1-promoted RPE cell apoptosis suggests a mechanism for HtrA1 on AMD development. Results in this thesis provide the support for *HTRA1* as an AMD-associated gene through a combination of genetic and functional studies.

摘要

年齡相關性黃斑變性(AMD)是在發達國家伍十歲或以上人群中導致嚴重視力損傷甚至失明的一種主要視網膜疾病。據統計，全球約有伍千萬人受此病影響。基因學研究在對 AMD 發病機制的探討中起到重要的作用，但僅有少數相關的研究被報導。全基因組相關性研究指出染色體 1q31 上的 *CFH* 及 10q26 上的 *HTRA1* 是 AMD 的相關基因，但上述位點的致病基因尚未明確。本論文通過闡述 *CFH* 和 *HTRA1* 的分子分析來證實其與滲出性 AMD 之間的相關性。

本研究對 163 位滲出性 AMD 患者及 390 位對照組進行突變篩查。統計學結果顯示 *CFH* (rs800292;p=0.00056)和 *HTRA1* (rs11200638;p=1.74x10^{12})的多態性與滲出性 AMD 相關，且具有肯定的相加作用(機會比率=23.3)。此外，本研究發現一個位於 *HTRA1* 基因上的變異(34delCinsTCCT)與滲出性 AMD 相關，此變異上的等位基因在對照組出現的頻率(7.9%)明顯高於滲出性 AMD 患者(1.2%)。單倍體型分析確認了這個變異位於保護性單倍體上以及其保護作用。在將此變異轉染到視網膜色素上皮細胞株(ARPE-19)後發現，與野生型相比，攜帶變異的細胞其存活率提高並且凋亡率降低，從而進一步證實以上結論。通過生物訊息分析發現，這個變異導致在 12 號位點絲胺酸的插入可影響訊號肽的識別，同時轉染研究揭示了此變異比野生型更集中於內質網而非高爾基體，使其對外分泌作用受阻礙。

為證實 HtrA1 與 AMD 發病機制之間的相關性，本論文對 55 位患者的活體玻璃體樣本進行研究，並探討 HtrA1 與其他 AMD 相關蛋白的相互作用。本研究首次揭示活體玻璃體的 HtrA1 水平與血管內皮生長因子(VEGF)水平呈正相關，在應激及炎症相關性視網膜脫離病人中尤其明顯(Pearson's 相關係數測試;

r=0.835, *p*=2.14x10^{-7})。在經衣霉素與二硫蘇糖醇處理的人胚胎視網膜色素上皮細胞內，*HTRA1* 和 *VEGFA* 的表達同時上調，這進一步確認它們與應激及炎症的相關性。然而，本研究發現蛋白酶抑制劑 MG132 可使它們的表達下調。不過，在體外研究中未能觀察到 HtrA1 與 VEGF 的直接相互作用。HtrA1 促使的細胞凋亡提示了 HtrA1 在 AMD 發病機制中的作用。本論文結合基因及功能研究證實了 *HTRA1* 是 AMD 的相關基因。

Acknowledgements

Table of Contents

Chapter 1: Introduction

Chapter 3: Results

Chapter 4: Discussion

Chapter 5: Conclusion and future prospects   150

References   151

List of Figures

List of Tables

Abbreviations

Nucleotides

A	adenine
T	thymine
C	cytosine
G	guanine
U	uracil

Amino acids

Ala	A	alanine
Arg	R	arginine
Asn	N	asparagine
Asp	D	aspartic acid
Cys	C	cysteine
Gln	Q	glutamine
Glu	E	glutamic acid
Gly	G	glycine
His	H	histidine
Ile	I	isoleucine
Leu	L	leucine
Lys	K	lysine
Met	M	methionine
Phe	F	phenylalanine
Pro	P	proline
Ser	S	serine
Thr	T	threonine
Trp	W	tryptophan
Tyr	Y	tyrosine
Val	V	valine
Ter	X	stop codon

General

ABCA4	ATP-binding cassette, subfamily A, member 4
AEBSF	4-(2-aminoethyl)benzenesulfonyl fluoride hydrochloride
AMD	age-related macular degeneration
ANOVA	analysis of variance
AP-2α	adaptor-related protein complex 2α
BF	complement factor B
BMP	bone morphogenetic protein
b	base
bp	base pair
BSA	bovine serum albumin
C2	complement component 2
C3	complement component 3

CARASIL	cerebral autosomal recessive arteriopathy with subcortical infarcts and leukoencephalopathy
cDNA	complementary DNA
CFH	complement factor H
CNV	choroidal neovascularization
Da	Daltons
DAPI	4',6-diamidino-2-phenylindole
DTT	dithiothreitol
E	embryonic day
ECL	enhanced chemiluminescence
E. coli	*Escherichia coli*
ER	endoplasmic reticulum
ERM	epi-retinal membrane
FGF	fibroblast growth factor
g	gram
GWAS	genome-wide association study
HH	Hamburger and Hamilton stages
HRP	horse-radish peroxidase
HtrA	high temperature requirement factor A
HTRA1	high temperature requirement factor A1
HTRA2	high temperature requirement factor A2
HTRA3	high temperature requirement factor A3
HTRA4	high temperature requirement factor A4
HWE	Hardy-Weinberg equilibrium
IAP	inhibitors of apoptosis protein
IGF	insulin-like growth factor
IGFBP	insulin-like growth factor binding protein
IgG	immunoglobulin-G
indel	deletion-insertion
IOL	intra-ocular lens re-operation
IP	immunoprecipitation
k	kilo
l	liter
LD	linkage disequilibrium
LM	lymph node metastasis
LOH	loss of heterozygosity
min	minutes
MG132	Z-Leu-Leu-Leu-H
m	meter
m	milli
M	Molar
mRNA	messenger RNA
MTT	3-(4, 5-dimethylthiazol-2-yl)-2,5-diphenyltetrazolium bromide
NFκB	nuclear factor-kappa B
n	nano
OD	optical density
OR	odds ratio
ORF	open reading frame
PAR	population attributable risk
PBS	phosphate buffer saline

PCR	polymerase chain reaction
PDZ	postsynaptic density protein 95-discs large-zona occludens 1
PEDF	pigment epithelial growth factor
PLEKHA1	pleckstrin homology domain containing, family A member 1
PMSF	phenylmethylsulfonylfluoride
RIPA	radioimmunoprecipitation
RPE	retinal pigment epithelium
SDS	sodium dodecyl sulphate
SNP	single nucleotide polymorphism
SRF	serum response factor
TGF	transforming growth factor
TNF	tumor necrosis factor
μ	micro
V	volt
VEGF	vascular endothelial growth factor
VMD2	vitelliform macular dystrophy

Publications

1. **Ng TK**, Yam GH, Tam PO, He J, Lai TY, Liu DT, Lee VY, Fan AH, Chen H, Chiang SW, Chen LJ, Zhang MZ, Yang Z, Choy KW, Lam DS, Pang CP. High temperature requirement factor A1 is a potential disease-causing gene for age-related macular degeneration: evidences from the protective effect of a variant. *Manuscript in preparation.*

2. **Ng TK**, Yam GH, Chen WQ, Lee VY, Chen H, Tam PO, Chen LJ, Liu DT, Choy KW, Yang Z, Lam DS, Pang CP. Interative expressions of HtrA1 and VEGF in human vitreous and retinal pigment epithelial cells. *Submitted.*

3. **Ng TK**, Chen LJ, Liu DT, Tam PO, Chan WM, Liu K, Hu YJ, Chong KK, Lau CS, Chiang SW, Lam DS, Pang CP. Multiple gene polymorphisms in the complement factor H gene are associated with exudative age-related macular degeneration in Chinese. *Invest Ophthalmol Vis Sci* 2008; 49:3312-3317.

4. Tam PO, **Ng TK**, Liu DT, Chan WM, Chiang SW, Chen LJ, DeWan A, Hoh J, Lam DS, Pang CP. HTRA1 variants in exudative age-related macular degeneration and interactions with smoking and CFH. *Invest Ophthalmol Vis Sci* 2008; 49:2357-2365.

Conference Presentations

1. **Ng TK**, Pang CP. High temperature requirement factor A1 is a potential disease-causing gene for age-related macular degeneration: evidences from the protective effect of a variant. 60th Annual American Society of Human Genetics Meeting. Washington DC, USA. November 2-6, 2010.

2. Pang CP, **Ng TK**, Yam GH, Liu DT, Chiang SW, Chen LJ, Tam PO, Lai TY. Interactive expressions of HtrA1 and VEGF in human vitreous and retinal pigment epithelial cells through a NFκB-related mechanism. 60th Annual American Society of Human Genetics Meeting. Washington DC, USA. November 2-6, 2010.

3. **Ng TK**, Chen LJ, Chan WM, Tam POS, Liu DTL, Lam DSC and Pang CP. Association of complement factor H polymorphisms with exudative age-related macular degeneration in ethnic Chinese. HUGO 12th Human Genome Meeting. Montreal, Canada. May 21-24, 2007.

4. **Ng TK**, Chen LJ, Tam POS, Liu DTL, Chan WM, Lam DSC and Pang CP. Complement factor H polymorphisms in exudative age-related macular degeneration. Yale CME Conference: Genome-Wide Association Study: Design & Analysis. New Haven, USA. Oct 24-26, 2006.

Chapter 1: Introduction

1.1 Retina, light perception and visual pathway

Eye is the organ in vertebrates for visual perception, which requires a sophisticated and well-engineered system for the missions to be performed accurately, rapidly and reliably in the natural environment. Retina, lining the interior of the eye, is a transparent neural tissue for light reception. Mature retina is composed of six types of neurons, one type of epithelial cell and one type of glial cell, all of which are derived from a single type of retinal progenitor cell, the neuroblast, in a sequential order. The six types of neurons (from posterior to interior: the rod and cone photoreceptors, the amacrine cells, the horizontal cells, the bipolar cells and the retinal ganglion cells) form a characteristic laminar structure with 11 layers (from posterior to interior: pigment epithelium, outer segment and inner segment of photoreceptors, outer limiting membrane, outer nuclear layer, outer plexiform layer, inner nuclear layer, inner plexiform layer, ganglion cell layer, nerve fibre layer and inner limiting membrane) (Cajal SR, 1892; reviewed in Glickstein M, 1969) (**Figure 1.1**). The neuron distribution in the retina is non-random and forms a crystalline-like order, mosaics (reviewed in Galli-Resta L et al, 2008). The central retina, called fovea or macula, which contains a dense population of cone photoreceptors, is responsible for the color vision.

Distant light rays from the environment enter the eye through the refraction and convergence by the cornea and the lens, and fall on the back of retina. The light energy activates the photopigments, opsin or rhodopsin, and causes the isomerization of 11-*cis* retinaldehyde to all-*trans* (reviewed in Ritter E et al, 2008). This leads to hyperpolarization and generation of electrical signals in the photoreceptors, which diverge and transmit the electrical signals to the horizontal cells and the bipolar cells at the synapses in the outer

1

plexiform layer (reviewed in Bloomfield SA and Dacheux RF, 2001; Field GD and Chichilnisky EJ, 2007; Balasubramanian V and Sterling P, 2009). After the information processing among the bipolar cells, the amacrine cells and the horizontal cells in the inner nuclear layer, the electrical signals are passed from the bipolar cells and the amacrine cells to the retinal ganglion cells at the synapses in the inner plexiform layers (reviewed in Field GD and Chichilnisky EJ, 2007; Balasubramanian V and Sterling P, 2009). The electrical signals from the retinal ganglion cells are converged in and transmitted through the optic nerve to the primary visual centres, superior colliculus or dorsal lateral geniculate nucleus, in the brain (reviewed in Glickstein M, 1969; van Essen DC et al, 1992; Schulte D and Bumsted-O'Brien KM, 2008). The generated vision cooperates with centres for motor control and cognitive processing, allowing the vertebrates to learn, react and response.

Human retina is able to receive light signal accurately and completely from the environment because of three cone types and a single rod type cells with different peak sensitivities for the full spectrum of visible light (reviewed in Bloomfield SA and Dacheux RF, 2001; Jacobs GH, 2008). In addition, different subtypes of intermediate neurons and retinal ganglion cells (at least 10 types of bipolar cells, 30 types of amacrine cells, 2 types of horizontal cells and 17 types of retinal ganglion cells) further compute the visual signal, allowing precise information passing to the brain (reviewed in Field GD and Chichilnisky EJ, 2007). Recently, a newly characterized retinal ganglion cell type, independent of cone and rod photoreceptors, is able to receive light signal by melanopsin and responsible for circadian rhythm of the biological clock (reviewed in He S et al, 2003).

1.2 Retinal diseases

Retina is the tissue within the eye responsible for light perception. Diseased or damaged retina would weaken the reception of the light and lead to vision loss or even

blindness. This is mainly caused by the death of neurons or separation of retina from the retinal pigment epithelium. There are a great number of retinal disease, including retinitis pigmentosa, glaucoma, diabetic retinopathy, retinal detachment, macular hole, age-related macular degeneration, and etc.

Retinitis pigmentosa is one of the subset of hereditary degenerative diseases, affecting 1 in 4000 individuals. Retinitis pigmentosa is characterized by a classic pattern of difficulties in dark adaptation and night blindness in adolescence, loss of mid-peripheral visual field in young adulthood and central vision in later life, which are due to the severe attenuation of rod and cone photoreceptors (reviewed in Hartong DT et al, 2006). The inner nuclear layer is fairly preserved, but many of them would degenerate later in the disease (reviewed in Hartong DT et al, 2006).

Diabetic retinopathy is the most common cause of vision impairment in working-age adults in the developed countries. It can be subdivided into non-proliferative and proliferative retinopathy. The retinal changes include the formation of retinal capillary microaneurysms, development of excessive vascular permeability, vascular occlusion, proliferation of new blood vessels and accompanying fibrous tissue on the surface of the retina and optic disk, and contraction of the fibrovascular proliferations and the vitreous (reviewed in D'Amico DJ, 1994; Wood AJ, 1999; Gariano RF and Gardner TW, 2005).

Retinal detachment, a separation within the retina between the photoreceptors and RPE, is characterized by the collection of fluid or blood in this area. Rhegmatogenous retinal detachment is defined as the presence of a hole or break in the retina that allows fluid from vitreous cavity to enter the subretinal space (reviewed in D'Amico DJ, 1994). Rhegmatogenous detachment is distinguished from traction detachment, in which the intact retina is forcibly elevated by contracting membranes on the surface of retina or by vitreous traction on areas of retinal neovascularization (reviewed in D'Amico DJ, 1994).

3

Rhegmatogenous retinal detachment is originated from retinal holes or as a result of subsequent scar formation. Retinal detachment would also initiate inflammatory and stress responses (Zacks DN et al, 2006; Hollborn M et al, 2008). Failure in surgery for rhegmatogenous detachment will cause the development of membranes on the retina, with reopening of retinal breaks and subsequent recurrent detachment, a condition known as proliferative vitreoretinopathy (reviewed in D'Amico DJ, 1994).

Macular hole is a full-thickness defect of retinal tissue involving the anatomic fovea of the eye. Macular hole was originally believed to be traumatic in young eyes; however, idiopathic, age-related macular hole represents more than 80% of cases (McDonnell PJ et al, 1982). A mechanism of idiopathic macular hole is proposed as "involutional macular thinning" (Morgan CM and Schatz H, 1986). Firstly, choroidal vascular changes lead to altered submacular choroidal vascular perfusion, leading to focal foveal, retinal and pigment epithelial changes. The vascular changes then lead to cystic degeneration of the retina (Coats G, 1907), producing permanent structural changes in the fovea or in the RPE and resulting involutional macular thinning. Finally, vitreous traction on thinned foveal tissue produces the macular hole (reviewed in Ho AC et al, 1998). Recently, with the application of optical coherence tomography, the understanding and management of macular hole have been improved, such as monitoring precursor lesions and progression, staging of macular hole, differentiating simulating lesions, and assisting in evaluating the results of surgery (Altaweel M and Ip M, 2003).

Age-related macular degeneration (AMD), firstly described as "symmetrical central choroido-retinal disease occurring in senile persons" (Hutchinson J et al, 1874), is the leading cause of irreversible blindness in people aged 50 years or above in the developed world, affecting about 50 million people worldwide (Pascolini D et al, 2004; Congdon N et al, 2004). AMD is a disease influencing the central portion of the retina, the

4

macula, on which the diagnosis of AMD relies, irrespective of visual acuity (Bird AC et al, 1995). In the Hong Kong Chinese population, AMD was observed in 5.9% of subjects aged 40 years or above (Van Newkirk MR, 1997), which is similar to 5.6% in Beijing (Li Y et al, 2008), but in contrast to 10.1% in Taiwan (Chen SJ et al, 2008). The overall prevalence of advanced AMD is projected to increase by more than 50% by the year 2020 (Friedman DS et al, 2004). Traditional AMD treatments, including ocular photodynamic therapy (Donati G et al, 1999) and vitreoretinal surgeries [surgical extraction of CNV (Hawkins BS et al, 2004), macular translocation surgery (Mruthyunjaya P et al, 2004) and subretinal tissue plasminogen activator injection combined with intravitreal air injection (Haupert CL et al, 2001)] can limit visual loss, but not a cure of the disease. Currently, the most common treatment, intravitreal injection of anti-angiogenic agents, such as pegaptanib sodium (Macugen) (Gragoudas ES et al, 2004), ranibizumab (Lucentis) (Rosenfeld PJ et al, 2006) and bevacizumab (Avastin) (Spaide RF et al, 2006), prevents the progression of the disease, with limited vision improvement. Therefore, in-depth understanding the pathological mechanisms of AMD is important for the development of new and safe therapies against this sight-threatening disease.

1.3 Pathology of age-related macular degeneration

The clinical hallmark and characteristic physical sign of AMD is the appearance of pale yellowish lesions, called drusen, during funduscopic examination (reviewed in D'Amico DJ, 1994; de Jong PT, 2006; Jager RD et al, 2008). This acellular, polymorphous debris is focally deposited between the RPE and Bruch's membrane. Drusen have a core of glycoproteins (Hageman GS et al, 2001; Rudnew A, 1871), and their outer domes contain crystallins, chaperone proteins, apolipoprotein E, vitronectin and other inflammatory proteins (Crabb JW et al, 2002; Nakata K et al, 2005; Umeda S et al, 2005). Drusen become

visible on ophthalmoscopy when their diameter exceeds 25 μm (Sarks SH et al, 1999). Drusen are categorized as small (<63 μm in diameter), medium (63 to 124 μm), or large (>124 μm) according to an international classification and grading system (Bird AC et al, 1995). The diameter of large drusen, on ophthalmoscopic examination, is roughly equivalent to the caliber of a retinal vein coursing towards the optic disk. Besides, drusen are also categorized as hard or soft on the basis of the appearance of their margins (Bird AC et al, 1995). Hard drusen have discrete margins while soft drusen are usually large with indistinct edges and confluent. Drusen are ubiquitous in people over 50 years of age and are considered as a part of normal aging. Therefore, an eye with few small, hard drusen is not regarded as having AMD (reviewed in Jager RD et al, 2008).

According to the international classification and grading system of age-related maculopathy and AMD (Bird AC et al, 1995), early AMD is characterized by drusen or by hyperpigmentations or small hypopigmentations, without visible choroidal vessels (reviewed in de Jong PT, 2006). The larger the drusen, the greater the covered area, and the larger the areas of hyperpigmentation and hypopigmentation of the RPE in the macula, the higher the risk of late AMD (Klein R et al, 2002). Late AMD is divided into two forms: "dry" and "wet". Dry (atrophic, non-exudative or non-neovascular) AMD, also named as geographic atrophy, starts with a sharply demarcated round or oval hypopigmented spot that is often juxtafoveal and in which large choroidal vessels are visible (reviewed in de Jong PT, 2006). The initial symptoms of dry AMD are usually indicated by gaps in an image. Serous or hemorrhagic fluid that causes the neuroretina or the RPE to detach from Bruch's membrane is the first sign of wet (exudative or neovascular) AMD, also called choroidal neovascularization (CNV) (reviewed in de Jong PT, 2006). The fluid originates from the subretinal neovascular membrane. The detachment disturbs the fine arrangement of photoreceptors and causes metamorphopsia, the first symptom of wet AMD. New subretinal

vessels tend to grow toward the fovea, and more extensive hemorrhages and scars can appear within days or months.

Excess drusen can lead to damage of RPE, which is important for regeneration of bleached visual pigments, formation and maintenance of the inter-photoreceptor matrix and Bruch's membrane, transport of fluids and nutrients between photoreceptors and the choriocapillaries, and phagocytosis of photoreceptors (reviewed in de Jong PT, 2006; Jager RD et al, 2008). Each RPE cell sheds about 3000 disks from 30 photoreceptors daily (Bok D and Young RW, 1979). The contents of phagolysosomes are incompletely degraded within acid lysosomal compartments and the residual bodies are the substrates for lipofuscin formation (reviewed in de Jong PT, 2006). Accumulation of lipofuscin imposes an ever-increasing burden on RPE cells; however, RPE cells have a limited capacity to sequester malfunctioning cytoplasm before delivering it to lysosomes (Streeten BW, 1961). The autophagic process of RPE cannot handle the immense amount of metabolic waste that accumulates within RPE cells before the onset of late AMD (reviewed in de Jong PT, 2006). Moreover, the number of RPE cells diminishes with age, increasing the phagocytic burden on the remaining cells (reviewed in de Jong PT, 2006).

Bruch's membrane, beneath the RPE, has three layers: a central elastic layer encompassed by two collagenous layers. The elastic layer is one third to one fifth as thick in the fovea as in the peripheral retina, lowering the tissue resistance for centripetal growth of wet AMD (Chong NH et al, 2005). Moreover, Bruch's membrane calcifies, doubles in thickness between the ages of 10 and 90 years (Ramrattan RS et al, 1994), and concentrates with lipid in later years (Bird AC and Marshall J, 1986). Furthermore, basal laminar deposits and membranous debris, considered as precursors of AMD, in Bruch's membrane cause a sharp reduction in fluid and nutrient transport across the membrane (Starita C et al, 1996), and instigate chronic local inflammation (Cousins SW et al, 2004). Abnormalities in

collagen or elastin in Bruch's membrane, the outer retina, or the choroid may also predispose to AMD development (Marneros AG et al, 2007).

Consequently, damage to the RPE and a chronic aberrant inflammatory response can lead to geographic atrophy and the expression of angiogenic cytokines, such as vascular endothelial growth factor (VEGF) (reviewed in D'Amico DJ, 1994; de Jong PT, 2006; Jager RD et al, 2008). Subsequently, CNV develops and is accompanied by increased vascular permeability and fragility. CNV may extend through breaks in Bruch's membrane and lead to subretinal hemorrhage, fluid exudation, lipid deposition, RPE detachment from the choroid and appearance of fibrotic scars (Hageman GS et al, 2001; Zarbin MA, 2004; Donoso LA et al, 2006; Grossniklaus HE and Green WR, 2006; Anderson DH et al, 2002; Kijlstra A et al, 2005).

CNV in AMD belongs to the angiogenic condition of ocular diseases, which is regulated by different angiogenic factors. Among the known angiogenic factors, vascular endothelial growth factor (VEGF) is widely accepted as the most important single regulator in physiological and pathological angiogenesis (Ferrara N, 2002). VEGF, a dimeric secreted glycoprotein, is an endothelial cell-specific mitogen, a vascular permeability factor (Keck PJ et al, 1989) and a cell survival factor (Nishijima K et al, 2007). Evidences from animal models (Baffi J et al, 2000; Spilsbury K et al, 2000) and anti-VEGF therapeutic treatments for human patients with ocular vascular diseases (Eyetech Study Group, 2003; Chan WM et al, 2008) suggested VEGF could be one of the initiators or inducers of neovascularization in the eye. Moreover, elevated expression of VEGF in the aqueous and vitreous humors of patients with different angiogenic ocular diseases (Tong JP et al, 2006; Wang X et al, 2006) indicated prognostic potential of VEGF for the prediction of angiogenic disease progression or severity. In addition, angiogenesis is a consequence of the equilibrium between stimulation by VEGF and inhibition by pigment epithelium-derived factor (PEDF)

8

(Folkman J, 1995). In retina tissue cells, there is a physiological balance between angiogenic VEGF and anti-angiogenic PEDF (Ohno-Matsui K et al, 2001). Accordingly, PEDF downregulates VEGF expression and inhibits VEGF-induced vascular changes (Zhang SX et al, 2006; Tong JP et al, 2006).

1.4 Genetics of age-related macular degeneration

AMD is a common late-onset progressive macular disorder. Twin and family-based studies have provided compelling evidences for a genetic basis of AMD (Meyers SM, 1994; Seddon JM et al, 2003). However, because of phenotypic variability and unavailability of large pedigree, mapping AMD loci with classical linkage analysis was not informative. Until now, more than 31 loci across multiple chromosomes are linked to AMD (reviewed in Haddad S et al, 2006). Apart from a polygenic nature of AMD, the inheritance could be influenced by environmental factors, such as smoking, greater body mass index, hypertension and chronic inflammation (reviewed in Katta S et al, 2009). Nonetheless, a meta-analysis of genome scans of AMD has revealed chromosome 10q26 to be a strongest AMD susceptibility locus, whereas chromosomes 1q, 2p, 3p and 16 are likely to contain linked loci (Fisher SA et al, 2005). In addition, the approach studying the candidate genes for hereditary macular dystrophies, such as Best's (*VMD2*), Stargardt's (*ABCA4*) and Sorsby's (*TIMP3*) diseases, which exhibit certain commonalities with AMD, were only able to show limited association with AMD (reviewed in Patel N et al, 2008) although some mutations were found in *ABCA4* (Baum L et al, 2003), *VMD2* (Lotery AJ et al, 2000) and fibulin-5 genes (Stone EM et al, 2004).

1.4.1 Association studies

The development of AMD genetics has been boosted with the application of genome-wide association study (GWAS), which attempts to identify disease-causing variants by using high-throughput genotyping technologies to assay hundreds of thousands of common single nucleotide polymorphisms (SNPs) and relate them to clinical conditions and measurable traits (Manolio TA and Collins FS, 2009). If a SNP is associated with a disease, the occurrence of the two characteristics will be more often than by chance alone, i.e. the associated SNP could be a disease-causing variant or in linkage disequilibrium (LD) with a true disease-causing variant.

The first AMD-associated gene identified by GWAS is the complement factor H (*CFH*) gene on chromosome 1q31 (Klein RJ et al, 2005; Edwards AO et al, 2005; Haines JL et al, 2005). Significant association of a non-synonymous variant (Tyr402His; rs1061170, T>C) in exon 9 of *CFH* with AMD has been widely replicated in Caucasian populations, but not in Chinese and Japanese populations (**Table 1.1**). The association follows a co-dominant, multiplicative genetic model, by which a meta-analysis has shown that patients with homozygous CC and heterozygous TC genotypes have 6.32 and 2.50 times higher chance to develop AMD than that with homozygous TT genotype, respectively (Thakkinstian A et al, 2006). Moreover, the Tyr402His variant represents a population attributable risk of 54% in Caucasian (Despriet DD et al, 2006). Furthermore, both advance type of AMD (geographic atrophy and neovascular AMD) are equally associated with *CFH* (Magnusson KP et al, 2006). In addition, the Tyr402His variant exhibits decreased binding affinity to C-reactive protein (Yu J et al, 2007), which affects the negative control of CFH on alternative complement pathway for innate immunity and inflammation (Donoso LA et al, 2006).

Just after the discovery of association between *CFH* gene and unrelated AMD patients, another locus on chromosome 10q26 was discovered to be associated with Hong Kong Chinese exudative AMD patients. The most significant SNP (rs11200638, G>A) resides in the promoter region of high temperature requirement factor A1 (*HTRA1*) gene (Dewan A et al, 2006). The positive association of rs11200638 with AMD is replicated in different studies (**Table 1.2**), implying that rs11200638 in *HTRA1*, unlike Tyr402His in *CFH*, can increase the risk of developing AMD in all races. A meta-analysis showed that patients with homozygous AA and heterozygous GA genotypes have 6.92 and 2.13 times higher chance to develop AMD than that with homozygous GG genotype, respectively (Chen W et al, 2009). Similar to *CFH*, the risk of *HTRA1* rs11200638 on wet and dry AMD is comparable (Cameron DJ et al, 2007). Moreover, the risk allele of rs11200638 is more prevalent in bilateral than unilateral AMD patients (Chen H et al, 2008). However, the functional role of HtrA1 on the development of AMD is still unclear although higher expressions of HtrA1 mRNA and protein were found in the eyes and leukocytes of patients with AA genotype compared to that with GG genotype (Yang Z et al, 2006; Tuo J et al, 2008).

Apart from *CFH* and *HTRA1*, other components of complement system, such as complement factor B (*BF*), complement component 2 (*C2*) and complement component 3 (*C3*), have been suggested to be associated with AMD (Gold B et al, 2006; Yates JR et al, 2007). Lys9His and Arg32Gln in *BF*, which are in LD with Glu318Asp in *C2*, may have a protective role in AMD since a higher frequency was observed in the normal Caucasian control (Gold B et al, 2006), whereas Arg102Gly in *C3* increases the risk of AMD in the British and Scottish cohorts (Yates JR et al, 2007).

1.4.2 Common Disease Common Variant versus Common Disease Rare Variant

Significant association of a common *HTRA1* promoter SNP (rs11200638) with AMD is consistently observed (reviewed in Chen W et al, 2009); however, extensive sequencing around this chromosome 10q26 region has not yet given a definite causal variation although some variants in *LOC387715* are suggested to be possible mutations (Kanda A et al, 2007; Fritsche LG et al, 2008; Wang G et al, 2009). The non-synonymous Ala69Ser change in the LOC387715 protein was suggested to affect the presumptive function of the protein in mitochondria (Kanda A et al, 2007). Moreover, the LOC387715 protein with Ala69Ser change is more likely associated with the cytoskeleton in COS7 cells compared with wildtype protein (Wang G et al, 2009). Furthermore, a deletion-insertion (indel) polymorphism (c.372_815del443 ins54) in *LOC387715* gene removes the polyadenylation signal of *LOC387715* transcript and mediates rapid mRNA turnover (Fritsche LG et al, 2008). However, this indel polymorphism has no correlation with *LOC387715* mRNA level in human retina and blood samples (Wang G et al, 2010). In addition, the indel in *LOC387715* gene, rather affecting the *LOC387715* mRNA levels, together with *HTRA1* promoter SNP (rs11200638) in the risk haplotype upregulates the expression of *HTRA1*, whereas a nonsense mutation (Arg38X) in a protective haplotype leads to loss of *LOC387715* mRNA (Yang Z et al, 2010). Therefore, the functions of the *LOC387715* to AMD are still controversial.

Considering rs11200638 alone, it has high contribution at the population level with a population attributable risk (PAR) of 57.7%, using the formula of PAR = (observed disease incidence – disease incidence in the absence of the genetic variant) / observed disease incidence (Bodmer W and Bonilla C, 2008) and considering a recessive mode of inheritance of this SNP from our previous genotyping study (Tam PO et al, 2008). Moreover, the contribution of this SNP to the individual's risk is also justifiable with a

12

penetrance of 9.1%, using the formula of penetrance = [disease incidence in the absence of the genetic variant x (odds ratio − 1)] / {1 + [disease incidence in the absence of the genetic variant x (odds ratio − 1)]} (Bodmer W and Bonilla C, 2008) and considering an odds ratio (OR) of 5.2 (Tam PO et al, 2008). However, the functional aspect of this SNP is only known to upregulate the transcription of *HTRA1* (DeWan A et al, 2006; Yang Z et al, 2006; Tuo J et al, 2008, Yang Z et al, 2010). The causal impact of this SNP to AMD is still not clear; therefore, it is possible that other variants, which are in linkage disequilibrium with this common SNP, can be a causative factor for AMD.

Recently, there is a debate in the cause of common, multifactorial diseases on whether common variants or rare variants would be the actual disease causal factor (reviewed in Bodmer W and Bonilla C, 2008; Schork NJ et al, 2009). This issue is raised since the ORs in most GWAS only reach 1.2 to 1.5 and the penetrances are also low (reviewed in Bodmer W and Bonilla C, 2008; Schork NJ et al, 2009). In contrast, although the frequency of rare variants is low, their penetrances are often high and the changes are functionally relevant (reviewed in Bodmer W and Bonilla C, 2008; Schork NJ et al, 2009). Good examples for rare variants in AMD could be observed from patients with AMD containing mutations in *ABCA4* (Baum L et al, 2003), *VMD2* (Lotery AJ et al, 2000) and *FIBULIN-5* genes (Stone EM et al, 2004). Unlike other GWAS, the OR and PAR of *HTRA1* discovered by GWAS is high (>5) (Dewan A et al, 2006). However, this does not mean the *HTRA1* common SNP is likely to be a causal variant because common SNP might not be a functionally relevant variant due to comparatively recent natural selection (Bodmer W and Bonilla C, 2008). An association in GWAS could act as a guide to uncover the effect of a closely linked functional variant in LD with the observed associated variant. This suggests *HTRA1* and adjacent genes (*LOC387715* and *PLEKHA1*) could be possible candidates for rare variant search. Ultimately, the potential consequences to the function of relevant gene

product have to be assessed in order to validate the causal effect of the (common or rare) variants.

1.5 High temperature requirement factor A1

1.5.1 HtrA family

High temperature requirement (HtrA) family of protein belongs to the trypsin clan SA of the serine proteases, which is characterized by the histidine-aspartic acid-serine catalytic triad with two six-stranded β barrel domains (reviewed in Clausen T et al, 2002). HtrA is defined as S1C endopeptidase within the SA clan and identified by a proteolytic domain with at least one C-terminal Postsynaptic density protein 95-Discs large-Zona occludens 1 (PDZ) domain (Pallen M and Wren B, 1997). There are over 180 members in this ATP-independent family, corresponding to 10% of trypsin-like proteases.

1.5.1.1 Prokaryotic HtrA

HtrA was initially identified in *Escherichia coli* (*E. coli*) from the observation of two phenotypes in corresponding mutants. Mutant of DegP was discovered to be defective in breakdown of abnormal periplasmic protein (Strauch KL and Beckwith J, 1988) while mutant of HtrA failed to maintain bacterial survival at temperatures above 42℃ (Lipinska B et al, 1988). As expected from the sequence analysis, DegP possessed proteolytic activity on a number of substrates, including colicin A lysis protein (Cavard C et al, 1989), K88 and K99 fimbriae (Bakker D et al, 1991), MalS (Spiess C et al, 1999), PapA pilin (Jones CH et al, 2002), and DPMFKLV-*para*-nitroaniline (Hauske P et al, 2009). However, DegP, as a general cage-forming protease (Krojer T et al, 2002), is proposed to degrade at least partially unfolded substrates (reviewed in Clausen T et al, 2002) instead of cleaving folded proteins (Spiess C et al, 1999; Kim KI et al, 1999; Swamy KH et al, 1983). The proteolytic

activity, which is shown to be inhibited by diisopropylfluorophosphate (Lipinska B et al, 1990) and SPMFKGV-chloromethyl ketone (Hauske P et al, 2009), is independent of ATP, pH, reducing agents and divalent cations (Swamy KH et al, 1983). The protease activity increases rapidly from 32℃ to 42℃ in a nonlinear fashion (Skorko-Glonek J et al, 1995; Spiess C et al, 1999). Recently, a report showed a hydrolyzed peptide-induced autocleavage process after the relief of stress conditions (Jomaa A et al, 2009). At temperatures below 20℃, however, almost no proteolytic activity is detected. Instead, DegP exhibits molecular chaperone activity only at low temperatures (Bass S et al, 1996; Spiess C et al, 1999). The protease and chaperone activities appear to be antagonistic to each other (Clausen T et al, 2002).

After initial identification of DegP, sequence-based homology search revealed another 2 proteases, named as DegQ and DegS, comprising the HtrA family of proteins in *E. coli*. DegS was identified in the *E. coli* mutant strains with the small colony phenotype under all growth conditions (Bass S et al, 1996; Waller PR and Sauer RT, 1996). DegS, as a membrane-bound periplasmic protease, is involved in the activation of the σ^E-stress response through the heat stress-induced PDZ domain binding of OMPs and subsequent cleavage of the periplasmic domain of RseA (Ades SE et al, 1999; Alba BM et al, 2001; Walsh NP et al, 2003). DegQ, as a functional substitute for DegP in overexpressing condition (Waller PR and Sauer RT, 1996), was initially identified as a multicopy *E. coli* suppressor with a *prc* null mutation (Bass B et al, 1996). Although the physiological functions of DegQ remain largely unknown, DegQ is neither heat-inducible nor relevant to cell growth under normal conditions (Waller PR and Sauer RT, 1996; Farn J and Roberts M, 2004). Because of the lack of DegP and DegS, the HtrA homologues in many bacteria are more suitable to be considered as DegQ homologues due to the sequence homology with Q-liner region in DegQ (reviewed in Kim DY and Kim KK, 2005). In addition to the

protease and chaperone activity, HtrA homologues are proposed to be involved in the biogenesis and maturation of natural secreted proteins through pro-peptide processing (Poquet I et al, 2000; Lyon WR and Caparon MG, 2004; Biswas S and Biswas I, 2005; Cole JN et al, 2007).

1.5.1.2 Eukaryotic HtrA

Compared with prokaryotes, eukaryotic HtrAs have less information because of their relatively recent discovery. There is only one HtrA-like protein in *Saccharomyces cerevisiae* reported, named as Nma111 or Ynm3. Nma111 was identified as a nuclear mediator of apoptosis under cellular stress conditions, as overexpression of Nma111 enhances apoptotic-like cell death and yeast cells lacking Nma111 survive better than wildtype cells (Fahrenkrog B et al, 2004). Moreover, Nma111 is described as a modulator of fatty acid metabolism for its role in the use of nonfermentable carbon source (Tong F et al, 2006). Furthermore, Ynm3 is a dual chaperone-protease, in which its proteolytic activity is crucial for cell survival at higher temperature and the chaperone activity is important to improve the efficiency of proteolysis of aberrant proteins (Padmanabhan N et al, 2009). Until now, Ynm3 is the only eukaryotic HtrA-like member carrying chaperone activity (Padmanabhan N et al, 2009).

Evolution of the chloroplasts of green algae and higher plants from a cyanobacterial ancestor by endocytobiosis suggests an ancestory origin of proteases in chloroplast (Adam Z et al, 2001; Huesgen PF et al, 2006; Sakamoto W, 2006). A total of sixteen HtrA homologues have been found in Arabidopsis thaliana, four of which are located in chloroplasts (Adam Z et al, 2001; Sokolenko A et al, 2002; Huesgen PF et al, 2005). Similar to its cyanobacterial ancestor (Silva P et al, 2002; Huesgen PF et al, 2007), the only suggested role for plant Deg proteases is the site-specific fragmentation of

photodamaged reaction center D1 protein participated in plant photosystem II under light stress (Haußuhl K et al, 2001; Kapri-Pardes E et al, 2007; Sun X et al, 2007a; Sun X et al, 2007b; reviewed in Huesgen PF et al, 2009).

The HtrA-like sequences are suggested to enter the lineages of Animal kingdom by horizontal acquisition from prokaryotes (Koonin EV and Aravind L, 2002). Different animals, such as Xenopus (Montesanti A et al, 2007), Syrian hamster (Zurawa-Janicka D, et al, 2008), chick (Oka C et al, 2004; Ferrer-Vaquer A et al, 2008), rabbit (Clouet J et al, 2009), rat (Bowden M et al, 2009) , mouse (Gray CW et al, 2000; De Luca A et al, 2004; Tocharus J et al, 2004) and rhesus monkey (Bowden MA et al, 2008) are reported to contain HtrA homologues in their genomes. Three HtrA homologous, HtrA1-3, are identified in animals. Because of the high sequence homology with human HtrA proteins (>90%), the HtrA homologues in different animal species have been used to study the functions with respect to human HtrAs, such as cell growth, apoptosis, cell fate determination and inflammatory reactions (Clausen T et al, 2002). However, despite sharing high sequence homology, expression pattern of *HTRA1* mRNA in chick is significantly different from its mouse homolog (Ferrer-Vaquer A et al, 2008).

1.5.1.3 Human HtrA

In human, four members of HtrA family have been identified, named as HtrA1-4 (**Figure 1.2**). *HTRA1* (PRSS11 or L56) is originally identified as a downregulated gene in the SV40 oncogenic virus-transformed human fibroblasts (Zumbrunn J and Trueb B, 1996), and subsequently isolated in osteoarthritic cartilage (Hu SI et al, 1998). HtrA1 has been implicated in different physiological and pathological conditions, such as placentation (Nie GY et al, 2003; De Luca A et al, 2003), cancers (Baldi A et al, 2002; Chien J et al, 2004), arthritis (Hu SI et al, 1998; Grau S et al, 2006) and age-related macular degeneration

17

(DeWan A et al, 2006; Yang Z et al, 2006). Moreover, HtrA1 is reported to be involved in TGFβ signaling (Oka C et al, 2004) and degradation of several extracellular matrix proteins through its protease activity (reviewed in Canfield AE et al, 2007).

HtrA2 (Omi) was initially identified as an interactive binding partner with presenilin-1 in a human fetal brain library. It is upregulated in response to stress induced by heat shock and tunicamycin in mammalian cells (Gray CW et al, 2000). HtrA2 contains a mitochondrial localization signal in the N-terminus and resides in the mitochondrial intermembrane space (reviewed in Vande Walle L et al, 2008). Missense mutations (Ala141Ser and Gly399Ser) in the *HTRA2* gene are associated with the development of Parkinson's disease in human (Strauss KM et al, 2005). Moreover, HtrA2 is associated with Alzheimer's disease by interacting with secretase factor, presenillin-1 (Gray CW et al, 2000), and generating a 28 kDa amyloid precursor fragment (Park HJ et al, 2006). In addition, HtrA2 participates in apoptosis by degrading inhibitors of apoptosis protein (IAP), such as XIAP and cIAP1 leading to activation of caspase 3, 7 and 9 (Yang QH et al, 2003; Srinivasula SM et al, 2003).

HtrA3 was originally identified as a pregnancy-related serine protease, which is uniquely regulated at the time of embryo implantation and placental development in mouse and human (Nie GY et al, 2003). HtrA3 contains similar structural domains as HtrA1 (Nie GY et al, 2003). Moreover, HtrA3 has overlapping TGFβ binding partners and proteolytic substrates with HtrA1 (Tocharus J et al, 2004). Furthermore, HtrA3 and HtrA1 are downregulated in human endometrial cancer (Bowden MA et al, 2006). However, HtrA3 has a different expression profile from HtrA1 (Nie GY et al, 2003; Tocharus J et al, 2004), suggesting a complementary functions with HtrA1 in certain types of tissues (Tocharus J et al, 2004).

HtrA4 (GenBank accession number: NM_153692.3) is a predicted gene according to its homology with the HtrA family. *HTRA4* gene, located at chromosome 8p11.22, contains 8 exons, sharing similar structural domains with HtrA1 and HtrA3 (reviewed in Clausen T et al, 2002). No biochemical characterization has yet been reported for HtrA4.

1.5.2 Structure of HtrA1

The open reading frame of HtrA1 contains 480 amino acids with a predicted molecular mass of 51 kDa and a calculated isoelectric point of 7.7 (Zumbrunn B and Trueb B, 1996). HtrA1 protein is characterized and defined by the presence of HtrA domain, which is consisted of a proteolytic domain with at least one PDZ domain (**Figure 1.3**). Apart from the HtrA domain, HtrA family members have variable components at the N-terminus (reviewed in Clausen T et al, 2002). HtrA1, like HtrA3, but in contrast to HtrA2, also contain a signal peptide, a mac25-like/insulin-like growth factor binding protein-like domain with Kazal-type trypsin inhibitor motif at the N-terminus.

1.5.2.1 Signal peptide

The first 22 amino acids of HtrA1 is the most hydrophobic region in the protein (Zumbrunn J and Trueb B, 1996) (average hydrophobicity of 1.5455 for signal peptide versus -0.1215 for whole HtrA1 protein; SOSUIsignal (Gomi M et al, 2004); http://bp.nuap.nagoya-u.ac.jp/sosui/sosuisignal/). A putative secretory signal peptide is suggested (Hu SI et al, 1998), in which residues 1 to 5 represent the N-region of a typical signal peptide, residues 6 to 17 represent the H-region and residues 18 to 22 represent the C-region, according to the bioinformatics analysis using Phobius (Kall L et al, 2004; http://phobius.binf.ku.dk/index.html). The pre-protein is predicted to be cleaved after alanine residue 22 and the starting glutamine residue of the mature protein would be

19

converted into pyroglutamic acid, blocking the N-terminus of the polypeptide (Zumbrunn J and Trueb B, 1996). The secretory property of HtrA1 signal peptide is confirmed by the existence of HtrA1 protein in the extracellular supernatant (Hu SI et al, 1998; Ajayi F et al, 2008; Gilicze A et al, 2007) although intracellular localization of HtrA1 was also reported (Clawson GA et al, 2008; Chein J et al, 2009b).

1.5.2.2 Mac25-like/Insulin-like growth factor binding protein-like domain

The first 140 amino acids at the N-terminus of HtrA1 protein is characterized by a cluster of 12 conserved cysteine residues (Zumbrunn J and Trueb B, 1996; Hu SI et al, 1998). This N-terminus region of HtrA1 has a homology of IGFBP3 (Zumbrunn J and Trueb B, 1996) and shows 61% sequence identity (**Figure 1.4A**). In contrast, a homology to mac25, rather than IGFBP3, is suggested from the degree of identity and the motif arrangement (Hu SI et al, 1998). The N-terminus of HtrA1 has a higher sequence identity (81%) with human mac25 protein than IGFBP3 (**Figure 1.4B**). Moreover, apart from the IGFBP-like domain, a conserved Kazal-type serine protease inhibitor motif is identified at the end of these 140 amino acid region (Zumbrunn J and Trueb B, 1996; Hu SI et al, 1998). Although mac25 is provisionally labeled as IGFBP7 (GenBank accession number: NM_001553.1), mac25 is more closely related to follistatin than IGFBP because both mac25 and folistatin contain the Kazal-type inhibitor motif (Kato MV et al, 1996). Nevertheless, HtrA1 preferentially cleaves IGFBP5 than other IGFBP *in vitro*; however, the mac25-like/IGFBP-like domain is not required for the cleavage (Hou J et al, 2005). Besides, the possibility for IGF-I or IGF-II binding to this domain is extremely low (Hou J et al, 2005). In addition, the removal of this N-terminus region enhances the proteolytic activity of HtrA1 towards the substrates (Hou J et al, 2005; Chien J et al, 2006), indicating the presence of auto-inhibitory property in this region, which might be mediated by the

20

Kazal-type inhibitor motif. However, the function and properties of this region for HtrA1 remains to be elucidated.

1.5.2.3 Proteolytic domain

HtrA domain is characterized by a proteolytic domain followed by at least one PDZ domain. The proteolytic domain is chymotrypsin-like and belongs to the S1C type endoprotease within the trypsin clan SA of the serine proteases (Pallen M and Wren B, 1997). The HtrA proteolytic domain is arranged in the histidine-aspartic acid-serine order of the catalytic triad with two six-stranded β barrel domain structure (reviewed in Clausen T et al, 2002). In HtrA1, the catalytic triad is composed of histidine at position 220, aspartic acid at position 250 and serine at position 328 (Zumbrunn J and Trueb B, 1996). In addition, the proteolytic activity of HtrA1, unlike other proteases, is ATP-independent (reviewed in Clausen T et al, 2002).

A preferred HtrA1 cleavage motif (P1' to P4') is identified as Arg-Pro-Asp-Phe, accounting for 13 to 27 % of total primary peptide library (Chien J et al, 2009a). Based on this post-proteolytic cleavage motif, a possible HtrA1 proteolytic cleavage site (P1 to P4) is generated as [AlaGluGlyArg] – [LysAlaGlyArg] – [IleAlaMetLysArg] – [TheVlaIleAlaLys], and the predicted potential substrates containing this motif include tubulins, CD44, ICAMs, ABCBs, BESTs, IAPs and caspases (Chien J et al, 2009a). However, the proteolytic domain of HtrA1 has wide range of *in vitro* substrates, such as aggrecan, decorin, fibromodulin, soluble type II collagen, fibronectin, tubulins, cartilage oligomeric matrix protein, biglycan and matrix Gla protein (Tocharus J et al, 2004; Murwantoko et al, 2004; Tsuchiya A et al, 2005; Grau S et al, 2006; Hadfield KD et al, 2008; Chamberland A et al, 2009; Chein J et al, 2009a). HtrA1 recognizes the interglobular domain of aggrecan and generates the HtrA1-cleaved aggrecan fragments containing the VQTV[356] neoepitope (Chamberland A et

al, 2009). Moreover, HtrA1 is also able to bind various TGFβ family proteins without cleavage, including TGFβ1, TGFβ2, activin, BMP2, BMP4 and Gdf5 (Oka C et al, 2004). The proteolytic activity depends strictly on the catalytic triad since mutation of serine 328 to alanine abolishes the proteolytic acitivity of HtrA1 (Hu SI et al, 1998). Furthermore, the removal of the N-terminus region of HtrA1 enhances the proteolytic activity of HtrA1 towards the substrates (Hou J et al, 2005; Chien J et al, 2006), indicating a self-regulatory mechanism. In addition, HtrA1 agonists, such as CPII, a C-terminal hexapeptide derived from the C-propeptide of procollagen IIα1 also enhances the protease activity of HtrA1 (Chamberland A et al, 2009). Recently, recombinant HtrA1 has been reported to cleave several RPE secretome, including fibromodulin, clusterin, ADAM9, vitronectin, α-2 macroglobulin, talin-1, fascin and chloride intracellular channel protein 1 (An E et al, 2010).

1.5.2.4 Postsynaptic density protein 95-Discs large-Zona occuldens 1 domain

Postsynaptic density protein 95-Discs large-Zona occuldens 1 (PDZ) domain is a common protein, which mediates protein-protein interactions through the recognition of specific motifs, 4 to 6 amino acid in length, at the C-terminus of target proteins or structurally related internal motifs (Harris BZ and Lim WA, 2001; Hung AY and Sheng M, 2002). In additional to complex assembly, PDZ domains are also involved in the regulation of receptor activation and protein trafficking (Hung AY and Sheng M, 2002). HtrA family is characterized by the HtrA domain, which is consisted of a proteolytic domain followed by at least one PDZ domain (reviewed in Clausen T et al, 2002). Mammalian HtrA1 harbors only one PDZ domain, which is located at the C-terminus of HtrA1 protein.

Analogous to other PDZ domain structures (Sheng M and Sala C, 2001), the PDZ fold in human HtrA1 is consisted of a five-stranded β-sandwich (β1 – β5) capped by two

22

α-helices (α1, α3) (Runyon ST et al, 2007). In addition, two short β-strands are present at N and C termini (Runyon ST et al, 2007). Compared to the canonical PDZ fold, PDZ fold in HtrA1 is cyclically permuted, where the first β-strand of the canonical fold corresponds to β5 of PDZ in HtrA1 (Runyon ST et al, 2007). From the NMR structure, Tyr382, Ile383, Gly384, Met387 and Ser389 are involved in direct contact with the peptide ligand (Runyon et al, 2007). Moreover, mutations in Ile415 and I418 of HtrA1-PDZ result in poor peptide recognition (Runyon et al, 2007). Similar to the structure of other HtrA family members, the peptide ligand binds to an extended conformation in the cleft between strand β1 and helix α3 (Runyon et al, 2007).

From a yeast-two-hybrid analysis, 11 PDZ-binding proteins are identified in day-17 mouse embryo and adult mouse brain cDNA libraries. These include collagen type III α1 (Col3a1), collagen type I α1 (Col1a1), collagen type II α1 (Col2a1), and *cis*-Golgi matrix Golgin subfamily protein (GM130) (Murwantoko et al, 2004). PDZ domain of HtrA1 recognizes only last 4 ligand positions of C-terminus of target peptide, yielding a consensus motif of $\Phi^{-3}\text{-}X^{-2}\text{-}\Phi^{-1}\text{-}[L/V/F/A]^{0}\text{-}COOH$, which Φ represents hydrophobic/non-polar amino acids and X represents any amino acid (Murwantoko et al, 2004). The consensus sequence for HtrA1-PDZ is different in another study, of which aliphatic side chains at position^{0}, more promiscuous at position^{-1}, Trp/Phe at position^{-2} and Ile at position^{-3} are highly selected (Runyon et al, 2007) although the preference of overall hydrophobic character is conserved. Binding of peptide ligand to HtrA1-PDZ stimulates the proteolytic activity, which is similar to the effect of truncating the PDZ domain from HtrA1 protein, indicating a suppressive function of the unengaged PDZ domain on the proteolytic activity (Martins LM et al, 2002; Murwantoko et al, 2004).

1.5.3 Localization of HtrA1

An exhaustive knowledge of the tissue expression pattern and specific subcellular localization of HtrA1 is an essential requirement for a critical evaluation of the exact role for HtrA1 in cell homeostasis as HtrA1 is involved in several physiological and pathological conditions, such as placentation, cancers, arthritis and age-related macular degeneration.

1.5.3.1 Tissue distribution of HtrA1

Tissue distribution of HtrA1 mRNA and protein has been reported in embryonic chick (Ferrer-Vaquer A et al, 2008), embryonic mouse (Oka C et al, 2004; De Luca A et al, 2004b; Ferrer-Vaquer A et al, 2008) and adult human (Zumbrunn J and Trueb B, 1996; Nie GY et al, 2003; De Luca A et al, 2003).

In chick embryo, *HTRA1* mRNA expression is detected throughout the ectoderm and in the head development at Hamburger and Hamilton stages (HH) 4-8 (Ferrer-Vaquer A et al, 2008). At HH12, the neural crest derived head mesenchyme, the notochord, the floor plate, the sclerotome of somites from somite stage IX-X and the primordium of the facial-acoustic ganglion shows strong *HTRA1* expression (Ferrer-Vaquer A et al, 2008). At HH15, in addition to the expression at HH12 except the floor plate, *HTRA1* is expressed in the ectoderm on the dorsal side of the forming otic pits, the trigeminal placode, pharyngeal pouch endoderm and the endothelium of the dorsal aorta (Ferrer-Vaquer A et al, 2008). At HH18, strong *HTRA1* staining is detected in the nasal pit region, the lens vesicle, the dorsal region of the otic vesicle, the core of the first branchial arch, the ectoderm covering the second branchial arch, the endoderm of the pharyngeal pouches, all cranial ganglia, the endocardial cushion of the heart, the sclerotome of all somites, the tail region of notochord, the mesenchyme of developing forelimb, the mesenchyme around developing gut

24

(Ferrer-Vaquer A et al, 2008). At HH20, the overall pattern of HTRA1 is similar to previous stages with expression in the head mesenchyme, a restricted domain of the tegmental neuroepithelium, the lens and otocyst epithelium, pharyngeal endoderm, cranial ganglia, pharyngeal arches, forelimb and the dorsal midline of the neuroepithelium of forebrain and midbrain (Ferrer-Vaquer A et al, 2008). At HH23, addition *HTRA1* expression is detected in the anterior wall of the lens vesicle, the dorsal part of otocyst, the pharyngeal region, the dorsal root ganglia and spinal nerves (Ferrer-Vaquer A et al, 2008). At embryonic day (E) 7, the lungs, the outflow tract of heart, the dorsal aorta, gut, gizzard and Müllerian duct are positive for *HTRA1* (Ferrer-Vaquer A et al, 2008). Moreover, strong expression is localized in regions of the mesenchyme of E8 chicken limbs (Ferrer-Vaque A et al, 2008). Furthermore, *HTRA1* is involved in skin morphogenesis as it is detected in the forming feather placodes and the underlying dermis at HH34, and the dermal core of forming feathers, but not epithelium, at HH36 (Ferrer-Vaque A et al, 2008).

Unlike chick at HH4, *HtrA1* mRNA is localized in the extra-embryonic ectoderm adjacent to the ectoplancental cavity and in intra-embryonic mesoderm of E7.5 mouse (Ferrer-Vaquer A et al, 2008), which is similar to the presumptive mesoderm location of *Xenopus HtrA1* around the blastopore lip (Hou S et al, 2007). At E8-9.5, HtrA1 mRNA and protein expressions are restricted to the notochord, neuroepithelial tissues, epithelium of gut diverticulum, mesodermal tissue, developing heart, base of allantois, dorsal aorta and vitelline artery walls (De Luca A et al, 2004b; Ferrer-Vaquer A et al, 2008). In E11.5-12.5 mouse, moderate signal for HtrA1 is localized in midbrain, neopallial cortex, epithelium surrounding ventricles, pons/midbrain junction, spinal cord, cartilage primordial of different bones, the heart, lungs, gonads and skin of the thoraco-abdominal region while intense signal is shown in auditory epithelium, olfactory epithelium, dorsal and lumbar root ganglia (Oka C et al, 2004; De Luca A et al, 2004b). At E14.5, *HtrA1* is expressed in rudiments of

tendons, ligaments along the vertebrae and mesenchymal cells surrounding precartilage condensations, as well as in specific regions of the neuroepithelium in the forebrain and hindbrain (Oka C et al, 2004). In E19 mouse, intense HtrA1 protein is expressed in mature and outer layers of stratified epithelium of skin, epithelia of esophagus, intestine, urinary duct and striated and cardiac muscle while moderate expression is detected in liver and brain (De Luca A et al, 2004b). In postnatal day 1 mouse, HtrA1 is highly expressed in liver, stratified epithelium of skin, epithelium of esophagus, intestine, cardiac and striated muscle and spinal cord, and moderately in brain and epithelia of lung and kidney (De Luca A et al, 2004b). HtrA1 expression level is increased from E12 to E16, but remains at the same level until birth (Oka C et al, 2004; De Luca A et al, 2004b).

In normal adult human, low level of HtrA1 is found in the mature and outer layers of stratified epithelia, such as from esophagus, cervix and vagina, and the stratified columnar epithelial of trachea, bronchi and adjacent glands, whereas high expression level is in the mature layers of epidermis in the skin, compared to the low level in hair follicles, sebaceous glands and sweat glands (De Luca A et al, 2003). Moreover, medium expression level is detected in the secretory breast epithelium compared to low level in breast duct epithelium (De Luca A et al, 2003). In the gastrointestinal system, intense HtrA1 staining in the duct cells of the liver, moderate level in the colon epithelia and exocrine portion of the pancreas, and low level in secretory ducts of salivary glands, hepatocytes, stomach, gallbladder and the endocrine portion of the pancreas are shown (Zumbrunn J and Trueb B, 1996; De Luca A et al, 2003). In the urinary system, medium level of HtrA1 is detected in all kidney tubules of cortex and prostate stroma, whereas low expression is shown in the tubules of medulla and in the glomeruli (Zumbrunn J and Trueb B, 1996; De Luca A et al, 2003). In the endocrine system, moderate HtrA1 level is found in thyroid follicles, but low in cortical cells of adrenal gland (De Luca A et al, 2003). The male reproductive system

displays low HtrA1 level (De Luca A et al, 2003). In contrast, several regions in the female reproductive system show intermediate HtrA1 levels, including epithelium of proliferating endometrium, the basal layer in exocervix and the stroma in ovary (Nie GY et al, 2003; De Luca A et al, 2003). Furthermore, greater HtrA1 expression is detected in third trimester placenta compared with that at the first trimester of gestation (Zumbrunn J and Trueb B, 1996; Nie GY et al, 2003; De Luca A et al, 2003; De Luca A et al, 2004a). In cardiovascular and connective tissues, medium HtrA1 level in chondrocytes, endothelial cells and fibroblasts and low levels in skeletal muscle cells and myocardial cells are shown (Zumbrunn J and Trueb B, 1996; Nie GY et al, 2003; De Luca A et al, 2003). In the nervous system, all neurons from different regions of the brain, such as frontal cortex and midbrain and cells of the granular level of the cerebellum, as well as perineural and endoneural cells of peripheral nerves and ganglion cells and microglial cells display low HtrA1 protein levels (De Luca A et al, 2003) although moderate *HTRA1* expression is detected in most of the compartments of the brain (Zumbrunn J and Trueb B, 1996; Nie GY et al, 2003). In addition, undetectable level of HtrA1 is reported in blood cells and several lymphoid tissues (De Luca A et al, 2003).

In human eye, immunoreactivity of HtrA1 is weakly found in the peripheral retina, retinal vascular endothelium, internal limiting membrane and RPE (Chan CC et al. 2007; Tuo J et al, 2008). In mouse, HtrA1 is expressed at the peripheral margin of neural retina and RPE at E12.5, in the ciliary body, iris and cornea at E16.5, and additionally, in the ganglion cell layer and inner nuclear layer in 8-week adult (Tocharus J et al., 2004).

From all the reports, it can be summarized that HtrA1 is widely expressed. However, variable HtrA1 intensities are quantitatively shown in different tissues and developmental stages, indicating its highly dynamic nature.

1.5.3.2 Subcellular localization of HtrA1

The 1st to 22nd amino acids of HtrA1 are predicted to be the signal peptide for HtrA1 protein secretion. This is confirmed by the existence of HtrA1 protein in HtrA1-transfected cell culture medium (Hu SI et al, 1998; Baldi A et al, 2002; Gilicze A et al, 2007). Moreover, the extracellular localization of HtrA1 is further supported by the immunofluorescent pattern of HtrA1-expressed extravillous trophoblast cell line (Ajayi F et al, 2008) and mast cells (Gilicze A et al, 2007), and the immunoelectron microscopy of HtrA1 in extracytoplasmic space of the stroma of placental villi and the spaces between and on the collagen fibers (De Luca A et al, 2004a). However, the secretion of HtrA1 is suggested to be constitutive rather than stored in secretory granules (Gilicze A et al, 2007). In contrast, perinuclear and nuclear staining for HtrA1 is reported in a human cervical cancer cell line, a human embryonic kidney cell line and a hepatocyte cell line without any detectable HtrA1 in the culture medium (Clawson GA et al, 2008). Moreover, HtrA1 is also localized in the cytosol of placental cells (De Luca A et al, 2004a). Recently, a microtubule-associated localization for HtrA1 has been shown in the ovarian cancer cell lines, respectively (Chien J et al, 2009b). These studies imply HtrA1 in different cell types may have different subcellular localizations, as well as different functions.

1.5.4 HtrA1-associated physiological and pathological conditions

Mutations in the *HTRA1* gene (Ala252Thr, Val297Met, Arg302X and Arg370X) are associated with cerebral autosomal recessive arteriopathy with subcortical infarcts and leukoencephalopathy (CARASIL) (Hara K et al, 2009). Moreover, a polymorphism in the promoter region of the *HTRA1* gene (rs11200638) increases about 7-fold of risk to develop AMD (DeWan A et al, 2006; Yang Z et al, 2006). Furthermore, elevated expression of HtrA1 has been found in several diseases, including rheumatoid arthritis and osteoarthritis

(Hu SI et al, 1998; Tsuchiya A et al, 2005; Grau S et al, 2006; Wu J et al, 2007), Alzheimer's disease (Grau S et al, 2005), and Duchenne muscular dystrophy (Bakay M et al, 2002). In contrast, HtrA1 is downregulated in cancers (Baldi A et al, 2002; Chien J et al, 2004). In normal physiology, HtrA1 participates in the development of uterine lining and placentation (De Luca A et al, 2003; Nie GY et al, 2005).

1.5.4.1 HtrA1 and cancers

Human *HTRA1* gene (*L56*) was originally identified as a missing gene in the SV40 oncogenic virus-transformed human fibroblasts (Zumbrunn J and Trueb B, 1996). Subsequently, downregulation of *HTRA1* (*PRSS11*) gene was found in malignant melanoma and autologous lymph node metastasis (LM)-derived cell lines (Baldi A et al, 2002). Coherently, expression of HtrA1 was shown to be downregulated in ovarian tumors, brain tumors, endometrial cancer, lung cancer, choriocarcinoma, mesothelioma, ovarian cancer cell lines, breast cancer cell lines, liver cancer cell lines and cervical cancer cell lines (Baldi A et al, 2008; Bowden MA et al, 2006; Chien J et al, 2004; Esposito V et al, 2006; Marzioni D et al, 2009; Narkiewicz J et al, 2009). The downregulation of HtrA1 expression is related with increasing grades of cancers and cancer progression (Baldi A et al, 2002; Bowden MA et al, 2006; Esposito V et al, 2006; Narkiewicz J et al, 2008; Narkiewicz J et al, 2009).

The reduced HtrA1 expression in ovarian cancer could be caused by loss of heterozygosity (LOH) on chromosome 10q25-26 (Chien J et al, 2004), a region commonly deleted in cancers (Albarosa R et al, 1996). Moreover, the repressed *HTRA1* transcirption could also be mediated by DNA methylation (Chien J et al, 2004). However, no tumor-specific mutations were detected in ovarian tumors (Chien J et al, 2004), suggesting that mutation in *HTRA1* gene may not be a route for tumorgenesis.

The role of HtrA1 in cancers could be seen from its regulation of cell cycle and

growth. Overexpression of *HTRA1* in metastatic LM cell line reduced the proliferative activity and the ability to invade extracellular matrix *in vitro* as well as retarded growth and metastases *in vivo* in nu/nu mice (Baldi A et al, 2002). Moreover, downregulation of *HTRA1* in ovarian cell line by RNA interference promoted anchorage-independent growth while exogenous expression of HtrA1 induced a serine protease-dependent cell apoptosis (Chien J et al, 2004). Furthermore, forced expression of HtrA1 enhanced cisplatin and paclitaxel-induced apoptosis through reduction of autoproteolysis and activation of HtrA1 (Chien J et al, 2006). HtrA1 modulating the outcome of chemotherapy could also be seen from the treatment of piroxicam and cisplatin in a mouse model of peritoneal mesothelioma (Spugnini EP et al, 2006) and reflected by its predictive potential, together with *MTSS1* and *CLPTM1*, for the response to doxorubicin-based therapy in breast cancer (Folgueira MA et al, 2005; Sobral RA et al, 2008). Recently, downregulation of HtrA1 has been reported to promote cell motility while enhanced expression of HtrA1 attenuated cell migration through its association with microtubules and tubulins (Chien J et al, 2009a; Chien J et al, 2009b). In addition, downregulation of HtrA1 reduces resistance to anoikis, whereas enhanced expression of HtrA1 induces cell death through inhibition of EGFR/AKT pathway (He X et al, 2010).

1.5.4.2 HtrA1 and placentation

The highest HtrA1 expression was detected in human third-trimester placenta, proliferative endometrium and uterus (De Luca A et al, 2003; Nie GY et al, 2003), compared to other organs. However, HtrA1 expression in the first-trimester placenta was very low while undetectable expression was reported in the secretory endometrium.

In mouse, *HTRA1* expression, depending on the presence of embryo (Kashiwagi A et al, 2007), begins in E7.5 implantation sites and peaks at E10.5 placentas, then the levels

decline dramatically in E17.5 placentas (Nie GY et al, 2005). During early stages of placental development (E7.5 to 8.5), HtrA1 is expressed in the differentiated trophoblasts (terminally differentiated giant cells) in the ectoplacental cone and the uterine cells immediately adjacent to the trophoblast giant cells. On the contrary, by E9.5 – 10.5, more intensive HtrA1 signal is detected in the deciduas capsularis specifically at the decidual-trophoblast interface where active involution occurs. In human, during menstrual cycle, *HTRA1* expression is low in the menstrual phase, but gradually increases through the proliferative and secretory phases, and peaks in the mid to late secretory phase (Nie GY et al, 2006). HtrA1 protein is found in the glandular epithelium during all stages of menstrual cycle and in decidual cells in the stroma in late secretory phase. During early (first-trimester) pregnancy, the deciduas expressed higher HtrA1 levels than the placenta and during menstrual cycle.

Preeclampsia, initiated by shallow trophoblast invasion into endometrium and improper spiral artery remodeling in the decidua (Lyall F, 2006; McMaster MT et al, 2004), is a pregnancy-associated hypertensive disorder (Redman CW and Sargent IL, 2005). Elevated expression of HtrA1 was detected in the villous trophoblasts from patients with early-onset preeclampsia compared to controls (Ajayi F et al, 2008; Nishizawa et al, 2007), which extravillous trophoblast cell motility, cell migration and cell invasion were attenuated by ectopic expression of HtrA1 (Ajayi F et al, 2008).

1.5.4.3 HtrA1 and arthritis

The involvement of HtrA1 (ORF480) in arthritis was originally identified in osteoarthritic cartilage, which elevated HtrA1 mRNA (~ 7 fold) and protein levels were reported in cartilage from patients with osteoarthritis compared with nonarthritic controls (Hu SI et al, 1998). Subsequently, elevated synovial HtrA1 levels were found in fluids from

31

rheumatoid (~ 3 fold) and osteoarthritis (~ 7 fold) patients (Grau S et al, 2006). Moreover, increase in HtrA1 expression was also shown in articular cartilage tissue from donors with and without osteoarthritis (Wu J et al, 2007). The role of HtrA1 in arthritis was confirmed in an experimental rheumatoid mouse model, which HtrA1 in cartilage was elevated by about 4-fold on day 9 after arthritis induction (Tsuchiya A et al, 2005). Consistently, the expression of HtrA1 is increased in the knee and TM joints of 2 transgenic and 2 surgically induced mouse osteoarthritic models (Polur I et al, 2010).

From the experimental rheumatoid mouse model, the origin of elevated HtrA1 is proposed to be the chondrocytes terminally differentiated to the hypertrophic stage in arthritic joints (Tsuchiya A et al, 2005). However, the synovial fibroblasts are also postulated as a major source of secreted HtrA1 (Grau et al, 2006).

Unlike the action in cancers (Chien J et al, 2004; Baldi A et al, 2002), the expression of HtrA1 does not coincide with the onset of apoptosis; rather, heavy local deposition of HtrA1 is shown in the areas with severely damaged joint surface, suggesting that HtrA1 may play a role in tissue damages after the initiation of apoptosis in chondrocytes (Tsuchiya A et al, 2005). Alternatively, HtrA1 is proposed to negatively regulate the availability of TGFβ family (Oka C et al, 2004) since interference in TGFβ signaling has shown phenotypes very similar to human osteoarthritis (Serra R et al, 1997; Yang X et al, 2001). Moreover, the deposition of HtrA1 protein in bone matrix was coherent with that of TGFβ (Tsuchiya A et al, 2005) and the inhibition of TGFβ-induced matrix synthesis in chondrocyte by HtrA1 (Wu J et al, 2007), indicating a close functional relationship between HtrA1 and TGFβ. Furthermore, HtrA1 could degrade extracellular matrix components of the cartilage (Tocharus J et al, 2004; Murwantoko et al, 2004; Tsuchiya A et al, 2005; Grau S et al, 2006; Hadfield KD et al, 2008; Chamberland A et al, 2009). Specifically, HtrA1 might disrupt the pericellular matrix network of type VI collagen,

resulting in alteration of chondrocyte metabolisms and eventually leading to osteoarthritis (Polur I et al, 2010). In addition, the HtrA1-regulated matrix calcification and inhibited mineral deposition by osteoblasts may implicate a possible pathology in skeletal development (Canfield AE et al, 2007; Hadfield KD et al, 2008).

1.5.5 Molecular biology of HtrA1

On the molecular level, HtrA1 modulates IGF signaling by cleaving the IGFBP-5 (Hou J et al, 2005). It might not regulate epidermal growth factor (EGF) or fibroblast growth factor 2 (FGF-2) as it does not bind to these molecules (Oka C et al, 2004). However, FGF signaling is necessary and sufficient for *HTRA1* expression in chick facial and forelimb mesenchyme (Ferrer-Vaquer A et al, 2008). Similarly, FGF signaling is sufficient but not required for *HtrA1* transcription in *Xenopus* embryos (Hou S et al, 2007). Moreover, HtrA1 inhibits mineral deposition by osteoblasts (Hadfoeld KD et al, 2008). Furthermore, intracellular HtrA1 regulates cell migration in an ovarian cancer cell line, SKOV3, since HtrA1 binds to the endogenous tubulins (Chien J et al, 2009b). Even though HtrA1 participates in a wide range of molecular functions, only the relationships of HtrA1 with TGFβ signaling and extracellular matrix have been well studied and elucidated.

1.5.5.1 HtrA1 and TGFβ signaling

HtrA1 protein possesses a mac25-like/follistatin-like domain at the N-terminus region (Hu SI et al, 1998). Since follistatin has an important role in the negative regulation of TGFβ family members (Kato MV, 2000; Krieglstein K et al, 2002), HtrA1 is proposed to have a regulatory role in TGFβ signaling. The first correlation comes from a coherent situation between the spatio-temporal expression patterns of HtrA1 and the functioning sites of various Tgfβ proteins in embryonic mice (Oka C et al, 2004). Moreover, HtrA1

binds to various Tgfβ family proteins, such as Tgfβ1, Tgfβ2, Bmp4, Gdf5 and activin, and subsequently inhibit the Bmp4, Bmp2 and TGFβ1 signaling (Oka C et al, 2004). The binding requires the proteolytic domain, but independent of the mac25-like domain and the proteolytic activity. However, the proteolytic activity is necessary for the inhibition of TGFβ signaling (Tocharus J et al, 2004). In addition, increased expression of TGFβ1 in the tunica media of patients with CARASIL further supports the negative regulation of the Tgfβ proteins availability (Hara K et al, 2009) and, therefore, the TGFβ signaling (Oka C et al, 2004).

Apart from the physical interaction between HtrA1 and Tgfβ family proteins, aberrant HtrA1 expression could induce smaller eyecup, shorter lens diameter, thinner lens, retinal detachment and transition of RPE to neuroepithelium-like tissue in chick eye (Oka C et al, 2004), which resemble the effect of noggin, an endogenous Bmp signal inhibitor (Adler R and Belecky-Adams TL, 2002). Furthermore, increasing HtrA1 expression co-exists with a progression loss of TGFβ signaling during in vitro neuronal maturation and brain development, whereas the blockage of HtrA1 proteolytic activity restores the TGFβ signaling and leads to neuronal death (Launay S et al, 2008). These evidences indirectly implicate a negative correlation between HtrA1 and TGFβ signaling.

1.5.5.2 HtrA1 and extracellular matrix

HtrA1 possesses a signal peptide guiding for protein secretion (Hu SI et al, 1998). Extracellular HtrA1 is proposed to degrade extracellular matrix proteins because of its proteolytic domain and activity, as well as their differential expression in arthritis (Hu SI et al, 1998; Grau S et al, 2006; Wu J et al, 2007). Apart from the proteolytic activity, the proximity of HtrA1 to the bone matrix also suggests its correlation with extracellular matrix turnover (Oka C et al, 2004; Tsuchiya A et al, 2005). Recombinant HtrA1 can cleave

extracellular matrix components, such as aggrecan, decorin, fibromodulin, soluble type II collagen, fibronectin, cartilage oligomeric matrix protein, biglycan and matrix Gla protein (Tocharus J et al, 2004; Murwantoko et al, 2004; Tsuchiya A et al, 2005; Grau S et al, 2006; Hadfield KD et al, 2008; Chamberland A et al, 2009). Moreover, *in vivo* involvement of HtrA1 in aggrecan proteolysis was shown by the higher abundance of HtrA1-generated aggrecan fragments in osteoarthritic cartilage compared with healthy cartilage (Chamberland A et al, 2009). Increased expression of the extra domain-A region of fibronectin and versican in the thickened tunica intima of patients with CARASIL further supports the role of HtrA1 in extracellular matrix degradation (Hara K et al, 2009). Furthermore, HtrA1-cleaved fibronectin fragments induce the expression of matrix metalloprotease (MMP) 1 and MMP3 in synovial fibroblasts, and this contributes to the destruction of extracellular matrix in an indirect mechanism (Grau S et al, 2006). In addition, HtrA1 also inhibit the TGFβ-induced matrix synthesis by chondrocytes (Wu J et al, 2007), further regulating the extracellular matrix composition. This evidence strongly suggests that HtrA1, possessing protelolytic activity, has a role in extracellular matrix turnover.

1.6 Objectives and research impacts

The knowledge on the AMD pathogenic mechanisms is limited. Genetics is a widely used approach to discover the molecular players involved in the disease pathogenesis. Previously, chromosome 1q31 (*CFH*) and 10q26 (*HTRA1* or *LOC387715*) were found to be associated with AMD. However, the disease-causing gene for AMD in these regions has yet to be identified. This thesis was aimed:

1.   To affirm the molecular linkage between AMD and the AMD-associated genes, *CFH* and *HTRA1*, their sequences were screened for possible mutations/variants in Chinese exudative AMD patients and age-matched controls to delineate their role in AMD.

2.   To characterize the biological features of HtrA1 variants identified in the screening study, together with the wildtype, to depict their association with AMD.

3.   To investigate the interaction of HtrA1 with other AMD-associated proteins in human vitreous humor to determine its relationship with AMD pathogenesis.

4.   To determine the regulation of HtrA1 and VEGF in the primary human fetal RPE cell culture system to reveal the possible link in actions between these two AMD-associated molecules and to throw light on the possible mechanisms of HtrA1 in AMD development.

Population	AMD Patients (n, %)			Controls (n, %)			p	Odds Ratio (95% CI)	References
	TT	TC	CC	TT	TC	CC			
Chinese	145 (89.0%)	17 (10.4%)	1 (0.6%)	225 (92.2%)	19 (7.8%)	0 (0%)	0.3	N/A	Chen LJ et al. 2006
Chinese	109 (75.7%)	34 (23.6%)	1 (0.7%)	114 (90.5%)	11 (8.7%)	1 (0.8%)	0.005	3.23 (1.56-6.70)	Chu J et al. 2008
Chinese	97 (80.2%)	23 (19.0%)	1 (0.8%)	111 (84.3%)	21 (15.7%)	0 (0%)	0.496	1.25 (0.65-2.40)	Xu Y et al. 2008
Chinese	123 (81.0%)	25 (15.3%)	6 (3.7%)	219 (94.4%)	13 (5.6%)	0 (0%)	< 0.0001	3.9 (2.0-7.8)	Lau LI et al. 2006
Korean	91 (79.8%)	22 (19.3%)	1 (0.9%)	164 (87.7%)	22 (11.8%)	1 (0.5%)	0.183	2.51 (0.13-49.55)	Kim NR et al. 2008
Japanese	158 (84.0%)	27 (14.4%)	3 (1.6%)	124 (89.2%)	15 (10.8%)	0 (0%)	0.246	0.66 (0.33-1.34)	Mori K et al. 2007
Japanese	51 (76%)	13 (19%)	3 (5%)	86 (80%)	18 (17%)	3 (3%)	0.52	1.3 (0.68-2.49)	Uka J et al. 2006
Japanese	73 (91.3%)	7 (8.8%)	0 (0%)	166 (86.5%)	24 (12.5%)	2 (1.0%)	0.41	0.58 (0.24-1.36)	Fuse N et al. 2006
Caucasian	30 (21.3%)	63 (44.7%)	48 (34.0%)	47 (51.6%)	33 (36.3%)	11 (12.1%)	< 0.0001	6.84 (3.07-15.21)	Souied EH et al. 2005
Caucasian	199 (17.1%)	530 (45.5%)	437 (37.5%)	355 (37.5%)	475 (50.2%)	116 (12.3%)	4.7×10^{-7}	6.72 (5.14-8.79)	Rivera A et al. 2005
Caucasian	264 (19.8%)	644 (48.4%)	422 (31.7%)	470 (37.2%)	613 (48.5%)	182 (14.4%)	5.9×10^{-12}	4.13 (3.28-5.20)	Magnusson KP et al. 2006
Caucasian	41 (15.0%)	119 (42.0%)	121 (43.0%)	380 (32.0%)	527 (44.0%)	278 (23.0%)	< 0.001	3.1 (2.2-4.3)	Seddon JM et al. 2007
Caucasian	24 (13.4%)	92 (51.4%)	63 (35.2%)	81 (49.7%)	68 (41.7%)	14 (8.6%)	< 0.001	5.78 (3.09-10.83)	Wegscheider BJ et al. 2007
Caucasian	55 (22.9%)	127 (52.9%)	58 (24.2%)	49 (41.5%)	54 (45.8%)	15 (12.7%)	0.00047	3.4 (1.7-6.8)	Chowers I et al. 2008

N/A: Data not available

Table 1.1: Genotypic distribution of *CFH* gene variant (Tyr402His) in different studies.

Population	AMD Patients (n, %)			Controls (n, %)			Odds Ratio (95% CI)	References
	GG	GA	AA	GG	GA	AA		
Chinese	18 (11.0%)	51 (31.3%)	94 (57.7%)	55 (30.1%)	90 (49.2%)	38 (20.8%)	5.20 (3.24-8.35)	Tam PO et al. 2008
Chinese	3 (3.3%)	34 (37.8%)	53 (58.9%)	28 (26.4%)	63 (59.4%)	15 (14.2%)	6.68 (2.98-14.98)	Lu F et al, 2007
Chinese	9 (9.5%)	33 (34.7%)	53 (55.8%)	24 (26.7%)	47 (52.2%)	19 (21.1%)	8.59 (3.28-22.49)	Lin JM et al. 2008
Chinese	13 (10.7%)	52 (43.0%)	56 (46.3%)	44 (33.3%)	64 (48.5%)	24 (18.2%)	7.90 (3.61-17.26)	Xu et al, 2008
Chinese	13 (8.2%)	47 (30.0%)	99 (62.3%)	42 (30.0%)	67 (47.9%)	31 (22.1%)	10.32 (4.92-21.66)	Jiang et al, 2009
Japanese	26 (21.1%)	52 (42.3%)	45 (36.6%)	54 (40.6%)	57 (42.9%)	22 (16.5%)	4.25 (2.13-8.49)	Mori K et al, 2007
Japanese	5 (6.8%)	39 (53.4%)	29 (39.7%)	38 (40.4%)	40 (42.6%)	16 (17.0%)	13.78 (4.52-41.98)	Kondo N et al. 2007
Indian	50 (21.8%)	89 (38.9%)	90 (39.3%)	78 (42.4%)	85 (46.2%)	21 (11.4%)	6.69 (3.69-12.10)	Kaur I et al, 2008
Caucasian	67 (27.7%)	108 (44.6%)	67 (27.7%)	99 (63.1%)	50 (31.8%)	8 (5.1%)	12.38 (5.58-27.43)	Weger M et al, 2007
Caucasian	37 (27.6%)	54 (40.3%)	43 (32.1%)	70 (52.2%)	43 (32.1%)	21 (15.7%)	3.87 (2.01-7.47)	Deangelis MM et al, 2007
Caucasian	172 (37.6%)	183 (40.0%)	102 (22.3%)	179 (63.9%)	90 (32.1%)	11 (3.9%)	9.65 (5.01-18.60)	Kanda A et al. 2007
Caucasian	29 (24.6%)	57 (48.3%)	32 (27.1%)	70 (60.3%)	41 (35.3%)	5 (4.3%)	15.45 (5.48-43.58)	Leveziel N et al, 2007
Caucasian	245 (31.6%)	400 (51.5%)	131 (16.9%)	156 (53.1%)	128 (43.5%)	10 (3.4%)	8.34 (4.25-16.36)	Chen H et al, 2008
Caucasian	316 (40.0%)	361 (45.7%)	113 (14.3%)	544 (60.4%)	316 (35.1%)	40 (4.4%)	4.86 (3.30-7.16)	Tuo J et al, 2008

Table 1.2: Genotypic distribution of *HTRA1* promoter SNP (rs11200638) in various studies.
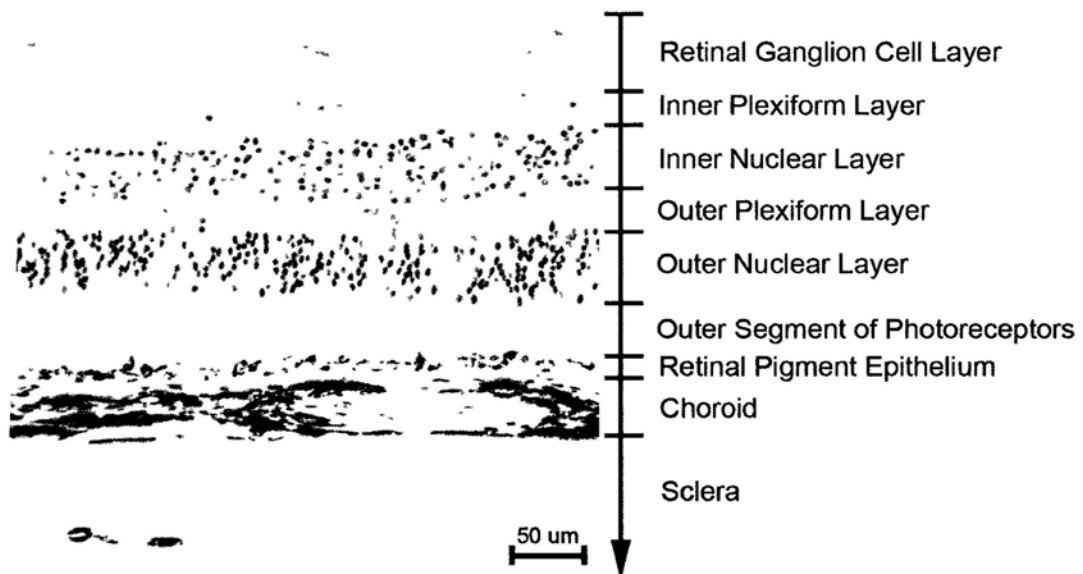
Figure 1.1: Anatomical structure of human retina.

Posterior part of the eye, including the sclera, choroid and retina was stained by haematoxylin and eosin. The retina forms a characteristic laminar structure with 8 layers, consisting of (from posterior to interior) retinal pigment epithelium, outer segment of photoreceptors, inner segment of photoreceptors (missing), outer nuclear layer, outer plexiform layer, inner nuclear layer, inner plexiform layer, and ganglion cell layer.
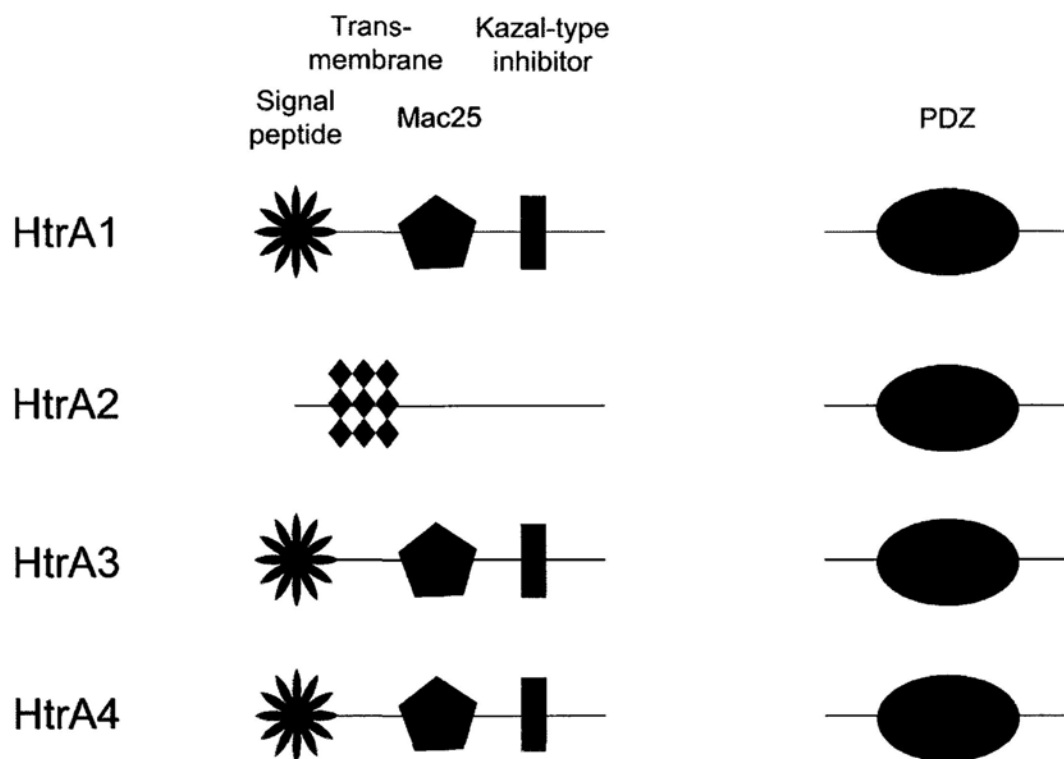
Figure 1.2: Structural comparisons among human HtrA proteins.

The HtrA family proteins are characterized by the presence of HtrA domain, which is composed of a chymotrypsin-like domain followed by at least one PDZ domain. In contrast, the N-terminus of HtrA proteins is variable. For HtrA1, HtrA3 and HtrA4, they contain a signal peptide, a mac25-like domain and a Kazal-type inhibitor at the N-terminus. Different from other paralog, HtrA2 possesses a transmembrane domain at the N-terminus.
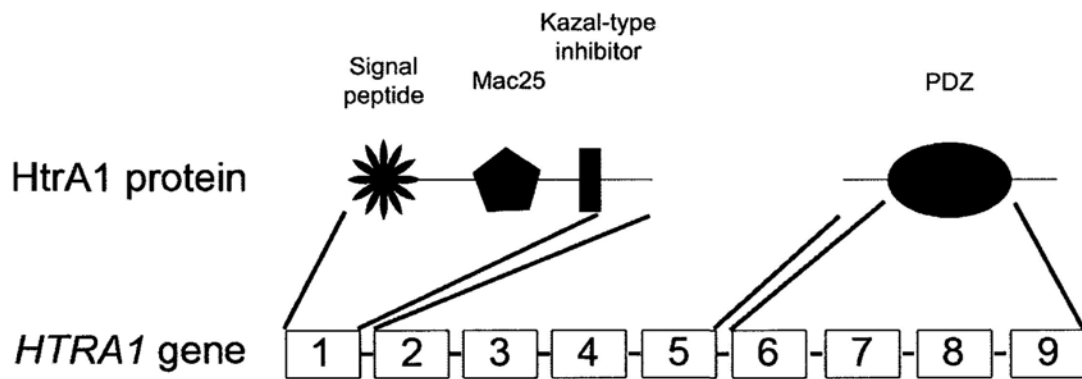
Figure 1.3: Gene structure and functional domains of HtrA1.

HTRA1 gene is composed of 9 exons. The first exon is coded for a signal peptide, a mac25-like domain and a Kazal-type inhibitor. The second to fifth exons are coded for the chymotrypsin-like domain while the PDZ domain is encoded by the sixth to ninth exons.

A

D AVG

*
HtrA1 : 61
IGFBP3 : 61
cons   61

HtrA1   PLLLLLLAAPASAQLS SAPLAAGC -----
IGFBP3 AAALTLLVLLRGPPVA SSG-GLGP CDARALA

cons   . * **. .. ! ! *: * .

HtrA1   VPF VPASATV
IGFBP3 GP-S HARDG

cons

HtrA1   RAQA GLGVGASGE-----------PVCGSD ANY -----------CQLRA
IGFBP3 LDGR GLGVNAS VSRLRAYLLPAPPPAPGNA SEGE EDRSAGSVESP STHRV

cons   :   *. *. *. . .

HtrA1   ASRRS HRPPVIVLQ-----------------------------------
IGFBP3 SDPKF HSK-IIIIKKGHAKDSQRYKVDYESQSTDTQNFSSESKRETEYGPC

cons   : · * · *:::

HtrA1   --RGA------
IGFBP3 RREMEDTLNHLKFLNVLSPRGVHIPNCDKKGFYKKKQCRPSKGRKRGFCWCVDK

cons   **

HtrA1   ---------------------C
IGFBP3 YGQPLPGYTTKGKEDVHCYSMQSK

cons

B

: 81
: 81
: 81

HtrA1   IPRAALL-----PLLLLLLLAAPASAQLS RAGRSAPLA CPD
Mac25   --RASLRALLFGPAGLLLLLLLPLSSSSS---------TCG

cons   **:*   *   **** * *:. *

HtrA1   -E PFGVPASA
Mac25   PL GGG -------S

cons   .   :

HtrA1   T A----------
Mac25   R AGAAAGGPGVS

cons   . *

HtrA1
Mac25   EQGPSIVTPPKDIWNVTGAQVYLSCEVIGIPTPVLIWNKVKR

cons

HtrA1   --
Mac25   GHYGVQRTELLPGDRDNLAIQTRGGPEKHEVTGWVLVSPLSKEDAGEYECHASN

cons

HtrA1   -------------------------
Mac25   SQGQASASAKITVVDALHEIASEKR

cons

42

Figure 1.4: Multiple sequence alignment of N-terminus of human HtrA1 with human insulin-like growth factor binding protein-3 and Mac25 protein.

The N-terminus region of human wildtype HtrA1 protein (NP_002766.1; 155 amino acids) is aligned with the full-length of human wildtype **(A)** IGFBP3 protein (NP_000589.2; 291 amino acids) and **(B)** Mac25 protein (NP_001544.1; 277 amino acids) using online analysis tool (T-coffee; http://tcoffee.vital-it.ch/cgi-bin/Tcoffee/ tcoffee_cgi/index.cgi). The N-terminus region of HtrA1 shares a homology of 61% with IGFBP3 protein and 81% with Mac25 protein.

Chapter 2: Materials and Methods

2.1 Variant identification in *CFH* and *HTRA1* genes

2.1.1 Study subjects

A total of 163 patients with exudative AMD and 390 age- and sex-matched control subjects were recruited. 155, 183 and 207 control subjects were used for the *CFH* screening, the first *HTRA1* screening and the second *HTRA1* screening, respectively. The characteristics of the study group for the first *HTRA1* screening were shown in **Table 2.1**. All study subjects received a detailed eye examination, including best corrected visual acuity test and slit lamp biomicroscopy of the fundus, and stereoscopic fundus photographs were recorded. For AMD diagnosis, the experienced clinicians followed an international classification and grading system for age-related maculopathy and age-related macular degeneration (Bird AC et al, 1995). Patients with exudative AMD were defined to have non-drusenoid RPE detachment, CNV, serous or hemorrhagic retinal detachments, subretinal or sub-RPE hemorrhage, or fibrosis. The clinical phenotype of polypoidal choroidal vasculopathy was excluded in all exudative AMD patients by the indocyanine green analysis. For the control subjects, they did not have a family history of AMD, sign of AMD, or any other major eye diseases except senile cataract and slight floaters. Their fundi were normal with no drusen, no abnormal RPE change and no foveal reflex. Informed consent was obtained from all participants after explanation of the nature of the study. The study protocol was approved by the Ethics Committee on Human Research of the Chinese University of Hong Kong, which is in accordance to the Declaration of Helsinki.

44

2.1.2 DNA collection and extraction

Five milliliters (ml) of peripheral venous blood was collected from each study subjects, and aliquots were stored in 1.5-ml EDTA tubes at -80℃ before extraction. Genomic DNA was extracted using a commercially available extraction kit (QIAamp DNA Blood Mini kit; Qiagen, Hilden, Germany). Briefly, 200 micro-liters (μl) of whole blood was lysed with 20 μl proteinase K and 200 μl Buffer AL at 56℃ for 10 minutes (min). Genomic DNA from the lysed blood sample was then bound to the column with 200 μl absolute ethanol. The column-bound DNA was sequentially washed by 500 μl Buffer AW1 and AW2, and eluted with 50 μl water through gravitational force. The quantity (ng/μl) and quality ($Absorbance_{260}/Absorbance_{280}$) of the extracted DNA would be measured by a spectrophotometer (Nanodrop ND-1000; Thermo Scientific, Wilmington, DE) at wavelengths of 260 nm and 280 nm. The extracted DNA samples were diluted to working concentration of 8 ng/μl.

2.1.3 Polymerase chain reaction

All the 22 exons of *CFH* gene (NM_000186.2) and 9 exons of *HTRA1* gene (NM_002775.4) as well as their 1 kilo-base (kb) upstream promoter regions were screened for sequence alterations. Genomic DNA was amplified by polymerase chain reaction (PCR) before sequencing. In brief, the PCR mixture consisted of 1x PCR buffer (Invitrogen, Carlsbad, CA), $MgCl_2$ (Invitrogen), 1 mM dNTP Mix (Roche, Indianapolis, IN), 1 μM sense primer, 1 μM antisense primer, 1 U platinum *Taq* DNA polymerase (Invitrogen) and 50 ng DNA, in a volume of 25 μl. PCR was performed in a thermal cycler (model 9700; Applied Biosystems Inc.) with an initial denaturation at 95℃ for 2 min, 35 cycles of 95℃ denaturation for 1 min, primer annealing for 1 min and 72℃ extension for 1 min, and a

final extension at 72℃ for 5 min. The primer sequences and amplification conditions were listed in **Table 2.2** for *CFH* gene and **Table 2.3** for *HTRA1* gene. The PCR products were resolved by 2% agarose gel electrophoresis (supplemented with ethidium bromide) at 135 V for 20 min, and the signals were visualized by gel documentation (Gel-Doc 2000; BioRad, Hercules, CA). For the haplotype analysis of 34delCinsTCCT with rs11200638 in the *HTRA1* gene, rs11200638 allele-specific primers were used for PCR (**Table 2.4**).

2.1.4 DNA Sequencing

The amplified PCR products (8 μl) were purified by 2 μl of exonuclease I and shrimp alkaline phosphatase (ExoSAP; USB Corporation, Cleveland, OH). The purified PCR products were then taken for dideoxy-sequencing reactions using commercially available reagents (BigDye Terminator Cycle Sequencing Reaction Kit, version 3.1; Applied Biosystems Inc., Foster City, CA). In brief, a total of 5 μl sequencing reaction mixture was consisted of 1 μl of BigDye 3.1 reaction mix, 1 μl of BigDye buffer, 0.5 μl of oligo primer and 2.5 μl purified PCR product. The sequencing reaction mixture underwent an initial denaturation at 96℃ for 2 min, and 30 cycles of sequencing reaction of 96℃ denaturation for 10 sec, 52℃ primer annealing for 5 sec and 60℃ extension for 4 min. The sequence reaction product was cleaned by ammonium acetate precipitation and 70% ethanol washing, before the electrophoresis on a capillary DNA sequencing machine (model 3130XL; Applied Biosystems Inc.). The output sequences were analyzed a DNA sequence analyzer (Chromas, version 2; Technelysium Pty Ltd.).

2.1.5 Statistical analysis

Hardy-Weinberg equilibrium (HWE) for each polymorphism was calculated by χ^2 test. Allelic and genotypic distribution of polymorphisms between patients and control

subjects were compared by χ^2 analysis or the Fisher exact test. The risk analysis was estimated by odds ratios (OR). Conservative Bonferroni correction was applied for multiple testing comparisons. All statistical analyses were performed by commercially available software (SPSS, version 16.0; SPSS Inc., Chicago, IL).

2.2 Characterization of HtrA1 wildtype and variant protein

2.2.1 Cloning of recombinant human *HTRA1* construct

HtrA1 open reading frame (ORF; 1440 base-pair in length) was generated by PCR using TaKaRa LA™ *Taq* DNA polymerase (TaKaRa Bio Inc, Japan) and specific amplification primers (**Table 2.5**) designed for the pcDNA6/*myc*-His© A (Invitrogen) mammalian expression vector (**Figure 2.1**). The reaction mixture consisted of: 1x GC Buffer I, 50 ng cDNA template, 1x dNTP mixture (Roche), 1 μM sense primer, 1 μM antisense primer, 1 U TaKaRa LA™ *Taq* DNA polymerase, and the final volume was made up to 25 μl by distilled water. The reaction mixture was incubated in a thermal cycler as follow: initial denaturation at 94℃ for 1 min, 40 cycles composed of denaturation at 94℃ for 30 sec, annealing at 60℃ for 30 sec and extension at 72℃ for 2 min, and final extension at 72℃ for 5 min. PCR products were resolved in 1% agarose gel electrophoresis at 135 V for 30 min and visualized by UV light (ChemiDoc, BioRad). Specific DNA band was cut from the gel, extracted and purified by Qiaquick gel extraction kit (Qiagen) following the manufacturer's protocol.

Purified PCR product containing HtrA1 ORF and mammalian expression vector pcDNA6/*myc*-His© A (Invitrogen) were digested with restriction enzymes *BamH*I (New England Biolabs, Ipswich, MA) and *Not*I (New England Biolabs). Both digestions were performed at 37℃ for 1 hour. The products were purified by Qiaquick PCR purification kit (Qiagen) following the manufacturer's protocol. The quantity (ng/μl) and quality

(Absorbance$_{260}$/Absorbance$_{280}$) of the HtrA1 ORF insert and vector DNA were monitored by a spectrophotometer (Nanodrop ND-1000).

One μg of purified restriction enzyme-cut vector DNA was dephosphorylated by 1 U rAPid alkaline phosphatase (Rapid DNA Dephos & Ligation kit, Roche) for 10 min at 37℃ to prevent self-ligation. 50 ng of vector DNA was ligated with 150 ng of HtrA1 ORF insert DNA in a reaction mixture of 1x T4 ligation buffer and 5 U T4 ligase (Rapid DNA Dephos & Ligation kit, Roche) at room temperature for 10 min.

One μl of ligation product was mixed with 25 μl *Escherichia coli* competent cells (DH5α^{TM}, Invitrogen) and incubated on ice for 30 min. The DNA-bacterial cell mixture was heat shocked at 42℃ for 45 sec, and immediately transferred to ice for another 2 min. SOC medium (Invitrogen) was added and incubated at 37℃ for 30 min with vigorous shaking at 250 rpm. The bacterial suspension was plated on LB Agar plates (Invitrogen) supplemented with ampicillin (100 μg/ml; Invitrogen) and incubated at 37℃ for overnight.

Twenty-four bacterial clones were separately picked and resuspended in 4 ml LB broth (Invitrogen) supplemented with ampicillin, and incubated at 37℃ for 6-8 hours with shaking. From 1 ml bacterial suspension, DNA was extracted by a modified protocol of Plasmid Midi Kit (Qiagen). Bacteria cells were pelleted at 6000 rpm centrifugation for 10 min at 4℃ (Heraeus Labofuge 400R, Thermo Scientific). Pellet was resuspended in 300 μl of chilled Buffer P1 supplemented with RNase A (100 ug/ml, Plasmid Midi kit, Qiagen) on ice. The mixture was mixed with 300 μl of Buffer P2, and incubated at room temperature for 5 min. Next, the mixture was mixed with 300 μl of pre-chilled Buffer P3, and incubated on ice for 10 min. The supernatant, which was collected after a 13000 rpm centrifugation at 4℃ for 20 min, was mixed with 500 μl isopropanol in a new tube to precipitate plasmid DNA, and centrifuged at 13000 rpm at 4℃ for 30 minutes. The DNA pellet was subsequently washed with 70% alcohol to remove the remaining isopropanol. Finally, the

48

resulted DNA pellet was briefly air-dried for 5 min and then resuspended in 20 µl distilled water.

The sequences of all plasmid DNA were verified by direct sequencing using BigDye Terminator Cycle Sequencing Reaction Kit (version 3.1; Applied Biosystems Inc.) on a capillary DNA sequencer (model 3130XL; Applied Biosystems Inc.) as described (**section2.1.4**).

Bacterial clone containing the construct with correct sequence and orientation were expanded in 100 ml of LB broth (Invitrogen) supplemented with ampicillin and incubated at 37°C for 12 – 16 hours with shaking. Bacterial pellet was collected by a 6000 g centrifugation at 4°C for 15 min. Pellet was resuspended in 4 ml of chilled Buffer P1 supplemented with RNase A and incubated on ice. The suspension was then mixed gently with 4 ml of Buffer P2 for alkali lysis at room temperature for 5 min, followed by a gentle mixing with 4 ml of pre-chilled Buffer P3 for neutralization. The mixture was subsequently poured into the barrel of QIAfilter Cartridge (Qiagen) and incubated at room temperature for 10 min. Pressure was applied to filter out the precipitated protein and chromosomal DNA from the plasmid DNA solution. The plasmid DNA was bound in a pre-equilibrated QIAGEN-tip and washed twice with 10 ml of Buffer QC. Plasmid DNA was eluted by 5 ml of Buffer QF, precipitated and pelleted by 3.5 ml of isopropanol with a 13000 rpm centrifugation at 4°C for 30 min. After washing with 70% ethanol to remove the remaining isopropanol, the DNA pellet was briefly air-dried and then resuspended in 200 µl of distilled water. The quantity (ng/µl) and quality (Absorbance$_{260}$/ Absorbance$_{280}$) of the plasmid DNA solution was measured by a spectrophotometer (Nanodrop ND-1000; Thermo Scientific) at wavelengths of 260 nm and 280 nm. The plasmid DNA was stored at −20°C until use.

49

2.2.2 Site-directed mutagenesis

An expression construct (pHis/myc-HtrA1-12insSer) for HtrA1 variant (34delCinsTCCT) was synthesized by site-directed mutagenesis using a commercially available mutagenesis kit (QuikChange Lightning Multi Site-Directed Mutagenesis Kit; Strategene, La Jolla, CA) based on the original HtrA1 construct (pHis/myc-HtrA1; **section 2.2.1**). In brief, a reaction mixture (25 ul in volume) was consisted of 2.5 μl of 10x QuikChange Lightning Multi reaction buffer, 0.75 μl of QuikSolution, 100 ng of pHis/myc-HtrA1 template, 100 ng of mutagenic sense primer, 100 ng of mutagenic antisense primer, 1 μl of dNTP mix (Roche) and 1 μl of QuikChange Lightning Multi enzyme blend, and distilled water. The reaction mixture was incubated in a thermal cycler as follow: initial denaturation at 95℃ for 2 min, 30 cycles of denaturation at 95℃ for 20 sec, annealing at 55℃ for 30 sec and extension at 65℃ for 8 min, and final extension 65 ℃ for 5 min. The mixture was then incubated with 1 μl of *Dpn* I restriction enzyme at 37 ℃ for 5 min. 1 μl of the mixture was transformed into 25 μl *Escherichia coli* competent cells (XLBlue^TM , Invitrogen) and incubated at 37℃ for overnight as described (**section 2.2.1**). The procedures of clonal selection, sequencing confirmation and clonal expansion were the same as described (**section 2.2.1**). The detail of the mutagenic primers was listed in **Table 2.6**.

2.2.3 Retinal pigment epithelial cell culture

Human retinal pigment epithelial cell line, ARPE-19 (CRL-2302, American Type Culture Collection) was maintained in Dulbecco's modified Eagle's medium and F-12 nutrient mixture (Gibco BRL, Rockville, MD) supplemented with 10% heat-inactivated

fetal bovine serum (Gibco BRL) and 1x penicillin/streptomycin (Gibco BRL) at 37℃ in a

humidified incubator containing 5% CO_2 balanced with air.

2.2.4 Transfection

ARPE-19 cells were seeded at a density of 2 x 10^5 cells/ml in a culture dish (60

mm in diameter; Corning Life Sciences, Lowell, MA). Cell transfection was performed on

the second day. In brief, 4 μg of HtrA1 expression constructs was mixed with 10 μl

transfection reagent (Lipofectamine-2000; Invitrogen) in 500 μl Opti-MEM I Reduced

Serum medium (Gibco BRL) and incubated at room temperature for 20 min. The cells were

washed with phosphate buffer saline (PBS; Gibco BRL) for 3 times and 0.5 ml Opti-MEM

I Reduced Serum medium was then added to the dish. The DNA-lipofectamine conjugate

was added to cells and incubated for 6 hours. 1 – 2 ml of culture medium (with or without

serum) was finally applied to the dish and the HtrA1-transfected cells were further

incubated for 12 – 48 hours before protein or medium collection for subsequent analysis.

The cells transfected with empty vector (pcDNA6/*myc*-His© A; Invitrogen) were used as

control.

2.2.5 Protein collection

The transfected cells at each time point were lysed by radioimmunoprecipitation

(RIPA) lysis buffer supplemented with 1 mM phenylmethylsulfonylfluoride (PMSF)

(Sigma-Aldrich, St. Louis, MO) and protease inhibitor cocktail tablet (Roche), and the

whole cell lysate was collected and incubated on ice for 20 min. The lysate was then

centrifuged at 13000 rpm at 4℃ for 20 min. Supernatant containing the soluble protein was

collected with the addition of sodium dodecyl sulphate (SDS) sample buffer to a final

concentration of 50 mM Tris base (pH 6.8), 2% SDS, 50 mM DTT and 10% glycerol. The

mixture was denatured at 95℃ for 5 min, cooled on ice for 2 min, and stored at -20℃ before immunoblotting analysis.

2.2.6 Immunoprecipitation

Serum-free medium for the post-incubation of HtrA1-transfected or empty vector-transfected ARPE-19 cells was collected at different time-point after transfection (0, 6, 12 and 18 hours). The collected medium was centrifuged at 1300 rpm for 5 min at 4℃ to remove the cell debris before harvesting the secreted-HtrA1 by immunoprecipitation (IP). In brief, the cell-free medium (1.5 ml) was incubated with 5 μg of mouse monoclonal antibody against polyhistidine tag (clone 4D11, 05-53; Upstate Biotechnoloy Inc., Lake Placid, NY) in 40 μl of buffer mixture (1% BSA (bovine serum albumin; Sigma-Aldrich), protease inhibitor cocktail tablet (Roche), 1mM PMSF (Sigma-Aldrich) and 0.1 mM AEBSF (4-(2-aminoethyl)benzenesulfonyl fluoride hydrochloride; Sigma-Aldrich)) at 4℃ for overnight. 10 μl of Protein A beads (Invitrogen) was suspended in 1x PBS and washed at 4℃ for 1 hour. After removing the washing PBS by centrifugation at full speed for 5 min at 4℃, the washed beads were then incubated with 1% BSA (Sigma-Aldrich) in PBS at 4℃ for 1 hour. After twice PBS wash, the beads were incubated with the antibody-treated medium at 4℃ for overnight. After PBS washes, the bound-HtrA1 was dissociated from the beads by 40 μl of 2x SDS loading buffer supplemented with 3% β-mercaptoethanol, denatured at 95℃ for 5 min and analyzed by immunoblotting.

2.2.7 Proteolytic activity analysis

Serum-free medium for the post-incubation of HtrA1-transfected or empty vector-transfected ARPE-19 cells was collected at 48 hours after transfection. The collected

52

medium was centrifuged at 1300 rpm for 5 min at 4℃ to remove the cell debris. The recombinant human HtrA1 protein in the cell-free condition medium was purified and concentrated by a commercially available centrifugal filter (Amicon Ultra-0.5, Ultracel-10 Membrane, 10 kDa; Millipore, Billerica, MA). Total protein of the concentrated condition medium was measured by Protein assay (BioRad). Equal amount of total protein (10 μg) in the condition medium from ARPE-19 cells transfected with transfected with pHis/myc-HtrA1, pHis/myc-HtrA1-12insSer and pcDNA6/*myc*-His© A was applied. The proteolytic activity analysis was performed by incubating 10 μg of protein in the condition medium with 5 μg of β-casein (Sigma Aldrich) in a buffer of 50 mM Tris/HCl (pH 7.5; Sigma Aldrich) and 150mM NaCl (Sigma Aldrich) at 37℃, added up to a volume of 30 μl by distilled water. At different time-points (0, 10, 20, 30, 40 and 50 min), 7.5 μl of SDS buffer will be added to the reaction mixture, which would then be denatured at 95 for 5 min to terminate the reaction. The denatured protein samples were resolved by 15% SDS-PAGE and visualized by Coomassie Blue staining. In brief, the resolved gel was fixed in a solution containing 10% acetic acid and 50% ethanol at room temperature for overnight. The fixed gel would then be stained with 0.025% Coomassie dye (Sigma Aldrich) in 10% acetic acid at room temperature for 15 min. The stained gel was destained in a solution of 5% acetic acid and 50% methanol at room temperature for several times until the blue bands were clearly visualized. The protein band pattern of the stained gel was captured and recorded by Quantity One® Image Analysis software (BioRad). The sample containing only β-casein and buffer was used as a negative control.

2.2.8 Immunoblotting

PROTEAN III SDS-polyacrylamide gel electrophoresis system (BioRad) was first applied to resolve the denatured protein. In brief, a resolving gel was made up of

12.5% acrylamide: 0.3% bis-acrylamide, 0.375 M Tris.HCl (pH 8.8), 0.1% SDS, 0.05% ammonium persulfate and 0.02% TEMED, and the gel mixture was set for polymerization at room temperature for 30 min. A stacking gel with a final concentration of 4% acrylamide: 0.15% bis-acrylamide, 0.125 M Tris.HCl (pH 6.8), 0.1% SDS, 0.05% ammonium persulfate and 0.02% TEMED was allowed to polymerize on top of the resolving gel for another 30 min. 50 µg of denatured total protein was applied to each sample well and mobilized through the gel encompassed in a Tris/glycine/SDS running buffer at 70 V for 30 min and then 150 V for 65 min.

After electrophoresis, the gel was equilibrated in chilled transfer buffer, which was consisted of 25 mM Tris, 192 mM glycine and 10% methanol, for 5 min before the electro-transfer of the mass-separated protein to a pre-wet nitrocellulose membrane (Amersham Pharmacia, Cleveland, OH) at a constant voltage of 100 V for 1 hour on ice.

The membrane containing immobilized protein was rinsed with distilled water to remove the residual methanol. After blocking with 5% non-fat milk powder (Santa Cruz Biotechnology) in TBST buffer (Tris buffered saline with 0.05% Tween-20; Sigma-Aldrich) at room temperature for 1 hour, the membrane was probed with primary mouse-monoclonal antibody against HtrA1 (a generous gift from Prof. Zhenglin Yang, Center for Human Molecular Biology and Genetics, Sichuan Academy of Medical Sciences and Sichuan Provincial People's Hospital) at 4℃ for 6 hour to overnight and secondary antibody conjugated with horse-radish peroxidase (HRP) against mouse (Jackson Immuno. Res, West Grove, PA) at room temperature for 1 hour at the specified concentration in TBST. The membrane was washed with TBST after incubation. The signals were detected by enhanced chemiluminescence (ECL) system (Amersham Pharmacia) and captured by ChemiDoc (BioRad). β-actin, detected by HRP conjugated mouse monoclonal antibody against β-actin (clone AC15, A3854; Sigma-Aldrich), was selected as housekeeping protein.

2.2.9 Immunocytochemistry

Transfected cells were fixed in freshly prepared 3% paraformaldehyde buffer (pH = 7; Sigma-Aldrich) at 37°C for 10 min, and then in pre-warmed neutral buffered 0.5% paraformaldehyde for another 30 min at ambient temperature. After washing with PBS, free aldehyde was quenched by freshly prepared 50 mM ammonium chloride (Sigma-Aldrich) in PBS on ice for 10 min. After washing, the cells were permeabilized and blocked in 0.1% BSA (Sigma-Aldrich) with 0.15% saponin (Sigma-Aldrich) for 15 min. Diluted primary antibody was applied and incubated for 2 hours at room temperature, followed by 5 times of PBS rinses. Secondary IgG antibody conjugated with a fluorescence probe (Invitrogen) was applied together with nuclear staining 4',6-diamidino-2-phenylindole (DAPI; Sigma-Aldrich), and incubated for 1 hour. If double-immunofluorescence was performed, the probing of primary and secondary antibodies was repeated for another protein epitope. The samples were washed and mounted with Fluoromount (Southern Biotech). The fluorescence signal was examined under a fluorescence microscope (DMRB; Leica, Wetzlar, Germany). The primary and secondary antibodies used in immunocytochemistry were listed in **Table 2.7**.

2.2.10 Quantitative analysis of ER-located HtrA1 protein

The number of transfected cells, in which the immunofluorescent signal of HtrA1 was partially overlapped with that of Golgi marker (giantin) or ER marker (Bip), was counted. The ER retention rate was calculated as the percentage of transfected cells with a partially overlapped signal of HtrA1 and giantin or Bip.

2.2.11 Apoptosis analysis

The number of transfected cells with normal and fragmented nuclei (representing end-staged apoptosis) was counted, respectively. The apoptosis rate was calculated as the percentage of transfected cells with fragmented nuclei.

2.2.12 Cell viability assay

ARPE-19 cells (2×10^5 cells/ml) were seeded on 24-well plates (Corning Life Sciences) one day before transfection, and the seeded cells were transfected with empty vectors or HtrA1 expression constructs (**section 2.2.4**). At 24 hours after transfection, 5 mg/ml MTT (3-(4, 5-dimethylthiazol-2-yl)-2,5-diphenyltetrazolium bromide) (Invitrogen) was applied to each well and incubated for 4 hours. The cells were washed with PBS and the purple crystals were resolved by 300 μl isopropanol. The absorbance at wavelength 570 nm with reference 650 nm was measured by a plate reader (Powerwave XS, Bio-Tek Instruments). The percentage of cell viability was calculated as: OD_{570} sample / OD_{570} control x 100%. The cells transfected with empty vector (pcDNA6/*myc*-His© A; Invitrogen) were used as control.

2.2.13 Bioinformatics analysis

The characteristics of the signal peptides of wildtype HtrA1 and HtrA1 variant were analyzed by open-accessible programs (SOSUIsignal (Gomi M et al, 2004); http://bp.nuap.nagoya-u.ac.jp/sosui/sosuisignal/) and (Phobius (Kall L et al, 2004); http://phobius.binf.ku.dk/index.html).

2.3 Association between HtrA1 and VEGF in human vitreous humors

2.3.1 Study subjects

Fifty-five unrelated Han Chinese patients underwent ocular surgery were recruited at the Prince of Wales Hospital in Hong Kong and the Joint Shantou International Eye Center of Shantou University and The Chinese University of Hong Kong (JSIEC). They were given complete ophthalmoscopic examinations. A standard three-port pars plana vitrectomy was performed in all subjects as a part of the regular surgical procedures. The clinical diagnosis, gender and age of 55 patients are summarized in **Table 2.8**. None of the subjects received treatment with anti-VEGF agents. The study protocol was approved by the Ethics Committee for Human Research at the Chinese University of Hong Kong and JSIEC, and was in accordance with the tenets of the Declaration of Helsinki. Informed consent was obtained from the study subjects after explanation of the nature and possible consequences of the study.

2.3.2 Sample collection

Undiluted vitreous humor samples (0.5 – 1 ml) from all study subjects were collected into sterile tubes at the time of surgery and aliquots were rapidly frozen at -80°C until assay. Venous blood samples (3 ml) from 51 subjects were collected simultaneously and stored at -80°C prior to DNA extraction.

2.3.3 Immunoblotting

The amounts of total protein in the vitreous humor samples were measured by Protein assay (BioRad). Equal amount (10 µg total protein) of the denatured (95°C for 5 min) vitreous humor samples were resolved on 4% SDS-polyacrylamide stacking gel at 70 volts (V) for 30 min and 12.5% SDS-polyacrylamide resolving gel at 150 V for 65 min. The

resolved protein was then electro-transferred to nitrocellulose membrane at 100 V for 75 min. The membrane was sequentially probed with the mouse monoclonal antibodies against (1) VEGF (Santa Cruz Biotechnology, Santa Cruz, CA) for 6 hours, (2) HtrA1 (a generous gift from Prof. Zhenglin Yang, Center for Human Molecular Biology and Genetics, Sichuan Academy of Medical Sciences and Sichuan Provincial People's Hospital) for overnight and (3) PEDF (Millipore) for 6 hours in the same blot, and subsequently with secondary antibody against mouse IgG conjugated with horseradish peroxidase (Jackson Immuno. Res., West Grove, PA) for 1 hour after each primary antibodies. The details of the antibodies used were listed in **Table 2.9**. The signals were detected by the enhanced chemiluminescence (ECL) system (Amersham Pharmacia, Cleveland, OH) and the band intensities were quantified by Quantity One® Image Analysis software (BioRad). Triplicates were performed. Detail protocol was described as before (**section 2.2.7**).

2.3.4 *HTRA1* genotyping

Genomic DNA was extracted from whole blood as described (**section 2.1.2**). The genotype of the SNP (rs11200638) in the promoter region of *HTRA1* gene was determined by PCR and direct sequencing as described (**section 2.1.3 and 2.1.4**).

2.3.5 Statistical analysis

The χ^2 test was used to calculate the statistical significance among categorical parameters. Pearson's correlation coefficient test was used to measure the linear association among the vitreous protein and with age while Spearman rank correlation test were used to measure the association in rank orders. Mann-Whitney U test and Kruskal-Wallis test were used to compare the vitreous levels with gender and grouped age, respectively. One-way Analysis of Variance (ANOVA) and the post-hoc Tukey HSD tests were used to compare

the vitreous levels with clinical diagnosis. With reference to analytical methods in previous publications (Baldi A et al, 2002; De Luca A et al, 2003; Chien J et al, 2004), the measured band intensities were categorized into 3 groups for association analysis according to the distribution, which weak (+) expression was defined as the vitreous humor sample distributed lower than 25 quartile, moderate (++) as 25 – 75 quartile and strong (+++) as higher than 75 quartile. For the analysis of the age effect, the parameter of age was grouped into 3 categories (< 40, 40 – 60 and > 60 years). All the analyses were performed on commercially available software (SPSS, version 16.0; SPSS Inc.). Significance was defined as $p < 0.05$

2.4 Association between HtrA1 and VEGF in human fetal retinal pigment epithelial cell culture

2.4.1 Human fetal retinal pigment epithelial cell culture

Previously established primary human fetal RPE cells (Choy KW et al, 2006) were cultured in Dulbecco's modified Eagle's medium and F-12 nutrient mixture (Gibco BRL) supplemented with 10% heat-inactivated fetal bovine serum (Gibco BRL) and 1x penicillin/streptomycin (Gibco BRL) at 37°C in a humidified incubator containing 5% CO_2. The human fetal RPE cells were characterized by gene expression analysis using a whole human genome oligo microarray (4x44K; Agilent Technologies, Santa Clara, CA). The gene expression was analyzed by an attached program (Genespring, version 11.0.2; Agilent Technologies). Expression of the reported RPE specific markers, such as *RPE65*, Bestrophin (*BEST1-4*) and *MERTK*, were found in these cells, suggesting that these culture cells belonged to the RPE cells. Passage 5 – 10 of human fetal RPE cells was used throughout the experiments in this study.

2.4.2 Transfection of HtrA1-construct

Human fetal RPE cells were seeded at a density of 2×10^5 cells/ml in a culture dish (60 mm in diameter; Corning Life Sciences). Cell transfection was performed on the second day. In brief, 4 µg of HtrA1 expression construct (pHis/myc-HtrA1; **section2.2.1**) was mixed with 10 µl transfection reagent (Lipofectamine-2000; Invitrogen) in 500 µl Opti-MEM I Reduced Serum medium (Gibco BRL) and incubated at room temperature for 20 min. The cells were washed with *phosphate buffer saline (PBS; Gibco BRL) for 3 times* and 0.5 ml Opti-MEM I Reduced Serum medium was then added to the dish. The DNA-lipofectamine conjugate was added to cells and incubated for 6 hours. 2 ml culture medium was finally applied to the dish and the HtrA1-transfected cells were further incubated for 24 hours before RNA collection for analysis. The cells transfected with empty vector (pcDNA6/*myc*-His© A; Invitrogen) were used as control. Triple experiments were performed.

2.4.3 Treatment of angiogenic factors

Human fetal RPE cells were seeded in a culture dish (60 mm in diameter) with FBS-containing medium 2 days before the treatment. Cell treatment was performed when the cells reached 95-100% confluence (Abcouwer SF et al, 2002). In brief, the cells were washed with PBS for 3 times, and treated with exogenous recombinant human VEGF (10ng/ml; Gibco BRL), recombinant human basic fibroblast growth factor (bFGF, 10 ng/ml; Invitrogen) or recombinant human tumor necrosis factor-alpha (TNFα, 10 ng/ml; Gibco BRL) in serum-free medium (Nagineni CN et al, 2003). The untreated cells were used as control. The cells were then incubated for 6 or 24 hours before RNA collection for analysis. Triple experiments were performed.

2.4.4 Cellular stress treatments

Human fetal RPE cells were seeded in a culture dish (60 mm in diameter) with FBS-containing medium 2 days before the treatment. Cell treatment was performed when the cells reached 95-100% confluence (Abcouwer SF et al, 2002). In brief, the cells were washed with PBS for 3 times, and treated with tunicamycin (0.5, 5 and 10 μg/ml; Sigma-Aldrich), dithiothreitol (DTT; 0.1, 1 and 2 mM; Sigma-Aldrich) or Z-Leu-Leu-Leu-H (MG132; 10μM; Sigma-Aldrich) in serum-free medium. The cells treated with 0.1% dimethyl sulfoxide (DMSO; Sigma-Aldrich) were used as control. The cells were then incubated for 18 hours before RNA collection for analysis. To evaluate the cellular stress treatments on cell viability of human fetal RPE cells, MTT assay was performed (**section 2.2.12**). Triple experiments were performed.

2.4.5 RNA collection and extraction

At each time point, total RNA from treated human fetal RPE cells was collected by 600 μl Buffer RLT (RNeasy extraction kit; Qiagen) freshly supplemented with 1:100 β–mercaptoethanol (Amresco, Solon, OH). Total RNA was extracted using a commercially available extraction kit (RNeasy extraction kit; Qiagen) following manufacture's protocol. In brief, Buffer RLT-extracted lysate was homogenized through a column with a full-speed centrifugation for 2 min. Total RNA from the homogenized lysate would then bind to the column with 600 μl 70% ethanol. The column-bound RNA would be washed twice by 500 μl Buffer RW1 and RPE sequentially, and eluted with 40 μl RNase-free water containing DEPC. The quantity (ng/μl) and quality ($Absorbance_{260}/Absorbance_{280}$) of the extracted RNA was measured by a spectrophotometer (Nanodrop ND-1000; Thermo Scientific) at wavelengths of 260 nm and 280 nm.

2.4.6 Reverse transcription

Total RNA extracted was used to synthesize the complementary DNA (cDNA) by SuperScript III cDNA synthesis kit (Invitrogen) following the manufacturer's protocol. The reverse transcription reaction mixture was consisted of 1 µg of total RNA, 1 µl of dNTP mixture (10 mM; Roche), 1 µl random hexamer (250 ng/µl; Qiagen), and was made up to a volume of 13 µl by RNase-free water. The mixture was heated to 65°C for 5 minutes and was incubated on ice for at least 1 minute. 4 µl 5X First-Strand Buffer (Invitrogen), 1 µl DL-DTT (0.1 M), 1 µl RNaseOUT™ Recombinant RNase Inhibitor and 1 µl SuperScript™ III reverse transcriptase were then added to the mixture. The mixture was incubated in conditions as followed: 25°C for 5 minutes, 50°C for 60 minutes, 70°C for 15 minutes, and finally 4°C. The synthesized cDNA was stored at -20°C until assay.

2.4.7 Gene expression analysis

The gene expressions of *HTRA1*, *VEGFA*, *PEDF*, superoxide dismutase (*SOD*; stress marker), interleukin-6 (*IL6*; inflammation marker) and housekeeping beta-actin (*β–ACTIN*) mRNA were analyzed using semi-quantitative PCR. The reaction mixture ingredients and the reaction procedures were same as described (**section 2.1.3**). The primer sequences, magnesium concentration and numbers of reaction cycles for each gene were listed in **Table 2.10**. The numbers of reaction cycles were optimized for each gene, which the band intensities was fallen in the exponential phase, but not in the stationery phase (**Figure 2.2**). The PCR products were resolved by 2% agarose gel at 135 V for 20 min. The signals were visualized by gel documentation (Gel-Doc 2000; BioRad) and the band intensities were semi-quantified by Quantity One® Image Analysis software (BioRad). The expressions of *HTRA1*, *VEGFA* and *PEDF* gene were normalized by the housekeeping *β–ACTIN* gene. Relative intensities, comparing the normalized band intensities of treated

cells with that of controls, were calculated and presented, which the normalized band intensity of control was set as 1. 2-fold or greater changes in the relative intensities were considered as significant change in gene expression level.

	Exudative AMD patients	Control subjects	p	OR (95% C.I.)
Total, n	163	183		
Male, n (%)	88 (54.0%)	91 (49.7%)	0.429	
Female, n (%)	75 (46.0%)	92 (50.3%)		
Smoker, n (%)	79 (51.6%)	54 (37.8%)	0.017	1.76
Non-smoker, n (%)	74 (48.4%)	89 (62.2%)		(1.11-2.80)
Age (mean ± SD)	75.5 ± 7.5 years	73.3 ± 6.5 years	0.005	

OR: odds ratio; C.I.: confident interval

Table 2.1: The characteristics of the study population of *CFH* and *HTRA1* sequencing.

Region		Primer Sequence (5' > 3')	Product size (bp)	Annealing Temp (°C)	MgCl$_2$ (mM)
Promoter	F	AGAATCGTGGTCTCTGTGTGTGG	547	57	1.5
	R	AGCAGCTGGTGATATCCTCTGG			
Promoter	F	TCAAATGAGAGTGAGCCAGTTGC	577	57	1 5
	R	CTGTTCACAACGTCCAGTTCTCC			
Exon 1	F	GTGGGAGTGCAGTGAGAATTGG	431	57	1.5
	R	AACTCAACAATGTCAAAAGCC			
Exon 2	F	GATAGACCTGTGACTGTCTAGGC	392	57	1.5
	R	GGCAATAGTGATATAATTCAGGC			
Exon 3	F	ACCTCAGCCTCCCAAAGTGC	632	Touch down 66-58	2.0
	R	TGCATACTGTTTTCCCACTCTCC			
Exon 4	F	AAGGAGGAGGAGAAGGAGGAAGG	445	57	1.0
	R	CAGGCTGCATTCGTTTTTGG			
Exon 5	F	CCACTCCCATAGAAAAGAATCAGG	647	58	2.5
	R	ACTTCTTTGCACCAGTCTCTTCC			
Exon 6	F	GATAAATCATTTATTAAGCGG	483	57	1.5
	R	GAACCTTGAACACAGAAAATGC			
Exon 7	F	GGATGACTTTGGAGAAGAAGG	572	57	1.5
	R	TATGAGTTTCGGCAACTTCG			
Exon 8	F	TCATCTTCATTAACAAAGACC	539	57	2.5
	R	AGATCTATTTTGGTCACTTTGC			
Exon 9	F	CTTTGTTAGTAACTTTAGTTCG	488	57	2.0
	R	TTATACACAGTTGAAAAACC			
Exon 10	F	GGCAACTCTGAGCTTATTTTCC	556	57	2.0
	R	AGAGTAGGAAAAGCCTGAATGG			
Exon 11	F	CATAGATTATTTTTGTACGG	468	57	2.5
	R	CAAAACTCCCTTCTTTTCCC			
Exon 12	F	ATCTGATGCCCCTCTGTATGACC	443	57	2.5
	R	ATTCAGTACTCAATACATGTCC			
Exon 13-14	F	CACCATTCTTGATTGTTTAGG	772	57	2.5
	R	ATTGAATTATAAGCAATATGC			
Exon 15	F	CATTTCAGCGACAGAATACAGG	555	57	1.5
	R	TCACAGGGCACAGTTAATATTAGG			
Exon 16	F	AACTGTTACACAGCTGAAAAG	536	Touch down 57-49	2.5
	R	GTGGTGATTGATTAATGTGC			
Exon 17	F	GGTGGAGGAATATATCTTTGC	509	57	2.5
	R	ATAGAATAGATTCAATCATGC			
Exon 18	F	CGATAGACAGACAGACACCAGAAGG	494	57	2.0
	R	CAGCTATAATTTCCCACAGCAGTCC			
Exon 19	F	GTGTAATCTCAATTGCTACGGCTACC	649	57	1.5
	R	CAAGTAGCTGGGACTTCAGATGC			
Exon 20	F	TAGTTTCATGTCTTTTCCTC	486	57	2.0
	R	GAATTTTAAGCACCATCAGTC			
Exon 21	F	CCAGGACTCATTTCTTTCACC	457	57	2.0
	R	CTTTCTGACAGAAATATTTGG			
Exon 22	F	TGATGTTTCTACATAGTTGGTTTGG	586	57	2.5
	R	AATTGCGTCTAATTTCTTGCC			

Table 2.2: The primer sequences and amplification conditions for *CFH* sequencing.

Region		Primer Sequence (5' > 3')	Product size (bp)	Annealing Temp (°C)	MgCl₂ (mM)	+DMSO
Promoter	F	CGGATGCACCAAAGATTCTCC	568	Touch down 62-55	2.5	Yes
	R	TTCGGGTCCTTCAAACTAATGG				
Exon 1	F	GTCCCCAAGGCGGCTCGT	819	Touch down 62-55	1.0	Yes
	R	CGCGAAGCTCGGTTCCGAGG				
Exon 2	F	ACGTTTTGTGGTGAACCTGAGC	688	Touch down 62-55	1.0	No
	R	GCAACAGCCACACACCTAGC				
Exon 3	F	GCCCGATATATAAAGGAGCGATGG	522	Touch down 62-55	1.0	No
	R	AGAAGTTTTCCTGAGCCCCTTCC				
Exon 4	F	GGGATGTTAGTTGTGAGCTCAGTTCC	485	Touch down 62-55	1.0	No
	R	GCACTAGCCTCCACATGGCTGG				
Exon 5	F	CTGGGCTTCAGAGAGAAAATCTCC	451	Touch down 62-55	1.0	No
	R	ATCCGTAGGGTCATTTGCAAGC				
Exon 6	F	AGTGCCGACCTGGAGTATGTGC	520	Touch down 62-55	1.0	No
	R	GGTGAAATGTCTGTGACCTTCTGC				
Exon 7	F	GTACCCTTCTGTGGCCCTTCC	343	Touch down 62-55	1.0	No
	R	AAGGGGCCAAGGCTAATGACC				
Exon 8	F	CAGTGAACTGAGATCGTACCACTGC	601	Touch down 66-58	3.0	Yes
	R	AGACAGAAGGCACCCTCCTATGG				
Exon 9	F	CGTGCCTGACCCACTGATGG	586	Touch down 62-55	1.0	No
	R	CCCAAGCTGGCAAGAAAAAGC				

Table 2.3: The primer sequences and amplification conditions for *HTRA1* sequencing.

Region	Primer Sequence (5' > 3')	Product size (bp)	Annealing Temp (°C)	MgCl$_2$ (mM)	+DMSO
Promoter - Exon 1	FG GACGCTGCCTTCGTCCG		Touch down 64-60	1.0	Yes
	FA GGACGCTGCCTTCGTCCA	895	Touch down 64-58 for 20 cycles; 58 for 40 cycles	1.0	Yes
	R TCGCAGCGGTCTGGGCA				

FG: G allele-specific primer
FA: A allele-specific primer

Table 2.4: The sequences of allele-specific primers and amplification conditions for *HTRA1* haplotype analysis.

Expression Vector		Primer sequence (5' > 3')	Product Size (bp)	Restriction site
pcDNA6/myc-His© A	F	TAATGGATCCCCATGCAGATCCCGCGC	1440	*BamH* I
	R	TAATGCGGCCGCGGGGTCAATTTCTTCGGG		*Not* I

Table 2.5: Primers for the amplification of full length *HTRA1* ORF.

HtrA1 variant		Primer sequence (5' > 3')
34delCinsTCCT	Sense	GCGCCGGCTCTTCCCGCTGTCCTTGCTGCTGCTGGCGGCG
	Anti-sense	CGCCGCCAGCAGCAGCAAGGACAGCGGGAAGAGCGGCGGC

Table 2.6: Primers for the site-directed mutagenesis of *HTRA1* variant.

Antibody	Source	Working concentrations
Mouse monoclonal anti-HtrA1 antibody	gift from Prof. Z Yang	1:2000 from stock
Rabbit polyclonal anti-BiP antibody	BD Biosciences 610978	2 ug/ml
Rabbit polyclonal anti-giantin antibody	Covance PRB-114C-200	2 ug/ml
Rabbit polyclonal anti-Sec23 antibody (clone H300)	Santa Cruz sc-20789	2 ug/ml
Rabbit polyclonal anti-TGN38 antibody (clone H300)	Santa Cruz sc-33783	2 ug/ml
Rabbit polyclonal anti-cytochrome C antibody (clone H104)	Santa Cruz sc-7159	2 ug/ml
Rabbit polyclonal anti-beta tubulin antibody (clone H235)	Santa Cruz sc-9104	2 ug/ml
Alexa Fluor^k 488-goat anti-rabbit IgG conjugate	Invitrogen A11008	1:1000 from stock
Rhodamine Red^{TM}-X-goat anti-mouse IgG conjugate	Invitrogen R6394	2 ug/ml

Table 2.7: Antibodies used for immunocytochemistry.

Study Subjects, n	55
Gender	
Male, n (%)	33 (60.0%)
Female, n (%)	22 (40.0%)
Clinical Diagnosis	
Vascular Disease, n (%)	12 (21.8%)
Retinal Detachment, n (%)	25 (45.5%)
Macular Hole, n (%)	8 (14.5%)
Traumatic, n (%)	7 (12.7%)
IOL, n (%)	2 (3.6%)
ERM, n (%)	1 (1.8%)
Age (mean ± SD)	50.8 ± 17 years

Vascular Diseases included vitreous hemorrhage, diabetic retinopathy and central retinal vein occlusion.

Retinal detachment included rhegmatogenous retinal detachment and recurrent retinal detachment.

Macular hole represented idiopathic macular hole.

IOL represented intra-ocular lens re-operation.

ERM represented epi-retinal membrane.

Table 2.8: A summary of the clinical diagnosis, gender and age of all 55 patients underwent ocular surgery.

Antibody	Source	Working concentrations
Mouse monoclonal anti-HtrA1 antibody	gift from Prof. Z Yang	1:2000 from stock
Mouse monoclonal anti-VEGF antibody (clone C1)	Santa Cruz sc-7269	1:500 from stock
Mouse monoclonal anti-PEDF antibody	Millipore MAB1059	1:1000 from stock
Goat anti-mouse IgG-HRP conjugate	Jackson ImmunoRes. Lab. 115-035-174	1:20000 from stock

Table 2.9: Antibodies used for immunoblotting analysis of vitreous humor.

Gene Symbol		Primer Sequence (5' > 3')	Tm (°C)	Cycles
HTRA1	F	CAAAGCCAAAGAGCTGAAGG	60	28
	R	ACCATGTTCAGGGTGCTTTC		
VEGFA	F	GAGCCTTGCCTTGCTGCTCTA	60	28
	R	CACCAGGGTCTCGATTGGAT		
PEDF	F	CAGTGTGCAGGCTTAGAGGGACTA	60	31
	R	AGGGTTCTGGCAGCTGCTGT		
SOD	F	AGGGCATCATCAATTTCGAGC	60	25
	R	CAAGGGAATGTTTATTGGGCG		
IL6	F	CTGGTCTTTTGGAGTTTGAGGTATACC	60	33
	R	CCATGCTACATTTGCCGAAGA		
β-ACTIN	F	CAACGGCTCCGGATGTGC	60	21
	R	CTCTTGCTCTGGGCCTCG		

Table 2.10: The primers and amplification conditions for gene expression analysis.
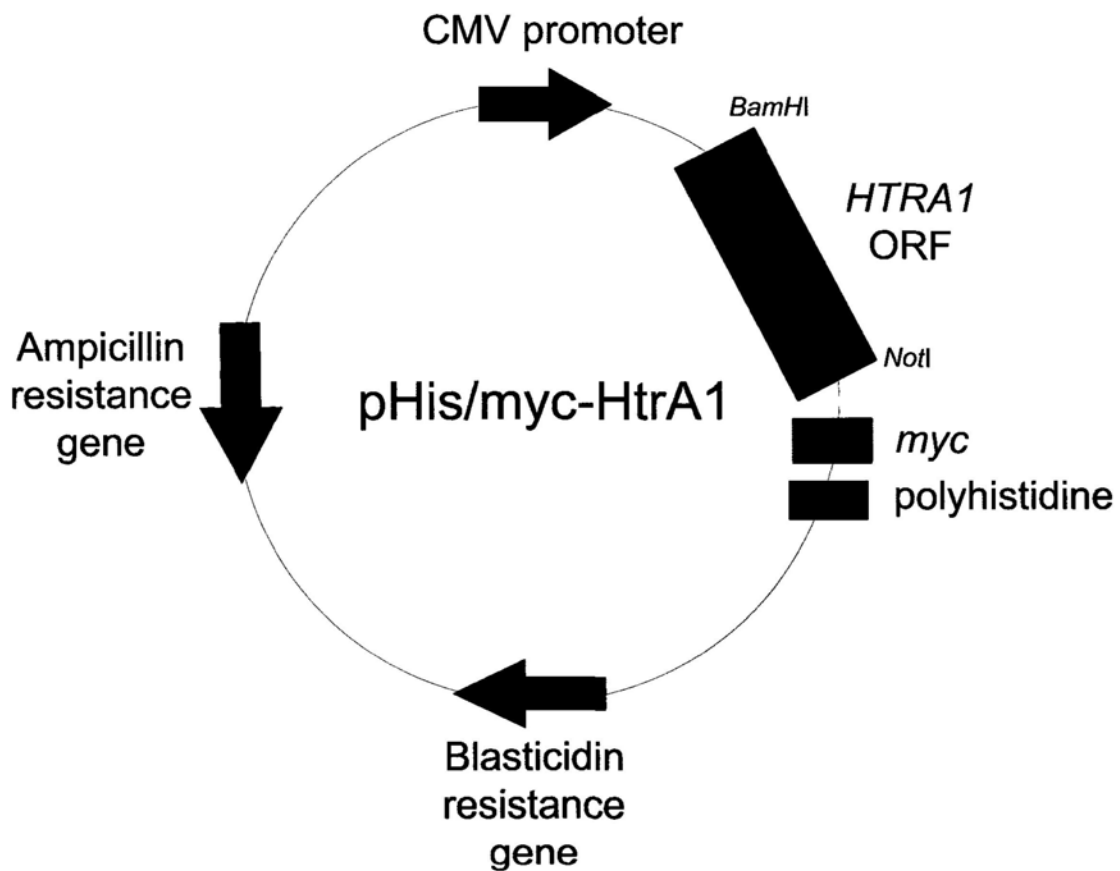
Figure 2.1: Vector map of pHis/myc-HtrA1.

HTRA1 open reading frame was cloned into an empty pcDNA6/*myc*-His© A (Invitrogen) mammalian expression vector through the *BamH*I and *Not*I restriction sites. The transcription of *HTRA1* gene is driven by a constitutively active pCMV promoter. The pcDNA6/*myc*-His© A expression vector is also composed of an ampicillin resistance gene for bacteria selection and blasticidin resistance gene for cell culture selection.
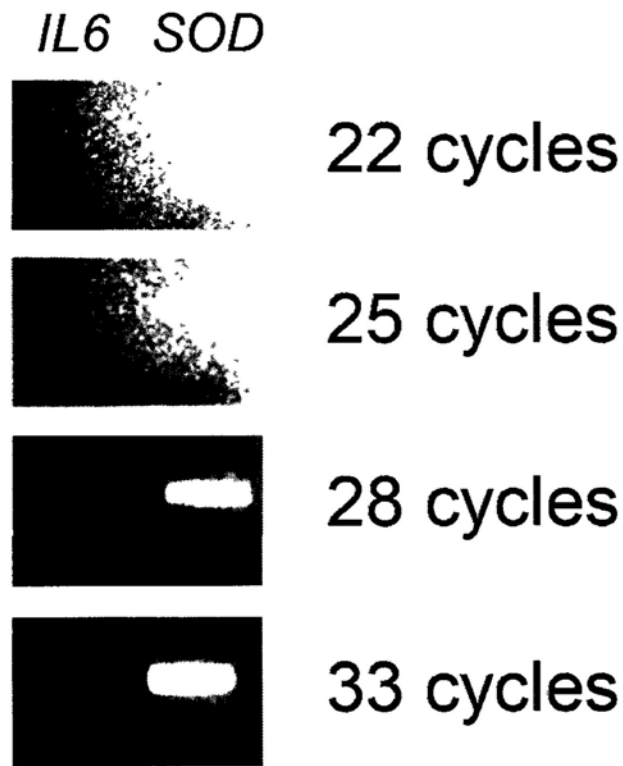
Figure 2.2: Polymerase chain reaction cycle optimization for gene expression analysis.

The polymerase chain reaction cycle was optimized for each gene by 2% agarose gel electrophoresis at every 3 cycles of reaction. Selection of the reaction cycle for gene expression analysis was based on the first appearance of the reaction product without over-saturation. For example, *SOD* gene was monitored after 25 reaction cycles while *IL6* gene was monitored after 33 reaction cycles.

Chapter 3: Results

3.1 Variant identification in *CFH* and *HTRA1* genes

3.1.1 Association between *CFH* gene and exudative AMD

A total of 58 sequence variations were identified in *CFH* gene in 163 Chinese patients diagnosed with exudative AMD and 155 sex- and age-matched control subjects (**Table 3.1**), all of which follow the Hardy-Weinberg equilibrium. Seven of them showed association with exudative AMD ($p < 0.05$). However, after multiple testing corrections by Bonferroni correction ($p < 0.05/58 = 0.00086$), only 2 polymorphisms (rs551397 and rs800292) were significantly associated with exudative AMD ($p = 0.00056$). Both polymorphisms were protective with odds ratio (OR) of 0.523 (95% CI: 0.373 – 0.735; $p = 0.00017$). Moreover, a major haplotype composed of rs551397 (T) and rs800292 (G) conferred an increased susceptibility for exudative AMD (OR = 1.91, 95% CI: 1.36 – 2.68; $p = 0.0001$). Notably, the Caucasian-associated AMD SNP, Tyr402His (rs1061170), was not associated with exudative AMD in our Hong Kong Chinese population ($p = 0.195$). The proposed risk allele C was not significantly higher in exudative AMD patients (5.8%) than in control subjects (2.9%) ($p = 0.072$).

3.1.2 Variants in *CFH* gene

Among the 58 sequence variations, 24 showed codon changes in the *CFH* open reading frame (ORF). Among them, 19 were non-synonymous changes. Excluding the variants showing similar biochemical properties with wildtype amino acids, 11 rare variants, including Tyr402His, could be considered to exert structural or functional impact on Cfh protein (**Table 3.2**). Although these 11 rare variants individually were not significantly associated with exudative AMD, grouping all of them together showed a significant

76

association with exudative AMD (p = 0.013). Exudative AMD patients (17.8%) carried more rare variants than the control subjects (8.4%). Individuals carrying these variants had 2.364-fold higher chance to develop AMD than those without. However, if Tyr402His was excluded, the 10 grouped rare variants were not associated with exudative AMD (p = 0.080).

3.1.3 Association between *HTRA1* gene and exudative AMD

Total 45 sequence variations were identified in *HTRA1* gene (**Table 3.3**), 41 of which obeyed the Hardy-Weinberg equilibrium. Coherent to our previous GWAS data (Dewan A et al, 2006), rs11200638 was confirmed to be significantly associated with exudative AMD in an extended cohort (p = 1.74 x 10^{-12}). Individuals carrying the risk allele A had 3.310-fold (95% CI: 2.403 – 4.559) higher chance to develop AMD than those carrying wildtype allele G (p = 9.24 x 10^{-14}). In addition to rs11200638, 4 other polymorphisms (rs2672598, 34delCinsTCCT, rs1049331 and rs2293870) were also significantly associated with exudative AMD, even after multiple testing corrections by Bonferroni method (p < 0.05/41 = 0.0012). These 5 polymorphisms were located in promoter region and exon 1. No polymorphism beyond exon 1 was associated with exudative AMD. Moreover, further interactive analysis revealed significant independent additive effects existed with smoking (OR = 15.7) and *CFH* (rs900292; OR = 23.3).

3.1.4 Variants in *HTRA1* gene

Among the 45 sequence variations, 11 showed codon changes in the *HTRA1* ORF (**Figure 3.1**). Among them, 7 were non-synonymous changes. Excluding the variants showing similar biochemical properties with wildtype amino acids, only 3 rare variants (34delCinsTCCT, 77G>C and 176G>C), all of which were located in exon 1, could be

considered to exert structural or functional impact on HtrA1 protein (**Table 3.4**). Unlike those rare variants in *CFH* gene, 34delCinsTCCT in *HTRA1* gene individually showed significant association with exudative AMD ($p = 0.001$) and exerted a protective effect with an odds ratio of 0.130 (95% CI: 0.029 – 0.575). Grouping together with the two insignificant rare variants, 77G>C and 176G>C, the protective effect was reduced with an odds ratio of 0.246 (95% CI: 0.081 – 0.746) although it remained significant ($p = 0.008$).

In order to validate the genotypic frequencies of these rare variants, especially 34delCinsTCCT, the study cohort of control subjects was extended to 390. Analogously, the protective rare variant, 34delCinsTCCT, was more prevalent in control subjects (7.9%) than in exudative AMD patients (1.2%) with an odds ratio of 0.144 (95% CI: 0.034 – 0.606; $p = 0.002$) (**Table 3.5**). Combining with 77G>C and 176G>C, the control subjects (9.0%) had more rare variants than the exudative AMD patients (2.5%) ($p = 0.006$), indicating these rare variants could protect the control subjects to develop AMD (odds ratio = 0.255, 95% CI: 0.089 – 0.730).

In order to validate the genetically protective effect of 34delCinsTCCT, the haplotypes of the 34delCinsTCCT variant with the rs11200638 polymorphism was determined. With the application of rs11200638 allele-specific primers (**Table 2.4**), the variant delCinsTCCT allele of 34delCinsTCCT was linked with the wildtype G allele of rs11200638 while the wildtype C allele of 34delCinsTCCT was linked with the risk A allele of rs11200638 (**Figure 3.2**), indicating that the variant delCinsTCCT allele was located in the protective haplotype, but not in the risk haplotype. Therefore, the protective effect of 34delCinsTCCT was confirmed in term of genetics.

3.2 Characterization of HtrA1 wildtype and variant protein

3.2.1 Bioinformatics analysis of HtrA1 variant

The codon containing wildtype C allele of 34delCinsTCCT coded for a leucine amino acid (CUG) at position 12 while the rare variant, 34delCinsTCCT, inserted a serine amino acid (UCC) at position 12 without affecting the leucine residue (UUG) at position 13. Insertion of a serine residue into HtrA1 protein was predicted to reduce the average hydrophobicity of whole protein from -0.1215 to -0.1229 by SOSUIsignal (Gomi M et al, 2004). As the first 22 amino acids at the N-terminus represented the signal peptide of HtrA1 protein (Zumbrunn J and Trueb B, 1996), the effect of serine insertion at position 12 on the signal peptide was analyzed. By SOSUIsignal (Gomi M et al, 2004), insertion of serine did not abolish the recognition of signal peptide in the HtrA1 variant, but reduced the average hydrophobicity of the signal peptide from 1.5455 to 1.4435. Moreover, from Phobius prediction (Kall L et al, 2004), insertion of serine at position 12 extended the N-region of the signal peptide from the first 5 residues (Met-Gln-Ile-Pro-Arg) in wildtype protein to first 6 residues (Met-Gln-Ile-Pro-Arg-Ala) in variant, and shifted the H-region (next 12 residues) from (Ala-Ala-Leu-Leu-Pro-Leu-Leu-Leu-Leu-Leu-Leu-Ala) in wildtype protein to (Ala-Leu-Leu-Pro-Leu-Ser-Leu-Leu-Leu-Leu-Leu-Ala) in variant without changing the C-region (Ala-Pro-Ala-Ser-Ala; last 5 residues) of the signal peptide (**Figure 3.3**). These predictions indicated that insertion of serine at position 12 in the HtrA1 variant might influence, but not abolish, the function of the signal peptide of HtrA1 protein.

3.2.2 Confirmation and verification of HtrA1 constructs and protein

Full-length human wildtype HtrA1 ORF (1440 bp) encompassed by a 27 bp *BamH*I forward primer and a 29 bp *Not*I reverse primer was inserted to the *BamH*I/*Not*I site of pcDNA6/*myc*-His© A vector to establish the HtrA1 expression construct,

pHis/myc-HtrA1 (**section 2.2.1**). The correct insertion of full-length human HtrA1 ORF was examined by agarose gel electrophoresis of the HtrA1 construct with appropriate restriction enzymes cut. HtrA1-containg construct was made of an approximate 1500 bp of HtrA1 fragment and an approximate 5000 bp of pcDNA6/*myc*-His© A vector fragment while the empty pcDNA6/*myc*-His© A vector only contained an approximate 5000 bp fragment (**Figure 3.4**). The correctly inserted sequence of HtrA1-containg construct was verified by direct sequencing and the full sequence of inserted HtrA1 with the restriction sites was shown in **Figure 3.5**.

The construct (pHis/myc-HtrA1-12insSer) for the HtrA1 variant, 34delCinsTCCT, was synthesized by site-directed mutagenesis on pHis/myc-HtrA1 construct with the application of specific mutagenesis primers (**section 2.2.2**). The correctly synthesized HtrA1 variant construct was verified by direct sequencing and the wildtype and the mutated sequences were shown in **Figure 3.6**.

Next, to validate the HtrA1 expression by the HtrA1-inserted constructs with correct sequences, pHis/myc-HtrA1 and pHis/myc-HtrA1-12insSer, HtrA1 mRNA and protein were examined by gene expression and immunoblotting analyses, respectively, through separate transfection to ARPE-19 cells. Gene expression analysis was performed by RT-PCR using specific expression primers for *HTRA1* (**Table 2.10**). An obviously strong single band (204 bp) of *HTRA1* was observed in HtrA1-transfected ARPE-19 cells (**Figure 3.7**). Empty vector-transfected cells also had *HTRA1* expression, but the band intensity was much weaker than the transfected ones, illustrating that endogenous *HTRA1* was present in ARPE-19 cells. The strong *HTRA1* signals demonstrated successful transfection of HtrA1 expression constructs and a steady state expression of *HTRA1* transcripts.

HtrA1 protein expression was examined by immuoblotting with the use of mouse monoclonal antibody against HtrA1 (**section 2.2.8**). In HtrA1-transfected ARPE-19 cells, a

specific band with molecular weight of ~ 53 kDa representing recombinant HtrA1 protein with *myc* epitope and polyhistidine (His$_6$) tag was observed in the RIPA soluble samples (**Figure 3.8**). The observed molecular weight was similar to the predicted size (51 kDa; Hu SI et al, 1998). On the other hand, minimal expression of HtrA1 was observed in the RIPA soluble sample of empty vector-transfected cells, indicating that the detection of endogenous HtrA1 protein in ARPE-19 cells by immunoblotting analysis was below limit. The immunoblotting results supported the cloning of right HtrA1 expression constructs, successful transfection of HtrA1 expression constructs and validated the expression of recombinant human HtrA1 protein.

As HtrA1 was suggested to function as a serine protease (Hu SI et al, 1998), the proteolytic activity of the recombinant human HtrA1 protein and variant was validated by the β-casein digestion. Recombinant human HtrA1 protein was collected from the serum-free condition medium of HtrA1-transfected ARPE-19 cells, purified and concentrated using a molecular size-restricted filter (**Figure 3.9A**). The concentrated condition medium containing the recombinant human HtrA1 was incubated with β-casein, which had a molecular weight of ~ 27 kDa (**Figure 3.9B**). The cleaved product of β-casein, which had a molecular weight of about 18 kDa, was only observed in the samples containing the recombinant human HtrA1, but not in the condition medium from empty vector-transfected ARPE-19 cells or without any condition medium (**Figure 3.9B**). In the sample containing the condition medium from the empty vector-transfected ARPE-19 cells, no cleaved product of β-casein was observed (**Figure 3.9B**), indicating that there was no protein other than HtrA1 cleaving β-casein in the medium from ARPE-19 cells. The cleaved product accumulated over time; however, the rate of cleaved product accumulation for the wildtype HtrA1 protein could not be differentiated from that for the HtrA1 variant protein (**Figure 3.9C**), indicating that the proteolytic domain of HtrA1 was not affected by the

81

insertion of serine residue in the signal peptide. These results confirmed that the recombinant HtrA1 protein and variant were proteolytically functional and suitable for further analysis.

3.2.3 Subcellular localization of recombinant human HtrA1 protein

ARPE-19 cells were transfected with pHis/myc-HtrA1 and cultured for 48 hours followed by collection for immunocytochemistry with mouse monoclonal antibody against HtrA1. A strong signal representing HtrA1 was observed in the juxtanuclear position of transfected cells (**Figure 3.10A**). Similar result was observed in RF/6A cells transfected with pHis/myc-HtrA1 (**Figure 3.10B**). This illustrated that the localization pattern of HtrA1 was not cell type specific.

The juxtanuclear localization pattern of recombinant human HtrA1 suggested a Golgi-related position. In order to verify this hypothesis, double immunofluorescence labelling of HtrA1 protein and the known markers for the Golgi apparatus, giantin or TGN38 (Linstedt AD and Hauri HP, 1993; Stankewich MC et al., 1998), was performed on ARPE-19 cells transfected with pHis/myc-HtrA1. Red fluorescence signal represented the recombinant human HtrA1 protein (**Figure 3.11**) while green fluorescence signal represented giantin (**Figure 3.11A**), which is a Golgi membrane protein. The multilamellar and tubular staining in the juxtanuclear position of Golgi apparatus was well demonstrated by giantin labeling and this was typical for Golgi apparatus staining. A substantial yellow overlay color was observed with merging of images of the same field, indicating that HtrA1 and giantin were co-localized (**Figure 3.11A**). Coherently, co-localization of HtrA1 and trans-Golgi network protein TGN38 was also observed when HtrA1-transfected ARPE-19 cells were double stained with HtrA1 antibody (red fluorescence signal) and TGN38 antibody (green fluorescence signal) (**Figure 3.11B**).

82

As the biosynthesis of secretory protein starts from the endoplasmic reticulum (ER), to Golgi apparatus and then secretory vesicles, the Golgi location might be an intermediate stage and might not be specific. In order to validate the specificity of Golgi location, double immunofluorescence labelling of HtrA1 protein with markers for the ER, Bip and ER exit site, Sec23 (Stankewich MC et al, 1998; Espenshade PJ et al, 2002), was examined on ARPE-19 cells transfected with pHis/myc-HtrA1. Red fluorescence signal represented the recombinant human HtrA1 protein (**Figure 3.11**) while green fluorescence signal represented Bip or Sec23 (**Figure 3.11C** and **Figure 3.11D**). The perinuclear gradient staining was demonstrated by Bip and Sec23 and this was typical for ER staining. Minimal yellow overlay color was observed (**Figure 3.11C** and **Figure 3.11D**), indicating that HtrA1 was not co-localized with these ER markers.

Human HtrA1 paralog, HtrA2, was shown to be localized in the mitochondria (Park HJ et al, 2006). To determine whether HtrA1 was also localized in mitochondria, double immunofluorescence labeling of HtrA1 protein with the mitochondrial marker, cytochrome C (Chance B et al, 1970), was performed on ARPE-19 cells transfected with pHis/myc-HtrA1. Red fluorescence signal represented the recombinant human HtrA1 protein (**Figure 3.11**) while green fluorescence signal represented cytochrome C (**Figure 3.11E**). The cytoplasmic punctate staining is typical for mitochondria. Minimal yellow overlay color was observed (**Figure 3.11E**), indicating that HtrA1 was not localized in mitochondria.

Recently, HtrA1 was suggested to be intracellularly associated with tubulin in the ovarian cancer cell lines (Chien J et al, 2009b). In order to verify this observation, double immunofluorescence labeling of HtrA1 protein with β-tubulin was performed on ARPE-19 cells transfected with pHis/myc-HtrA1. Red fluorescence signal represented the recombinant human HtrA1 protein (**Figure 3.11**) while green fluorescence signal

represented β-tubulin (**Figure 3.11F**). The cytoplasmic filamentous staining was typical for the intermediate filament containing β-tubulin. Exclusive red and green colors were observed (**Figure 3.11F**), indicating that recombinant HtrA1 protein was not associated with β-tubulin in ARPE-19 cells.

3.2.4 Quantitative analysis of ER-located HtrA1 protein

Although the immunocytochemistry profile of HtrA1 variant was similar to that of wildtype HtrA1 protein, a difference was also noticed. In the ARPE-19 cells transfected with HtrA1 variant, a prominent number of cells with HtrA1 localization in both the Golgi apparatus and ER was observed, which the fluorescence signal of HtrA1 variant was partially overlapped with that of Golgi marker and partially overlapped with that of ER marker (**Figure 3.12A**). This might be due to the HtrA1 variant located in the ER. Therefore, the ER localization efficiency of transfected HtrA1 (wildtype and variant) in ARPE-19 cells was determined by counting the number of transfected cells with HtrA1 signal overlapped with Golgi or ER markers (**section 2.2.10**). It was 2.7% for HtrA1 wildtype protein and 8.8% for HtrA1 variant protein (**Figure 3.12B**). This indicated that HtrA1 variant was most likely (3.2-fold) to be located in the ER but not for the wildtype protein.

3.2.5 Secretion of recombinant human HtrA1 protein

The difference of the ER localization between the wildtype protein and the variant protein might influence the trafficking and secretion of the protein. To verify this, serum-free media for post-incubation of the HtrA1-transfected ARPE-19 cells were collected at different time-points (12, 18, 24 and 36 hours). Secreted HtrA1 in media was detected by combined immunoprecipation and immunoblotting (**section 2.2.8**). For both

transfections, HtrA1 in media was not detected within 12 hours post-transfection (data not shown). Weak band of secreted HtrA1 was only observed at 12-hour post-transfection in ARPE-19 cells transfected with pHis/myc-HtrA1, but not in that transfected with pHis/myc-HtrA1-12insSer (**Figure 3.13**). From 18 to 36-hour post-transfection, stronger signals of secreted HtrA1 were detected for the cells transfected with pHis/myc-HtrA1 compared to that transfected with pHis/myc-HtrA1-12insSer. From the whole cell lysate, HtrA1 was detected similarly for both constructs. This indicated that the secretion of HtrA1 variant was delayed compared to that of wildtype protein.

3.2.6 Cell viability in HtrA1-transfected cells

HtrA1 was shown to be involved in the growth regulation of cancer cell lines (Baldi A et al, 2002; Chien J et al, 2004). This phenomenon might also exist in cell lines other than cancer, such as RPE cells. ARPE-19 cells transfected with pHis/myc-HtrA1, pHis/myc-HtrA1-12insSer and pcDNA6/*myc*-His© A were analyzed by MTT cell survival assay 24 hours after post-transfection (**section 2.2.12**). ARPE-19 cells expressing wildtype HtrA1 protein had a mean of 34% reduction of MTT signal compared to that transfected with empty vector, while ARPE-19 cells expressing HtrA1 variant protein had a mean of 15.4% reduction of MTT signal compared to that transfected with empty vector (**Figure 3.14**). This indicated that overexpression of HtrA1 protein reduced cell viability of ARPE-19 cells, but higher viability was found in cells expressing HtrA1 variant protein.

3.2.7 Cell apoptosis in HtrA1-transfected cells

Reduction in cell viability could be resulted from increased apoptosis or reduced proliferation; therefore, the apoptotic rates of ARPE-19 cells transfected with pHis/myc-HtrA1, pHis/myc-HtrA1-12insSer and pcDNA6/*myc*-His© A were analyzed by

counting the number of transfected cells with fragmented nuclei (**section 2.2.11**). 25.4% of ARPE-19 cells expressing wildtype HtrA1 protein, 15.6% of ARPE-19 cells expressing HtrA1 variant protein and 9.4% of empty vector-transfected ARPE-19 cells possessing fragmented nuclei were observed (**Figure 3.15**). This represented a 2.70-fold increase of apoptotic rate in ARPE-19 cells expressing wildtype HtrA1 protein and a 1.66-fold increase of apoptotic rate in ARPE-19 cells expressing HtrA1 variant protein, indicating that ectopic expression of HtrA1 protein would increase cell apoptosis in ARPE-19 cells and the ARPE-19 cell apoptotic rate was higher in cells expressing wildtype HtrA1 protein than those expressing HtrA1 variant protein. Reduction of cell viability in HtrA1-transfected ARPE-19 cells could be due to the increase in cell apoptotic rate by HtrA1 expression.

3.3 Association between HtrA1 and VEGF in vitreous humors

3.3.1 Association among vitreous levels of HtrA1, VEGF and PEDF

HtrA1, VEGF and PEDF protein were constitutively expressed in human vitreous humor as illustrated by immunoblotting analysis (**Figure 3.16**). Different expression levels were observed in different vitreous samples. Quantification by band densitometry using Quantity One® Image Analysis software (BioRad), the expression levels of HtrA1, VEGF and PEDF in 55 of vitreous samples collected from patients underwent ocular surgeries showed bell-shape distribution pattern (**Table 3.6**). With reference to previous publications, the expression levels were categorized into 3 groups (weak, moderate and strong) according to the distribution (**section 2.3.5**). Weak levels were below 25% quartile, moderate levels were between 25 to 75% quartile and high levels were above 75% quartile.

The vitreous levels of HtrA1, VEGF and PEDF had no clear association with gender (Mann-Whitney U test; $p = 0.250$, $p = 0.683$ and $p = 0.121$, respectively), age (Pearson's correlation coefficient test; $r = 0.146$, $p = 0.301$, $r = 0.140$, $p = 0.323$ and $r =$

0.140, $p = 0.322$, respectively) or grouped age (Kruskal-Wallis test; $p = 0.093$, $p = 0.108$ and $p = 0.203$, respectively). When analyzed with the categorized vitreous levels of HtrA1, VEGF and PEDF, no association was again observed with gender (χ^2 test; $p = 0.442$, $p = 0.160$ and $p = 0.265$, respectively) or grouped age (χ^2 test; $p = 0.251$, $p = 0.056$ and $p = 0.365$, respectively; Spearman rank correlation test; $\rho = 0.203$, $p = 0.148$, $\rho = 0.239$, $p = 0.088$ and $\rho = 0.035$, $p = 0.808$, respectively).

The trends of correlation for the mutual expressions of HtrA1, VEGF and PEDF across different vitreous humor samples were analyzed. The vitreous humor levels of HtrA1 were significantly associated with that of VEGF (Pearson's correlation coefficient test; r = 0.650, $p = 7.91 \times 10^{-8}$) (**Figure 3.17A**). However, no association was found between PEDF and VEGF or PEDF and HtrA1 (Pearson's correlation coefficient test; r = 0.023, $p = 0.865$ for PEDF and VEGF; r = 0.077, $p = 0.575$ for PEDF and HtrA1) (**Figure 3.17B** and **Figure 3.17C**). For the threshold analysis, significant association was observed between the grouped vitreous humor levels of HtrA1 and VEGF (χ^2 test; $p = 9.09 \times 10^{-10}$; Spearman rank correlation test; $\rho = 0.668$, $p = 2.55 \times 10^{-8}$) (**Table 3.7**). On the contrary, the grouped vitreous levels of PEDF were consistently not associated with that of VEGF or HtrA1 (χ^2 test; $p = 0.765$ for VEGF and $p = 0.607$ for HtrA1; Spearman rank correlation test; $\rho = -0.145$, $p = 0.292$ for VEGF and $\rho = -0.110$, $p = 0.422$ for HtrA1). When the grouped vitreous levels of PEDF were adjusted, the significant association between the grouped vitreous levels of HtrA1 and VEGF was mainly contributed by the low and moderate PEDF level (low PEDF level: χ^2 test for the association between grouped HtrA1 and grouped VEGF levels; $p = 1.42 \times 10^{-4}$; Spearman rank correlation test; $\rho = 0.955$, $p = 1.07 \times 10^{-7}$; moderate PEDF level: χ^2 test; $p = 6.12 \times 10^{-5}$; Spearman rank correlation test; $\rho = 0.736$, $p = 1.19 \times 10^{-5}$ and strong PEDF level: χ^2 test; $p = 0.043$; Spearman rank correlation test; $\rho = 0.189$, $p = 0.518$).

3.3.2 Association of vitreous levels of HtrA1 and VEGF in sub-clinical diagnosis

Vitreous humor samples were recruited from 55 subjects without AMD but underwent different ocular surgeries. According to similar disease phenotypes and clinical diagnosis, the subjects were categorized into 6 groups, vascular diseases, retinal detachment, idiopathic macular hole, traumatic injury, epi-retinal membrane (ERM) and intra-ocular lens re-operation (IOL). Vascular diseases include vitreous hemorrhage, diabetic retinopathy and central retinal vein occlusion, and retinal detachment includes rhegmatogenous retinal detachment and recurrent retinal detachment (**Table 2.8**). Excluding the group with less than 6 patients (ERM and IOL), the correlation of vitreous levels of HtrA1 with VEGF were analyzed within different clinical diagnosis. Significant positive association was observed between vitreous levels of HtrA1 and VEGF levels in retinal detachment (Pearson's correlation coefficient test; r = 0.835, p = 2.14 x 10^{-7}) (**Figure 3.18A**). However, only mild association was found in vascular diseases (Pearson's correlation coefficient test; r = 0.778, p = 0.003) (**Figure 3.18B**). In contrast, no association was observed in macular hole and traumatic injuries (Pearson's correlation coefficient test; r = -0.390, p = 0.340 and r = 0.706, p = 0.077, respectively) (**Figure 3.18C and 3.18D**).

3.3.3 Association among vitreous levels of HtrA1 and rs11200638 genotype

The mRNA and protein expressions of HtrA1 were reported to elevate in the individuals carrying the risk A allele of rs11200638 (Dewan A et al, 2006; Yang Z et al, 2006; Tuo J et al, 2008). The association between the vitreous HtrA1 levels and rs11200638 genotype was investigated. The rs11200638 genotype was not associated with vitreous HtrA1 levels (Kruskal-Wallis test; p = 0.668). Association remained not significant between the grouped vitreous levels of HtrA1 and the rs11200638 (χ^2 test; p = 0.529; Spearman rank correlation test; ρ = 0.129, p = 0.368) (**Table 3.8**), even after age-adjustment.

3.4 Association between HtrA1 and VEGF in human fetal retinal pigment epithelial cell culture

3.4.1 Association of *HTRA1* and *VEGFA* under cell stress response

As vitreous humor analysis showed a positive association between vitreous levels of HtrA1 and VEGF in retinal detachment (**Figure 3.18B**), their association in human fetal RPE cell culture under cell stress response was also speculated because retinal detachment is related to the inflammatory and stress responses (Zacks DN et al, 2006; Hollborn M et al, 2008). In addition, HtrA1 and VEGF could be associated with the cellular stress response as human HtrA1 paralog, HtrA2, is involved in cellular stress response (Gray CW et al, 2000; Han C et al, 2008), and VEGF is a stress-responsive gene (Abcouwer SF et al, 2002; Roybal CN et al, 2004; Li J et al, 2009). Cell stress response, which was assessed by gene expression analysis of *SOD* and *IL6*, was induced by treating human fetal RPE cells with tunicamycin, DTT and MG132. All of the chemical were able to induce cell stress response, as indicated by the upregulation of *SOD* (**Figure 3.19**). Moreover, inflammatory response (*IL6* upregulation) has also been induced in tunicamycin and DTT-treated cells (**Figure 3.19**).

First, tunicamycin, which induces cellular stress by the blockage of N-linked glycosylation in the ER (Elbein AD, 1984), simultaneously upregulated *HTRA1* and *VEGFA* expressions as compared to DMSO-treated control (**Figure 3.20B**). The elevated expressions of both *HTRA1* and *VEGFA* were dose-dependent, which the expression levels of *HTRA1* and *VEGFA* under 10 µg/ml tunicamycin treatment (3.53-fold and 3.14-fold, respectively) were higher than that with 5 µg/ml tunicamycin (2.16-fold and 2.19-fold, respectively). Nonetheless, *PEDF* was not altered under different tunicamycin concentrations.

To confirm the effect of cell stress response, human fetal RPE cells were treated

with DTT, which induces cellular stress by reducing the disulphide bond formation between cysteine residues (Jamsa E et al, 1994). Similar to tunicamycin treatment, both *HTRA1* and *VEGFA* were upregulated as compared to DMSO-treated control (**Figure 3.20C**). The change of *HTRA1* and *VEGFA* expression was dose-dependent, which the expression levels of *HTRA1* and *VEGFA* under 2 mM DTT treatment (4.51-fold and 3.89-fold, respectively) were higher than that with 1 mM DTT treatment (2.71-fold and 1.90-fold, respectively). Nevertheless, the expression of *PEDF* was not altered at any time-points or under different DTT concentrations.

To validate the effect of cell stress response, MG132, which is a reversible inhibitor of ubiquitin proteasome pathway (UPP) to induce ER stress (Lee AH et al, 2003), was applied. In contrast to tunicamycin and DTT, a substantial downregulation of *HTRA1* and VEGFA (by 2.4-fold and 2.2-fold, respectively) was observed upon treatment with 10μM MG132 (**Figure 3.20D**). Consistently, the expression of PEDF was unchanged. These results implicated that specific properties of MG132 might override the effect of cellular stress.

3.4.2 *VEGFA* expression in response to HtrA1

Since the association of HtrA1 and VEGF was validated in stress and inflammatory conditions, their mutual regulation was next investigated. Firstly, elevated HtrA1 expression was achieved by transfection of HtrA1 expression construct (**section 2.2.1**) into the human fetal RPE cells. Endogenous *HTRA1* mRNA expression was detected, indicating human fetal RPE cells were expressing *HTRA1*. The *HTRA1* expression was 7.2-fold higher in the HtrA1-transfected cells than in the empty vector-transfected cells (**Figure 3.21**), suggesting that overexpression of HtrA1 was done by transfection. In HtrA1 overexpressing cells, the *VEGFA* expression was unaltered (0.96-fold) as that in the empty

vector-transfected cells at 24 hours (**Figure 3.21**). This unchanged *VEGFA* expression was obtained in both shorter (6 – 12 hours) and longer (48 hours) collection time after transfection. In addition, similar *PEDF* levels were found in HtrA1-transfected and empty vector-transfected cells (0.81-fold). These results indicated that overexpression of HtrA1 did not upregulate or downregulate the expression of *VEGFA* in human fetal RPE cells.

3.4.3 *HTRA1* expression in response to vascular endothelial growth factor

VEGF-enriched environment was achieved by exogenous addition of recombinant human VEGF protein (10 ng/ml). 24 hours after treatment, *HTRA1* (0.94-fold), *VEGFA* (1.03-fold) and *PEDF* (1.12-fold) expressions in VEGF-treated cells were not different from that in the untreated cells (**Figure 3.22**). Shorter (10 min – 12 hours) or longer (48 hours) treatment time did not alter the expression of *HTRA1*. In addition, higher or lower dose of recombinant human VEGF also did not affect the *HTRA1* expression. These suggested that exogenous application of recombinant human VEGF did not change the expression of *HTRA1* and *PEDF* in human fetal RPE cells.

3.4.4 *HTRA1* and *VEGFA* expression in response to angiogenic factors

Although HtrA1 and VEGF were not transcriptionally regulated with each other, their expressions could be indirectly related. This experiment was to investigate the effect of angiogenic factors, such as bFGF and TNFα, on the expression of *HTRA1* and *VEGFA*. Firstly, application of recombinant human bFGF (10 ng/ml) for 24 hours did not alter the expression levels of *HTRA1* (0.93-fold) and *VEGFA* (0.64-fold) compared with untreated control (**Figure 3.23**). Rather, the *PEDF* expression level was reduced by 3 folds in the bFGF-treated cells compared with the untreated control. This indicates HtrA1 and VEGF were not associated under the treatment of bFGF on human fetal RPE cells.

Secondly, *HTRA1* (1.78-fold and 1.54-fold, respectively) and *VEGFA* (1.54-fold and 1.18-fold, respectively) remain unchanged although *PEDF* expressions showed a time-dependent decrease (0.70-fold to 0.19-fold) with 10 ng/ml TNFα treatment from 6 to 24 hours (**Figure 3.24**). The results were the same even with higher (50 ng/ml) or lower (1 ng/ml) concentration of TNFα. This suggested that *HTRA1* and *VEGFA* were not regulated by TNFα. Since MG132, apart from the UPP inhibition, also attenuates nuclear factor-kappa B (NFκB) activation by TNFα (Wang X et al, 1999), this result might suggest these 2 genes might not be regulated by the NFκB pathway.

3.4.5 Cell viability in response to cellular stress

Overexpression of human recombinant HtrA1 protein reduced cell viability and induced cell apoptosis in ARPE-19 cell line (**Figure 3.14** and **Figure 3.15**). Since *HTRA1* expression was upregulated in tunicamycin and DTT-treated human fetal RPE cells (**Figure 3.20**), it would be questioned whether the upregulation of *HTRA1* would be linked to the influence in cell viability. Therefore, the cell survival of human fetal RPE cells in response to cellular stress was analyzed by MTT cell survival assay after 18 hours of treatment (**section 2.4.4**). Human fetal RPE cells treated with 5 and 10 μg/ml of tunicamycin had a mean of 22.6% and 49.7% reduction of MTT signal, respectively, compared to the untreated cells, while human fetal RPE cells treated with 1 and 2 mM of DTT had a mean of 19.8% and 42.9% reduction of MTT signal, respectively, compared to the untreated cells (**Figure 3.25**). In contrast, the cell viability of human fetal RPE cells was not affected by the treatment of MG132, which reduced the *HTRA1* expression (**Figure 3.20**). These indicated that tunicamycin and DTT treatments would reduce cell viability of human fetal RPE cells and the upregulation of *HTRA1* expression in tunicamycin and DTT-treated human fetal RPE cells could be related to the reduction of cell viability.

Location	dbSNP ID	Sequence Change	Codon Change	Exudative AMD (Homo/Hetero/WT)	Control Subjects (Homo/Hetero/WT)	p
Promoter	Novel	-674C>G	-	0/0/163	0/1/154	NS
Promoter	Novel	-650A>G	-	0/3/160	0/8/147	NS
Promoter	Novel	-482G>A	-	0/0/163	0/1/154	NS
Promoter	rs3753394	-331T>C	-	22/58/83	32/69/54	0.013
Promoter	Novel	-261G>C	-	0/0/163	0/4/151	NS
Promoter	rs35836460	-195T>C	-	0/3/160	0/12/143	0.013
Intron 1	Novel	IVS1+95T>C	-	0/1/162	0/0/155	NS
Intron 1	rs551397	IVS1-36C>T	-	13/55/95	22/76/57	0.00056
Intron 1	Novel	IVS1-34C>T	-	0/1/162	0/0/155	NS
Exon 2	rs800292	184G>A	Val62Ile	13/55/95	22/76/57	0.00056
Intron 3	Novel	IVS3+9T>C	-	0/4/159	0/1/154	NS
Intron 3	Novel	IVS3+88T>C	-	0/3/160	0/6/149	NS
Intron 3	Novel	IVS3+175C>A	-	0/1/162	0/3/152	NS
Intron 3	Novel	IVS3-125_-131del7	-	0/1/162	0/1/154	NS
Intron 3	Novel	IVS3-63T>A	-	0/0/163	0/1/154	NS
Intron 3	Novel	IVS3-61G>A	-	0/1/162	0/0/155	NS
Intron 4	Novel	IVS4+57insT	-	0/3/160	0/8/147	NS
Intron 4	Novel	IVS4+108delT	-	0/4/159	0/3/152	NS
Intron 4	rs3766403	IVS4-44A>T	-	0/1/162	0/0/155	NS
Exon 5	Novel	476 G>C	Ser159Thr	0/0/163	0/1/154	NS
Intron 5	Novel	IVS5+195C>T	-	0/2/161	0/8/147	NS
Exon 6	Novel	647T>C	Ile216Thr	0/2/161	0/1/154	NS
Exon 7	Novel	907C>T	Arg303Trp	0/1/162	0/0/155	NS
Exon 7	rs1061147	921C>A	Ala307Ala	1/17/145	0/9/146	NS
Intron 7	Novel	IVS7+25C>T	-	0/2/161	0/3/152	NS
Intron 7	Novel	IVS7+54C>T	-	0/0/163	0/1/154	NS
Intron 7	rs482934	IVS7-53T>G	-	1/17/145	0/9/146	NS
Exon 9	rs1061170	1204T>C	Tyr402His	1/17/145	0/9/146	NS
Exon 9	Novel	1310C>A	Ser437Tyr	0/1/162	0/0/155	NS
Exon 9	Novel	1330C>T	Arg444Cys	0/1/162	0/0/155	NS
Intron 9	Novel	IVS9+10C>A	-	0/1/162	0/0/155	NS
Intron 9	Novel	IVS9-46G>T	-	0/1/162	0/0/155	NS
Exon 10	rs2274700	1419 G>A	Ala473Ala	16/57/90	27/66/62	0.015
Exon 10	Novel	1456 G>C	Gly486Arg	0/1/162	0/0/155	NS
Intron 10	Novel	IVS10+40T>C	-	0/0/163	0/1/154	NS
Intron 10	Novel	IVS10+168A>G	-	0/2/161	0/8/147	NS
Intron 10	rs203674	IVS10-98T>G	-	1/17/145	0/9/146	NS
Exon 11	rs35453854	1652T>C	Ile551Thr	0/1/162	0/1/154	NS
Exon 12	Novel	1735G>A	Val579Ile	0/2/161	0/0/155	NS
Exon 12	Novel	1736T>C	Val579Ala	0/1/162	0/1/154	NS
Exon 13	Novel	1935 G>T	Thr645Thr	0/2/161	0/8/147	NS
Exon 13	rs3753396	2016 G>A	Gln672Gln	21/66/76	34/69/52	0.024
Exon 14	Novel	2089C>T	Leu697Phe	0/1/162	0/0/155	NS
Exon 14	Novel	2114C>T	Ser705Phe	0/0/163	0/1/154	NS
Intron 14	Novel	IVS14-52T>C	-	0/0/163	0/2/153	NS
Intron 15	Novel	IVS15+20T>G	-	0/0/163	0/1/154	NS
Intron 15	Novel	IVS15-32A>T	-	0/1/162	0/0/155	NS
Intron 15	rs375046	IVS15-28A>C	-	4/14/145	0/12/143	NS
Exon 16	Novel	2509G>A	Val837Ile	0/2/161	0/8/147	NS
Exon 17	Novel	2637A>G	Gly879Gly	0/2/161	0/8/147	NS
Exon 17	Novel	2669G>C	Ser890Thr	0/0/163	0/1/154	NS
Exon 18	rs1065489	2808 T>G	Asp936Glu	23/67/73	34/69/52	NS
Exon 18	Novel	2944C>T	Pro982 Ser	0/1/162	0/0/155	NS
Intron 18	rs16840522	IVS18-89T>C	-	0/4/159	0/12/143	0.031
Intron 19	Novel	IVS19+8G>T	-	0/6/157	0/5/150	NS
Exon 20	Novel	3172T>C	Tyr1058His	0/2/161	0/1/154	NS
Exon 20	rs410232	3178G>C	Val1060Leu	0/2/161	0/1/154	NS
Exon 22	Novel	3696+99G>A	-	0/2/161	0/1/154	NS

Labeling of CFH gene was referred to GenBank database (NM_000186.2).
Homo: Homozygous change to the reference
Hetero: Heterozygous change to the reference
WT: Wildtype to the reference
NS: Not significant

Table 3.1: *CFH* variants identified in exudative AMD patients and control subjects.

Location	dbSNP ID	Sequence Change	Codon Change	Exudative AMD (Homo/Hetero/WT)	Control Subjects (Homo/Hetero/WT)	p	Odds Ratio (95% CI)
Exon 6	Novel	647T>C	Ile216Thr	0/2/161	0/1/154	NS	-
Exon 7	Novel	907C>T	Arg303Trp	0/1/162	0/0/155	NS	-
Exon 9	rs1061170	1204T>C	Tyr402His	1/17/145	0/9/146	NS	-
Exon 9	Novel	1310C>A	Ser437Tyr	0/1/162	0/0/155	NS	-
Exon 9	Novel	1330C>T	Arg444Cys	0/1/162	0/0/155	NS	-
Exon 10	Novel	1456 G>C	Gly486Arg	0/1/162	0/0/155	NS	-
Exon 11	rs35453854	1652T>C	Ile551Thr	0/1/162	0/1/154	NS	-
Exon 14	Novel	2089C>T	Leu697Phe	0/1/162	0/0/155	NS	-
Exon 14	Novel	2114C>T	Ser705Phe	0/0/163	0/1/154	NS	-
Exon 18	Novel	2944C>T	Pro982 Ser	0/1/162	0/0/155	NS	-
Exon 20	Novel	3172T>C	Tyr1058His	0/2/161	0/1/154	NS	-
		Number of variants with property change (including Tyr402His):		29 (17.8%)	13 (8.4%)	0.013	2.364 (1.179-4.739)
		Number of variants with property change (excluding Tyr402His):		11 (6.7%)	4 (2.6%)	0.080	-

Labeling of *CFH* gene was referred to GenBank database (NM_000186.2).
Homo: Homozygous change to the reference
Hetero: Heterozygous change to the reference
WT: Wildtype to the reference
NS: Not significant
CI: Confident interval

Table 3.2: Variants in *CFH* gene.

Location	dbSNP ID	Sequence Change	Codon Change	Exudative AMD (Homo/Hetero/WT)	Control Subjects (Homo/Hetero/WT)	p
Promoter	rs11200638	-625G>A	-	94/51/18	38/90/55	1.74×10^{12}
Promoter	Novel	-502C>T	-	0/10/153	0/20/163	NS
Promoter	Novel	-497C>T	-	0/4/159	0/8/175	NS
Promoter	rs2672598	-487T>C	-	138/24/1	97/68/18	3.03×10^{10}
Exon 1	Novel	34delCinsTCCT	Leu12insSer	0/2/161	0/16/167	0.001
Exon 1	Novel	59C>T	Ala20Val	3/36/124	2/56/125	NS
Exon 1	Novel	77G>C	Arg26Pro	0/1/162	0/0/180	NS
Exon 1	rs1049331	102C>T	Ala34Ala	18/52/93	55/90/38	3.73×10^{12}
Exon 1	rs2293870	108G>T	Gly36Gly	18/52/93	55/90/38	3.73×10^{12}
Exon 1	Novel	176G>C	Arg59Pro	0/1/162	0/1/182	NS
Intron 1	rs12267142	IVS1-176C>G	-	0/16/147	0/25/158	NS
Intron 2	Novel	IVS2+34G>A	-	0/1/162	0/0/183	NS
Intron 2	Novel	IVS2+81C>T	-	0/0/163	0/1/182	NS
Intron 2	Novel	ISV2+99T>C	-	0/1/162	0/0/183	NS
Intron 2	Novel	IVS2+100C>T	-	0/3/160	0/8/175	NS
Intron 2	Novel	IVS2+172_179del8	-	0/1/162	0/0/183	NS
Intron 2	Novel	IVS2+216A>G	-	0/0/163	0/1/182	NS
Intron 2	Novel	IVS2+317C>T	-	0/2/161	0/1/182	NS
Exon 3	Novel	663G>A	Val221Val	0/0/163	0/1/182	NS
Intron 3	rs2239586	IVS3+93C>T	-	15/77/71	22/92/69	NS
Intron 3	rs2239587	IVS3+167G>A	-	15/77/71	22/92/69	NS
Exon 4	Novel	834C>T	Phe278Phe	0/0/163	0/1/182	NS
Intron 4	rs2672582	IVS4+99C>T	-	46/90/27	67/86/30	NS
Intron 4	Novel	IVS4-34G>A	-	0/0/163	0/1/182	NS
Exon 5	Novel	996A>G	Leu332Leu	0/0/163	0/1/182	NS
Intron 5	Novel	IVS5+21delG	-	0/0/163	0/1/182	NS
Intron 5	Novel	IVS5+51G>C	-	0/0/163	0/1/182	NS
Intron 5	Novel	IVS5+76_79del4	-	0/59/104	0/48/135	NS
Intron 5	Novel	IVS5+168C>T	-	0/0/163	0/1/182	NS
Intron 5	rs2672583	IVS5+169G>A	-	42/90/31	68/87/28	NS
Intron 5	Novel	IVS5-133G>A	-	0/1/162	0/0/183	NS
Intron 6	Novel	IVS6+90G>T	-	0/0/163	0/1/182	NS
Intron 6	Novel	IVS6+111G>A	-	4/32/127	1/57/125	NS
Intron 6	rs2672585	IVS6 +115C>G	-	45/92/26	67/88/28	NS
Intron 7	Novel	IVS7+17C>A	-	0/1/162	0/0/183	NS
Intron 7	Novel	IVS7+130G>T	-	0/0/163	0/1/182	NS
Intron 7	Novel	IVS7+149C>G	-	4/33/126	1/57/125	NS
Intron 7	Novel	IVS7-123G>C	-	0/1/162	0/0/183	NS
Exon 8	rs11538140	1221C>T	Asp407Asp	0/3/160	0/5/178	NS
Exon 8	Novel	1249G>A	Val417Ile	0/0/163	0/1/182	NS
Intron 8	rs2272599	IVS8+14G>A	-	43/92/28	67/85/31	NS
Intron 8	Novel	IVS8+61A>G	-	0/0/163	0/1/182	NS
Intron 8	rs2293871	IVS8-36C>T	-	62/77/24	57/102/24	NS
Exon 9	Novel	1487C>T	-	0/0/163	0/1/182	NS
Exon 9	Novel	1537C>G	-	0/0/163	0/1/182	NS

Labeling of HTRA1 gene was referrred to GenBank database (NM_002775 3)
Homo Homozygous change to the reference
Hetero Heterozygous change to the reference
WT Wildtype to the reference
NS Not significant

Table 3.3: *HTRA1* variants identified in exudative AMD patients and control subjects.

95

Location	dbSNP ID	Sequence Change	Codon Change	Exudative AMD (Homo/Hetero/WT)	Control Subjects (Homo/Hetero/WT)	p	Odds Ratio (95% CI)
Exon 1	Novel	34delCinsTCCT	Leu12insSer	0/2/161	0/16/167	0 001	0 130 (0 029-0 575)
Exon 1	Novel	77G>C	Arg26Pro	0/1/162	0/0/180	NS	-
Exon 1	Novel	176G>C	Arg59Pro	0/1/162	0/1/182	NS	
		Number of variants with property change		4 (2 5%)	17 (9 3%)	0 008	0 246 (0 081 0 746)

Labeling of *HTRA1* gene was referred to GenBank database (NM_002775 3)
Homo Homozygous change to the reference
Hetero Heterozygous change to the reference
WT Wildtype to the reference
NS Not significant
CI Confident interval

Table 3.4: *HTRA1* variants in 163 patients and 183 controls.

Location	dbSNP ID	Sequence Change	Codon Change	Exudative AMD (Homo/Hetero/WT)	Control Subjects (Homo/Hetero/WT)	p	Odds Ratio (95% CI)
Exon 1	Novel	34delCinsTCCT	Leu12insSer	0/2/161	1/30/359	0 002	0 144 (0 034-0 606)
Exon 1	Novel	77G>C	Arg26Pro	0/1/162	0/2/388	NS	-
Exon 1	Novel	176G>C	Arg59Pro	0/1/162	0/2/388	NS	-
		Number of variants with property change		4 (2 5%)	35 (9 0%)	0 006	0 255 (0 089-0 730)

Labeling of *HTRA1* gene was referred to GenBank database (NM_002775 3)
Homo Homozygous change to the reference
Hetero Heterozygous change to the reference
WT Wildtype to the reference
NS Not significant
CI Confident interval

Table 3.5: *HTRA1* variants in 163 patients and 390 controls.

	HtrA1 Intensity	VEGF Intensity	PEDF Intensity
Study Subjects, n	55	55	55
Mean	8477.47	7663.08	8175.42
Standard deviation	4949.31	4292.13	4692.91
Median	7994.37	7176.17	7858.36
25% quartile	4605.86	4316.77	5098.33
75% quartile	11706.48	11076.71	11087.24
Maximum	21713.16	18944.29	20978.64
Minimum	586.35	748.64	64.29

Table 3.6: Quantification of vitreous levels of HtrA1, VEGF and PEDF.

Grouped HtrA1 Level	Grouped VEGF Level		
	+	++	+++
+	9 (16.4%)	3 (5.5%)	1 (1.8%)
++	4 (7.3%)	23 (41.8%)	1 (1.8%)
+++	1 (1.8%)	2 (3.6%)	11 (20.0%)

'+'   : Weak expression
'++' : Moderate expression
'+++': Strong expression

Table 3.7: Correlation of grouped vitreous levels of HtrA1 with grouped vitreous levels of VEGF.

Grouped HtrA1	rs11200638 Genotype		
Level	GG	GA	AA
+	4 (7.8%)	8 (15.7%)	1 (2.0%)
++	4 (7.8%)	14 (27.5%)	8 (15.7%)
+++	3 (5.9%)	6 (11.8%)	3 (5.9%)

'+'   : Weak expression

'++' : Moderate expression

'+++': Strong expression

Table 3.8: Correlation of grouped vitreous levels of HtrA1 with rs11200638 genotype.
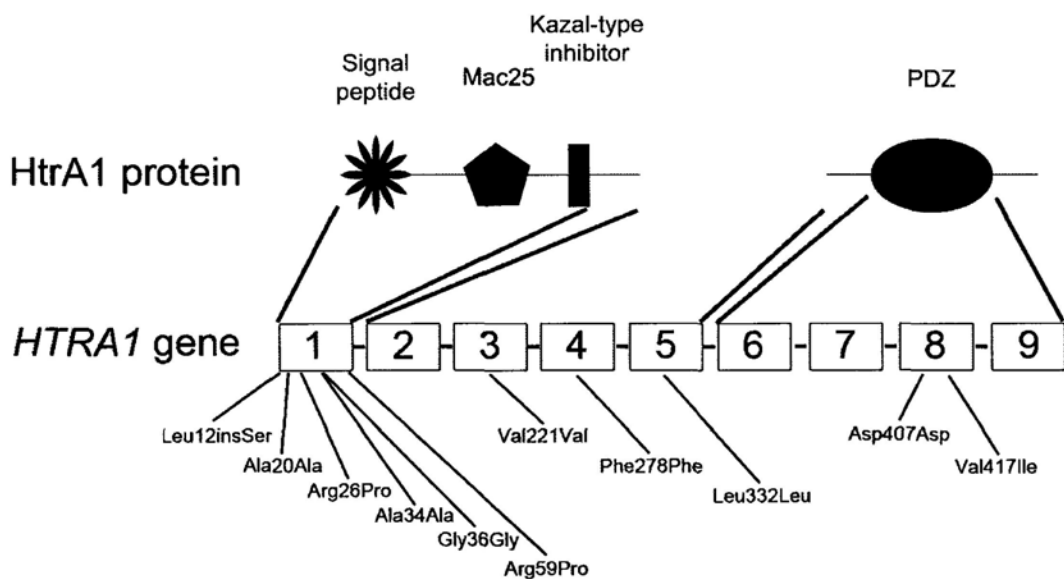
Figure 3.1: The eleven variants discovered in *HTRA1* open reading frame.

Total eleven variants were found in the *HTRA1* ORF. Among them, 7 were non-synonymous changes (Ala20Ala, Ala34Ala, Gly36Gly, Val221Val, Phe278Phe, Leu332Leu and Asp407Asp). Excluding the variants showing similar biochemical properties with wildtype amino acids (Val417Ile), only 3 variants (Leu12insSer, Arg26Pro and Arg59Pro), all of which were located in exon 1, could be considered to exert structural or functional impact on HtrA1 protein.
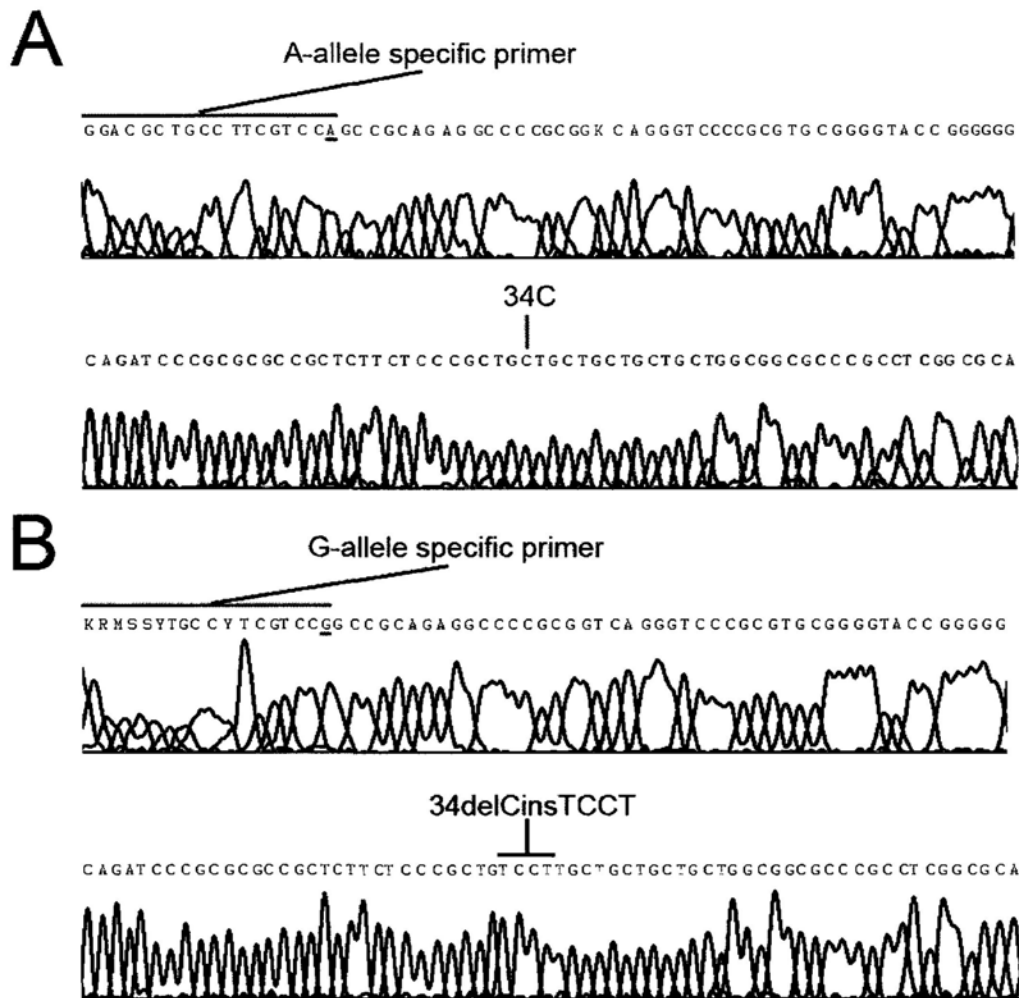
Figure 3.2: Haplotype analysis of rs11200638 and 34delCinsTCCT.

DNA from individual with a genotype of heterozygous 34delCinsTCCT and rs11200638 was amplified by PCR using allele-specific primers controlling the rs11200638, followed by direct sequencing. **(A)** The risk A allele of rs11200638 formed a haplotype with wildtype C allele of 34delCinsTCCT. **(B)** The wildtype G allele of rs11200638 formed a haplotype with variant delCinsTCCT allele of 34delCinsTCCT. The variant allele of 34delCinsTCCT is not located on the same haplotype with the risk allele of rs11200638, indicating a potential protective effect.

	N-region	H-region	C-region
Wildtype	Met-Gln-Ile-Pro-Arg	Ala-Ala-Leu-Leu-Pro-Leu-Leu-Leu-Leu-Leu-Leu-Ala	Ala-Pro-Ala-Ser-Ala
Variant	Met-Gln-Ile-Pro-Arg-Ala	Ala-Leu-Leu-Pro-Leu-Ser-Leu-Leu-Leu-Leu-Leu-Ala	Ala-Pro-Ala-Ser-Ala

Figure 3.3: Signal peptide structure of wildtype and variant HtrA1 protein.

From Phobius prediction (Kall L et al, 2004), insertion of serine at position 12 extended the N-region of the signal peptide from the first 5 residues (Met-Gln-Ile-Pro-Arg) in wildtype protein to first 6 residues (Met-Gln-Ile-Pro-Arg-Ala) in variant, and shifted the H-region (next 12 residues) from (Ala-Ala-Leu-Leu-Pro-Leu-Leu-Leu-Leu-Leu-Leu-Ala) in wildtype protein to (Ala-Leu-Leu-Pro-Leu-Ser-Leu-Leu-Leu-Leu-Leu-Ala) in variant without changing the C-region (Ala-Pro-Ala-Ser-Ala; last 5 residues) of the signal peptide.
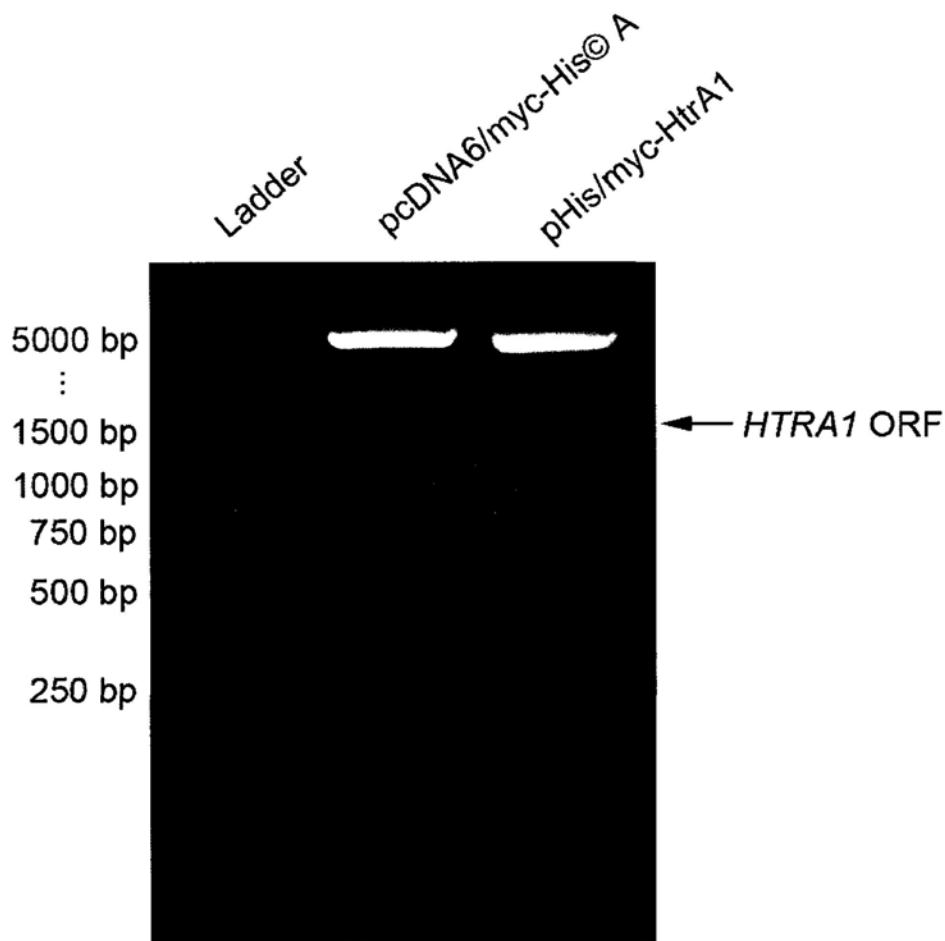
Figure 3.4: Confirmation of full-length _HTRA1_ open reading frame insertion into pcDNA6/_myc_-His© A expression vector by restriction enzyme analysis.

Insertion of full-length human _HTRA1_ ORF was confirmed by 1% agarose gel electrophoresis after restriction enzyme digestion using _BamH_I and _Not_I. The sizes of full-length _HTRA1_ ORF (about 1.5 kb) and the pcDNA6/myc-His© A expression vector (about 5.1 kb) are correctly indicated.

BamHI site | Met Gln Ile Pro Arg Ala Ala Leu Leu Pro Leu Leu Leu Leu Leu Leu Ala Ala Pro Ala Ser Ala Gln Leu Se

GGATCC CCATGCA GAT CCCGCGCGCC CGCTCTTCT CCCGCTGCTGCTGCTGCTGCTGGCGGCGCCCGCCTCGGCGCAGCTGTC

5 26 27 28 29 30 31 32 33 34 35 36 37 38 39 40 41 42 43 44 45 46 47 48 49 50 51 5
r Arg Ala Gly Arg Ser Ala Pro Leu Ala Ala Gly Cys Pro Asp Arg Cys Glu Pro Ala Arg Cys Pro Pro Gln Pro Glu H

CCC GG CCG GCCGC TCG GCGGCCT TTG GCCGCCGGG TGCCCAG ACCGCTGCG AGCCGGCGCGC TGCCCGCCGCAGCCGG AGC
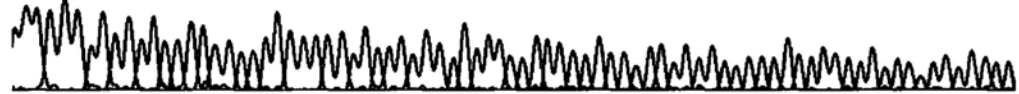
2 53 54 55 56 57 58 59 60 61 62 63 64 65 66 67 68 69 70 71 72 73 74 75 76 77 78 7
is Cys Glu Gly Gly Arg Ala Arg Asp Ala Cys Gly Cys Cys Glu Val Cys Gly Ala Pro Glu Gly Ala Ala Cys Gly Leu G

ACTGCGAGGGCGGCCGGGCCCGGGACGCSTGCGGCTGCTGCGAGGTGTGTGGCGCGCCCGAGGGCGCCGCGTGCGGCCTGC

9 80 81 82 83 84 85 86 87 88 89 90 91 92 93 94 95 96 97 98 99 100 101 102 103 104 105
ln Glu Gly Pro Cys Gly Glu Gly Leu Gln Cys Val Val Pro Phe Gly Val Pro Ala Ser Ala Thr Val Arg Arg Arg Ala

AGG AGG GCCCG TGCGGCG AGG GGCTGCAG TGCG TGG TGCCCTTCG GGG TGCCAGCC TCGGCCACGG TGCGGCGGCGCGCG
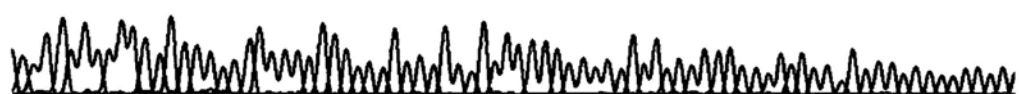

106 107 108 109 110 111 112 113 114 115 116 117 118 119 120 121 122 123 124 125 126 127 128 129 130 131 132 1
Gln Ala Gly Leu Cys Val Cys Ala Ser Ser Glu Pro Val Cys Gly Ser Asp Ala Asn Thr Tyr Ala Asn Leu Cys Gln Leu A

CAGGCCGGCCTCTGTGTGTGCGCCAGCAGCGAGCCGGTGTGCGGCAGCGACGCCAACACCTACGCCAACCTGTGCCAGCTGC

33 134 135 136 137 138 139 140 141 142 143 144 145 146 147 148 149 150 151 152 153 154 155 156 157 158 159 16
rg Ala Ala Ser Arg Arg Ser Glu Arg Leu His Arg Pro Pro Val Ile Val Leu Gln Arg Gly Ala Cys Gly Gln Gly Gln Gl

GCGCCGCCAGCCGCCGCTCCGAGAGGCTGCACCGGCCGCCGGTCATCGTCCTGCAGCGCGGAGCCTGCGGCCAAGGGCAGGA


0 161 162 163 164 165 166 167 168 169 170 171 172 173 174 175 176 177 178 179 180 181 182 183 184 185 186 187 1
u Asp Pro Asn Ser Leu Arg His Lys Tyr Asn Phe Ile Ala Asp Val Val Glu Lys Ile Ala Pro Ala Val Val His Ile Glu L

AGATCCCAACAGTTGCGCCATAAATAAAACTTATCGCGGACGGGTGGAGAAGATCGCCCCTGCCGTGGTTCATATCGAAT
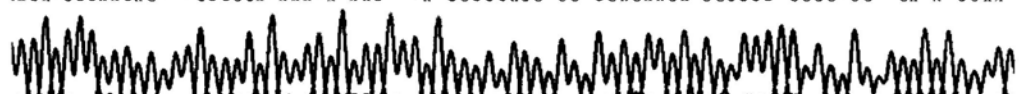

88 189 190 191 192 193 194 195 196 197 198 199 200 201 202 203 204 205 206 207 208 209 210 211 212 213 214 2
eu Phe Arg Lys Leu Pro Phe Ser Lys Arg Glu Val Pro Val Ala Ser Gly Ser Gly Phe Ile Val Ser Glu Asp Gly Leu I

TGTTTCGCAAGCTTCCGTTTTTCTAAACGAGAGGTGCCGGTGGCTAGTGGGTCTGGGTTTATTGTGTCGGAAGATGGACTGAT
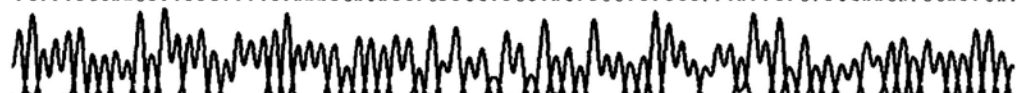
15 216 217 218 219 220 221 222 223 224 225 226 227 228 229 230 231 232 233 234 235 236 237 238 239 240 241
le Val Thr Asn Ala His Val Val Thr Asn Lys His Arg Val Lys Val Glu Leu Lys Asn Gly Ala Thr Tyr Glu Ala Lys

TCGTGACAAATGCCCACGTGGTGACCAACAAGCACCGGGTCAAAGTTGAGCTGAAGAACGGTGCCACTTACGAAGCCAAA
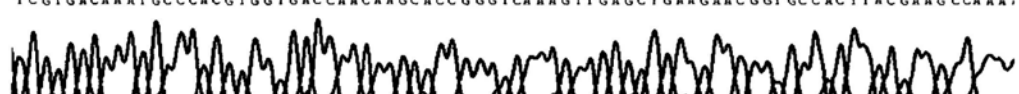
242 243 244 245 246 247 248 249 250 251 252 253 254 255 256 257 258 259 260 261 262 263 264 265 266 267 26
Ile Lys Asp Val Asp Glu Lys Ala Asp Ile Ala Leu Ile Lys Ile Asp His Gln Gly Lys Leu Pro Val Leu Leu Leu Gl

AATCAAGGATGTGGATGAGAAAGCAGACATCGCACTCATCAAAATTGACCACCAGGGCAAGCTGCCTGTCCTGCTGCTTGG
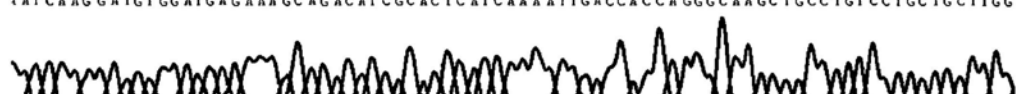
8 269 270 271 272 273 274 275 276 277 278 279 280 281 282 283 284 285 286 287 288 289 290 291 292 293 294 29
y Arg Ser Ser Glu Leu Arg Pro Gly Glu Phe Val Val Ala Ile Gly Ser Pro Phe Ser Leu Gln Asn Thr Val Thr Thr Gl

CCGCTCCTCAGAGCTGCGGCCGGGAGAGTTCGTGGTCGCCATCGGAAGCCCGTTTTCCCTTCAAAACACAGTCACCACCGG

105
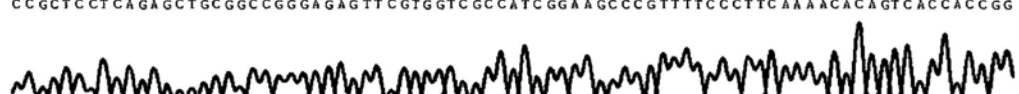
5 296 297 298 299 300 301 302 303 304 305 306 307 308 309 310 311 312 313 314 315 316 317 318 319 320 321 322
y Ile Val Ser Thr Thr Glu Arg Gly Gly Lys Glu Leu Gly Leu Arg Asn Ser Asp Met Asp Tyr Ile Gln Thr Asp Ala Ile
GATCGTGAGCACCACCCAGCGAGGCGGCAAAGAGCTGGGGCTCCGCAACTCAGACATGGACTACATCCAGACCGACGCCATC

323 324 325 326 327 328 329 330 331 332 333 334 335 336 337 338 339 340 341 342 343 344 345 346 347 348 349 35
Ile Asn Tyr Gly Asn Ser Gly Gly Pro Leu Val Asn Leu Asp Gly Glu Val Ile Gly Ile Asn Thr Leu Lys Val Thr Ala Gl
ATCAACTATGGAAACTCGGGAGGCCCGTTAGTAAACCTGGACGGTGAAGTGATTGGAATTAACACTTTGAAAGTGACAGCTGG
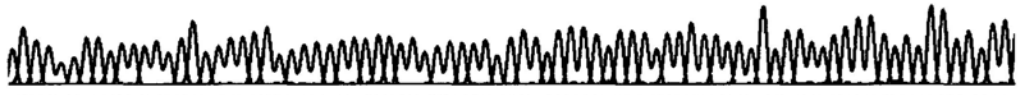
0 351 352 353 354 355 356 357 358 359 360 361 362 363 364 365 366 367 368 369 370 371 372 373 374 375 376 377
y Ile Ser Phe Ala Ile Pro Ser Asp Lys Ile Lys Lys Phe Leu Thr Glu Ser His Asp Arg Gln Ala Lys Gly Lys Ala Ile
AATCTCCTTTGCAATCCCATCTGATAAGATTAAAAAGTTCCTCACGGAGTCCCATGACCGACAGGCCAAAGGAAAAGCCATCA
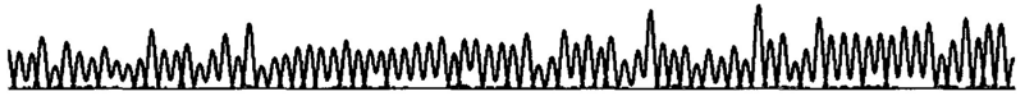

378 379 380 381 382 383 384 385 386 387 388 389 390 391 392 393 394 395 396 397 398 399 400 401 402 403 404 40
Thr Lys Lys Lys Tyr Ile Gly Ile Arg Met Met Ser Leu Thr Ser Ser Lys Ala Lys Glu Leu Lys Asp Arg His Arg Asp Ph
ACCAAGAAGAAGTATATTGGTATCCGAATGATGTCACTCACGTCCAGCAAAGCCAAAGAGCTGAAGGACCGGCACCGGGACTT

5 406 407 408 409 410 411 412 413 414 415 416 417 418 419 420 421 422 423 424 425 426 427 428 429 430 431 432
e Pro Asp Val Ile Ser Gly Ala Tyr Ile Ile Glu Val Ile Pro Asp Thr Pro Ala Glu Ala Gly Gly Leu Lys Glu Asn Asp
CCCAGACGTGATCTCAGGAGCCGTATATAATTGAAGTAATTCCTGATACCCCAGCAGAAGCTGGTGGTCTCAAGGAAAACGAC
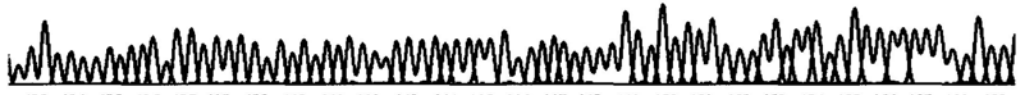
433 434 435 436 437 438 439 440 441 442 443 444 445 446 447 448 449 450 451 452 453 454 455 456 457 458 459
Val Ile Ile Ser Ile Asn Gly Gln Ser Val Val Ser Ala Asn Asp Val Ser Asp Val Ile Lys Arg Glu Ser Thr Leu Asn
CGTCATAATCAGCATCAATGGACAGTCCGTGGTCTCCGCCAATGATGTCAGCGACGTCATTAAAAGGGAAAGCACCCTGAAC
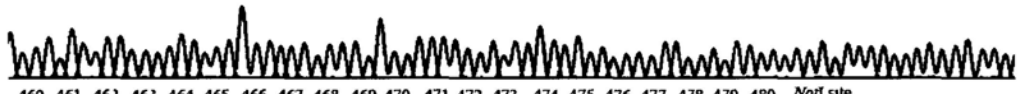
460 461 462 463 464 465 466 467 468 469 470 471 472 473 474 475 476 477 478 479 480 _Not_I site
Met Val Val Arg Arg Gly Asn Glu Asp Ile Met Ile Thr Val Ile Pro Glu Glu Ile Asp Pro Arg Pro Leu Glu Ser Arg G
ATGGTGGTCCGCAGGGGTAATGAAGATATCATGATCACAGTGATTCCCGAAGAAATTGACCCGCGGCCGCTCGAGTCTAGAG

myc epitope   Polyhistidine tag

ly Pro Phe Glu Gln Lys Leu Ile Ser Glu Glu Asp Leu Asn Met His Thr Glu His His His His His His Stop
GGCCCTTCGAACAAAAACTCATCTCAGAAGAGGATCTGAATATGCATACCGGTCATCATCACCATCACCATTGAGTTTAAACC

106

Figure 3.5: Full sequence of cloned *HTRA1* open reading frame inserted in pcDNA6/*myc*-His© A expression vector.

Recombinant human *HTRA1* ORF was inserted into the pcDNA6/myc-His© A expression vector. The sequence was labeled with the codon translation according to the start codon (ATG) of *HTRA1*. *HTRA1* ORF was inserted into the pcDNA6/myc-His© A expression vector using the *BamH*I and *Not*I restriction sites. All the amino acids labeled in *HTRA1* ORF by the codon translation were the same as the reference protein sequence (NP_002766.1). The stop codon of *HTRA1* ORF was removed so that the in-frame translation continued, and the *myc* epitope and polyhistidine tag were produced. The final synthesized recombinant protein is predicted to be a 510 amino acid protein consisting of a 480 amino acid full-length human HtrA1 protein with a 10 amino acid *myc* epitope and a 6 amino acid polyhistidine tag.
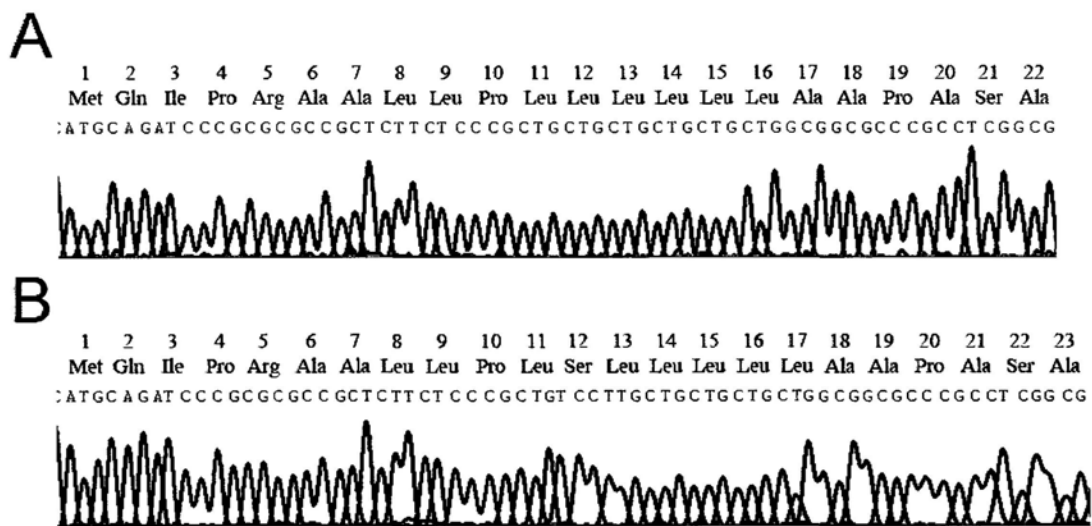
Figure 3.6: Sequences of signal peptide of human wildtype HtrA1 and HtrA1 variant.

The chromatograms of **(A)** first 66 nucleotides for *HTRA1* wildtype transcript and **(B)** first 69 nucleotides for *HTRA1* variant transcript, starting from the start codon (ATG), are presented with codon translation. The first 22 amino acids at the N-terminus of wildtype HtrA1 protein and first 23 amino acids of HtrA1 variant protein were predicted to be the signal peptide. The variation of HtrA1 variant protein is indicated with an insertion of serine residue at position 12.
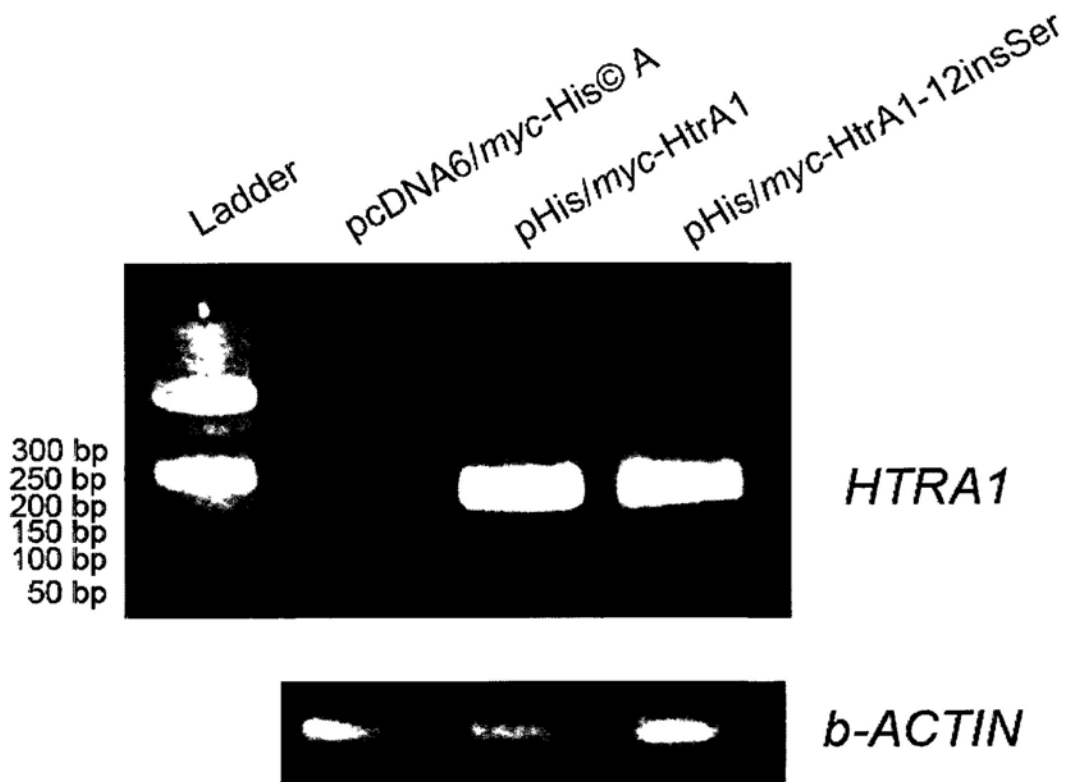
Figure 3.7: Gene expression analysis of ARPE-19 cells transfected with wildtype or variant HtrA1 expression construct.

Total RNA from transfected ARPE19 cells was analyzed for human HtrA1 expression by RT-PCR using specific primers for *HTRA1* and *β-ACTIN*. A strong single band (approximately 200 bp in size) representing *HTRA1* transcript was observed in samples transfected with pHis/myc-HtrA1 and pHis/myc-HtrA1-12insSer. Empty vector-transfected cells showed *HTRA1* expression, but the specific band intensity was much weaker than the transfected ones, illustrating that the endogenous *HTRA1* was present in ARPE-19 cells. Constant processing of template and loading of PCR samples was verified by the even expression levels of housekeeping *β-ACTIN*.
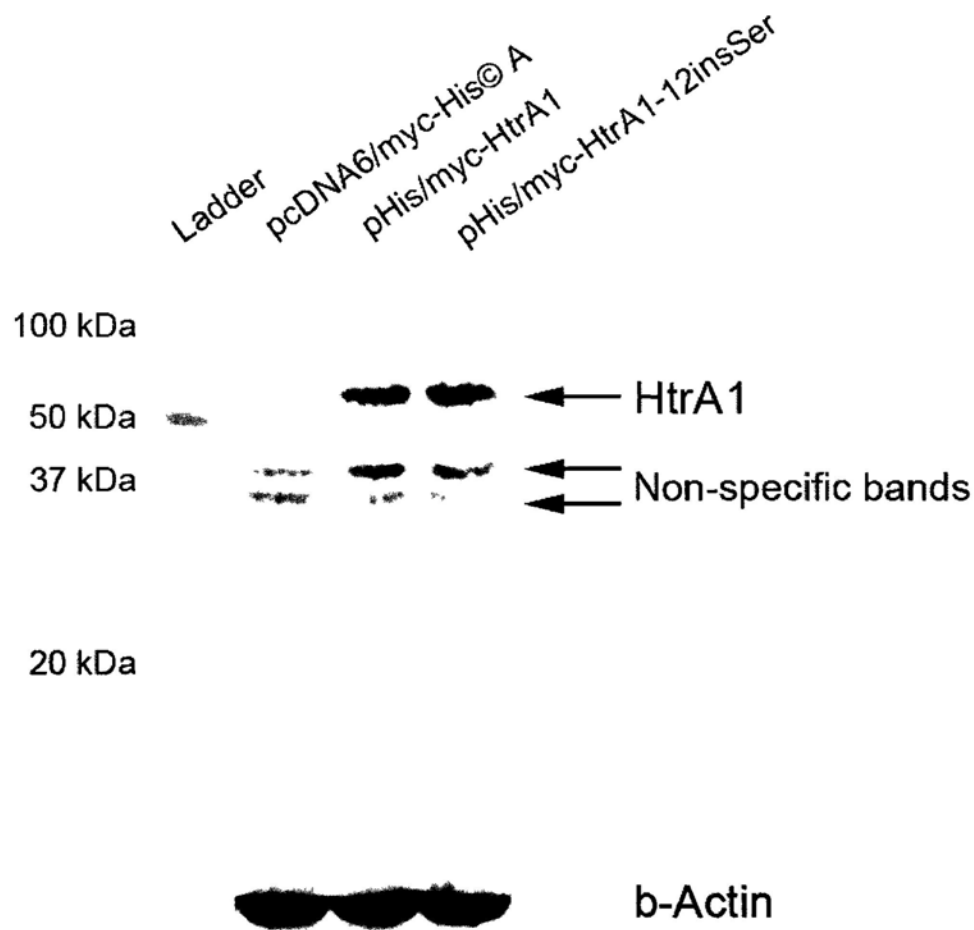
109

Figure 3.8: Protein expression analysis of ARPE-19 cells transfected with wildtype or variant HtrA1 expression construct.

Total RIPA soluble protein from ARPE-19 cells transfected with pHis/myc-HtrA1 and pHis/myc-HtrA1-12insSer was analyzed by western blotting for recombinant human wildtype and variant HtrA1 protein expression with mouse monoclonal antibody against human HtrA1 protein. Specific single band in the position of ~53 kDa was observed in HtrA1-transfected cells compared to empty vector-transfected cells. β-Actin expression was used as the housekeeping controls. Non-specific bands were noted, which might be due to the background of antibody staining.

A

pHis/myc-HtrA1
pHis/myc-HtrA1-12insSer
pcDNA6/myc-His© A

← HtrA1

B

| Ladder | pHis/myc-HtrA1 | | | | | | pHis/myc-HtrA1-12insSer | | | | | | pcDNA6/myc-His© A | Buffer only | |
| | 0 | 10 | 20 | 30 | 40 | 50 | 0 | 10 | 20 | 30 | 40 | 50 | 50 | 50 | (Minutes) |

25 kDa
20 kDa
15 kDa

← Casein

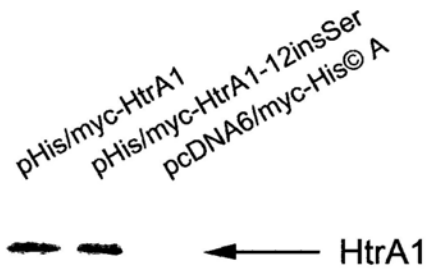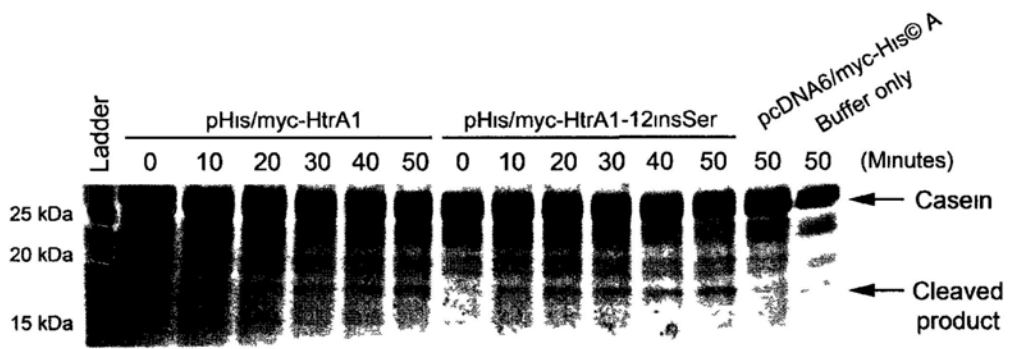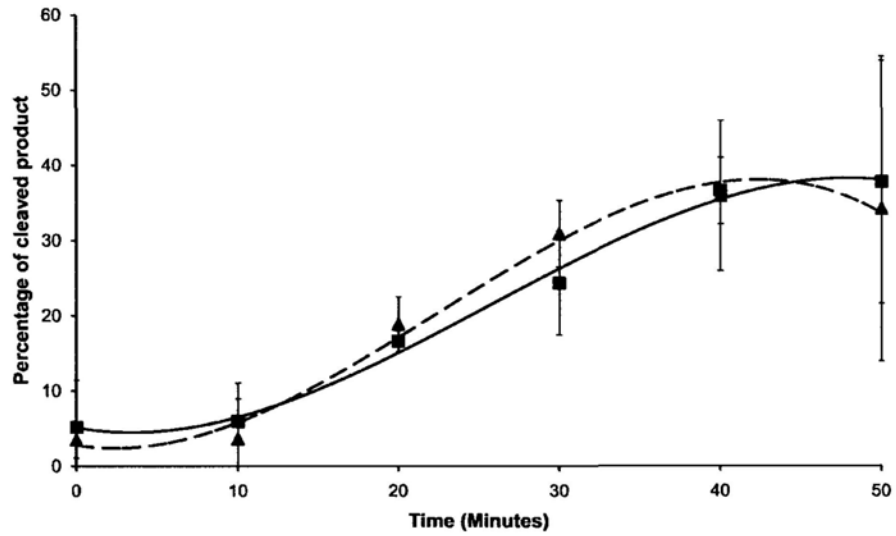← Cleaved product

C

Percentage of cleaved product vs Time (Minutes)

Figure 3.9: Proteolytic activity analysis of the recombinant human wildtype and variant HtrA1 protein.

HtrA1-transfected or empty vector-transfected ARPE-19 cells were incubated in serum-free medium which was collected at 48 hours after transfection. Recombinant human HtrA1 protein in the cell-free conditioned medium was purified and concentrated by 10-kDa centrifugal filter. Equal amount of total protein (10 μg) in the conditioned medium from ARPE-19 cells transfected with pHis/myc-HtrA1, pHis/myc-HtrA1-12insSer or pcDNA6/*myc*-His© A was applied. Proteolytic activity analysis was performed by incubating 10 μg protein in the conditioned medium with 5 ug of β-casein in a buffer of 50 mM Tris/HCl (pH 7.5) and 150mM NaCl at 37℃, added up to a volume of 30 μl by distilled water. At different time-points (0 – 50 min at 10 min-interval), 7.5 μl of SDS buffer was added to the reaction mixture, which was then denatured at 95℃ for 5 min to terminate the reaction. The denatured protein samples were resolved by 15% SDS-PAGE and visualized by Coomassie blue staining. The sample containing only β-casein and buffer was used as a negative control. **(A)** The quantity of HtrA1 protein in the conditioned medium with same amount of total protein was validated by immunoblotting analysis using mouse monoclonal antibody against HtrA1. **(B)** β-casein had a molecular weight of about 27 kDa while the cleaved product of β-casein had a molecular weight of about 18 kDa. The cleaved product was only observed in the samples containing recombinant human HtrA1, but not in the conditioned medium from empty vector-transfected ARPE-19 cells or without any conditioned medium. **(C)** The band intensities of the cleaved product were measured and compared with β-casein from the sample without conditioned medium. The rate of cleaved product accumulation for wildtype HtrA1 was similar to that for HtrA1 variant. Mean ± SD was presented.

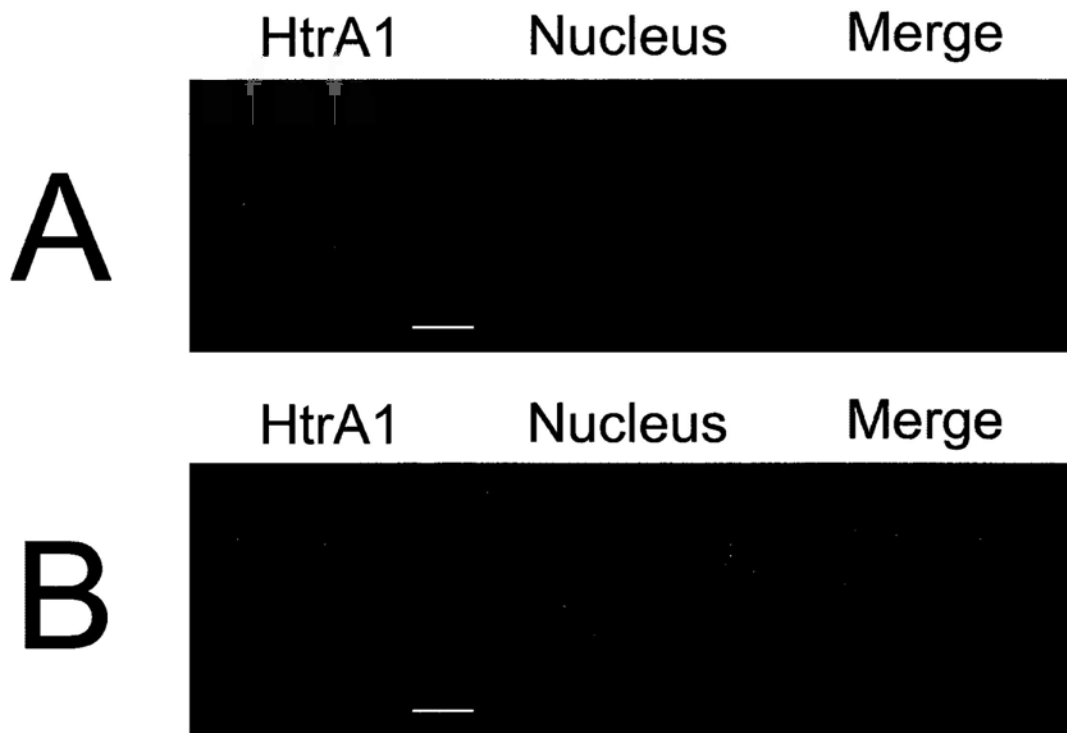**Figure 3.10: Immunocytochemical analysis of recombinant human HtrA1 protein in ARPE-19 and RF/6A cells.**

(A) ARPE-19 and **(B)** RF/6A cells transfected with pHis/myc-HtrA1 were fixed and immunostained for HtrA1 (in red fluorescence), followed by contrast staining of nuclei with DAPI (in blue fluorescence). A specific HtrA1 staining located in the juxtanuclear position was observed in both cell types. Scale bar: 10 μm.
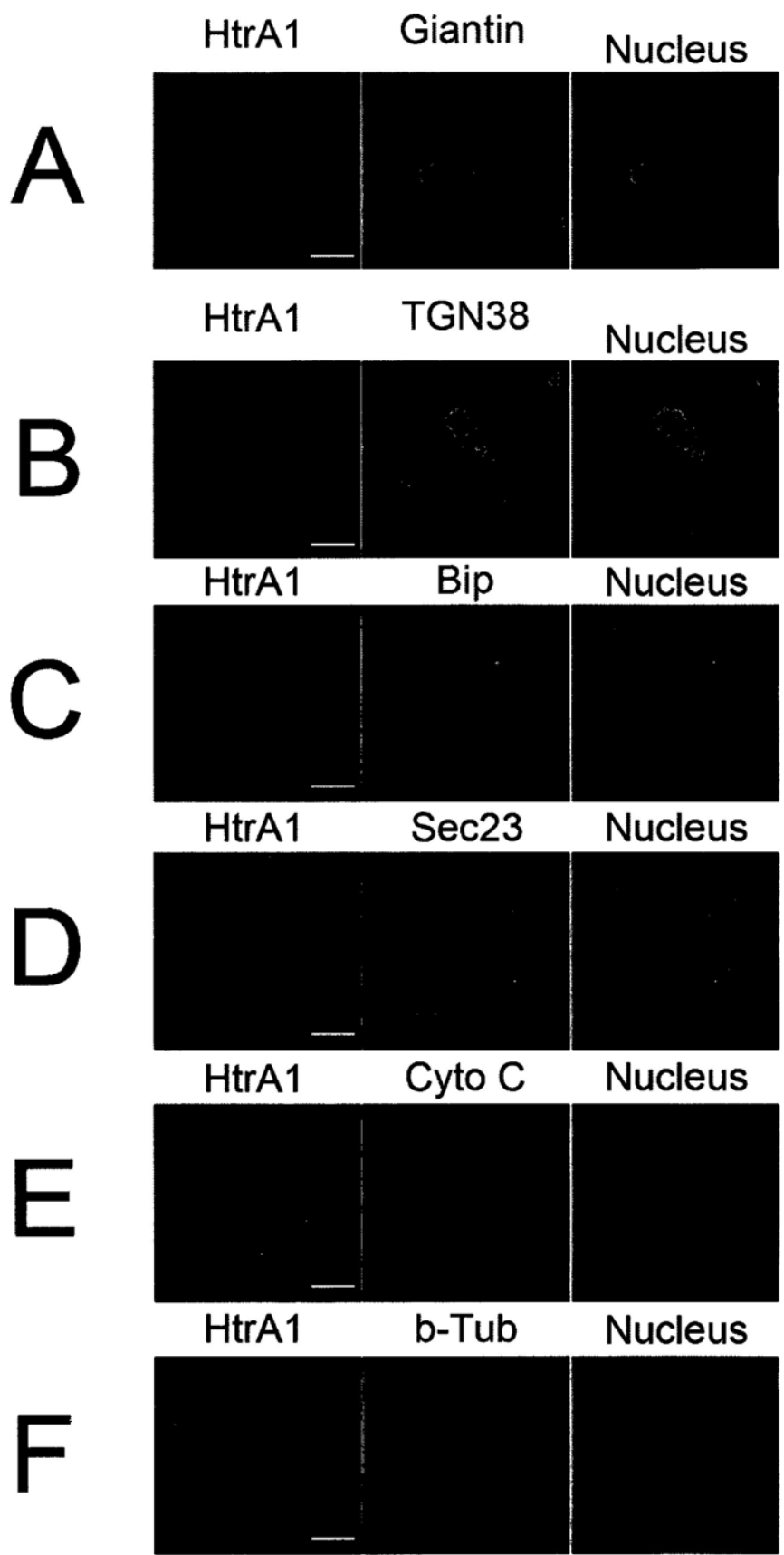
Figure 3.11: Subcellular localization analysis of recombinant human HtrA1 protein in ARPE-19 cells.

ARPE-19 cells transfected with pHis/myc-HtrA1 were fixed, double immunolabeled for HtrA1 protein (in red fluorescence) and different localization markers (in green fluorescence), including **(A)** giantin (a marker for Golgi apparatus), **(B)** TGN38 (a marker for Golgi and trans-Golgi network), **(C)** BiP (a marker for the ER), **(D)** Sec23 (a marker for transition ER / ER exit site), **(E)** cytochrome C (a marker for mitochondria) and **(F)** β-tubulin, and contrast-stained the nuclei with DAPI (in blue). Specific HtrA1 staining was found to be co-localized with giantin and TGN38 (in yellow overlay fluorescence), but not with other markers. Scale bars: 10 μm.

A

HtrA1 Giantin Nucleus

B

HtrA1 Bip Nucleus

C

116
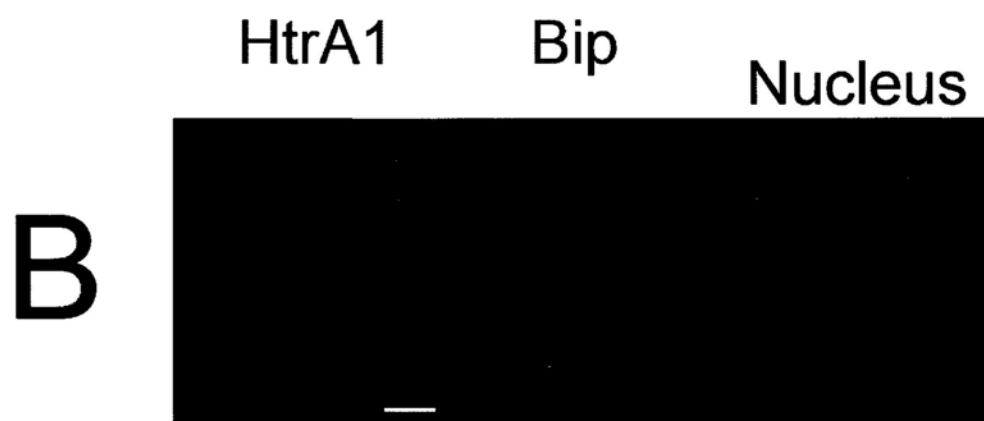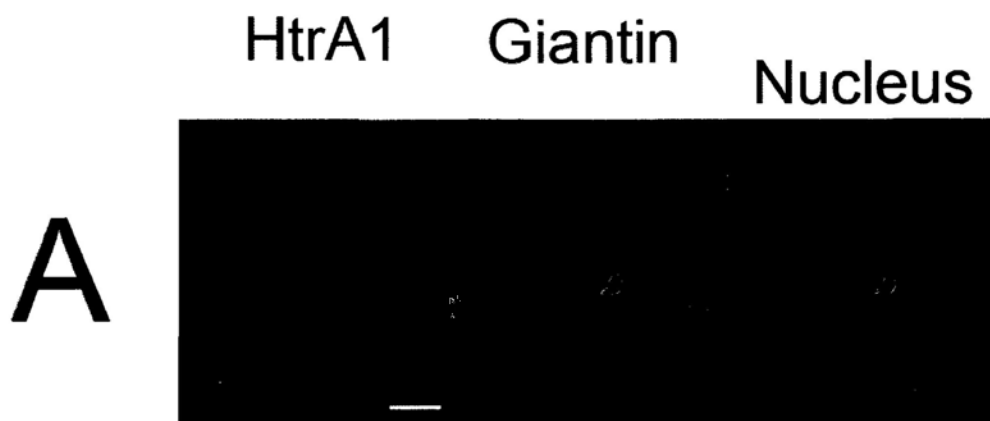
Figure 3.12: Quantitative analysis of ER-located HtrA1 protein in ARPE-19 cells transfected with pHis/myc-HtrA1 or pHis/myc-HtrA1-12insSer.

ARPE-19 cells transfected with pHis/myc-HtrA1 were fixed, double immunolabeled for HtrA1 protein (in red fluorescence) and **(A)** gaintin (a marker for Golgi apparatus) or **(B)** BiP (a marker for the ER) (in green fluorescence), and contrast-stained the nuclei with DAPI (in blue). Specific HtrA1 staining was partially co-localized with giantin and BiP (in yellow overlay fluorescence). Scale bars: 10 μm. **(C)** The ER localization was examined as the number of cells showing HtrA1 staining partially overlapped with giantin or BiP / the number of cells showing HtrA1 staining completely overlapped with giantin or exclusively with BiP. About 2.7% of ARPE-19 cells transfected with pHis/myc-HtrA1 showed partial co-localization compared to 8.8% of ARPE-19 cells transfected with pHis/myc-HtrA1-12insSer. Mean ± SD was presented.

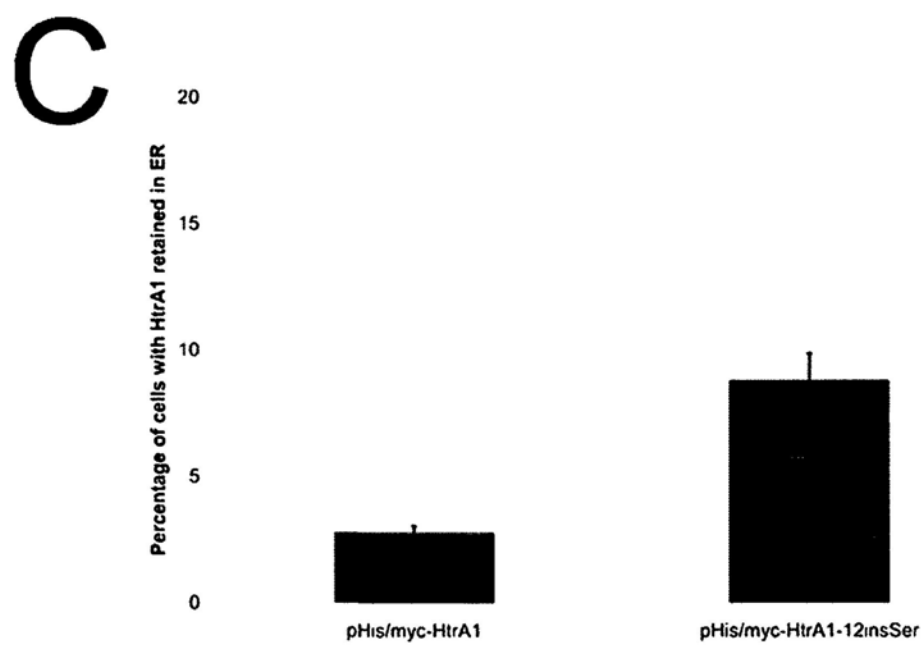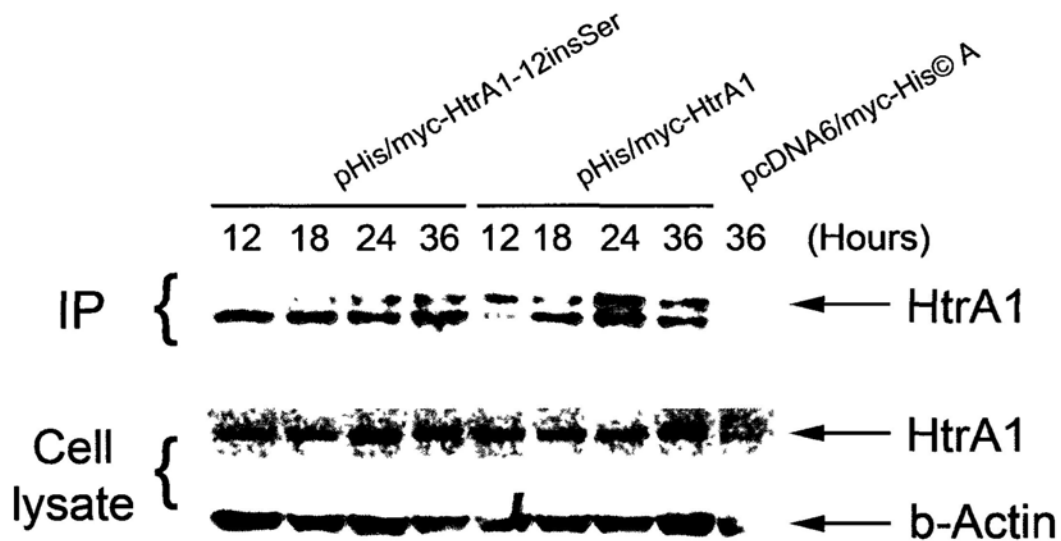**Figure 3.13: Secretion of recombinant HtrA1 protein in ARPE-19 cells transfected with pHis/myc-HtrA1 or pHis/myc-HtrA1-12insSer.**

Supernatant of ARPE-19 cells transfected with pHis/myc-HtrA1 and pHis/myc-HtrA1-12insSer incubated in serum-free medium was collected at different time-point after transfection (12, 18, 24 and 36 hours). Secreted HtrA1 was identified by immunoprecipitation using anti-His$_6$ antibody on the collected supernatant. The immunoprecipitates were then quantified by immunoblotting using mouse monoclonal antibody against HtrA1. Secreted HtrA1 was not detected before 12 hours post-transfection (data not shown). Weak band of secreted HtrA1 was only observed at 12-hour post-transfection in ARPE-19 cells transfected with pHis/myc-HtrA1, but not in that transfected with pHis/myc-HtrA1-12insSer. From 18 to 36-hour post-transfection, stronger signals of secreted HtrA1 were detected for the cells transfected with pHis/myc-HtrA1 compared to that transfected with pHis/myc-HtrA1-12insSer. From the whole cell lysate, the expression of HtrA1 protein was similar for both constructs, suggesting a similar HtrA1 synthesis.
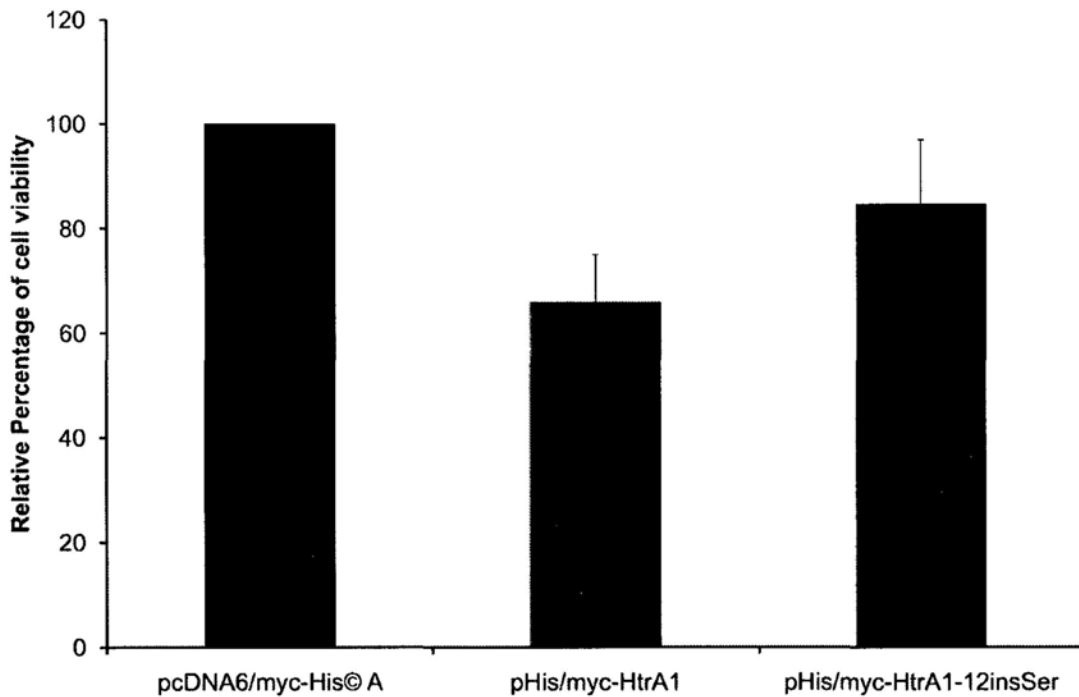
Figure 3.14: Cell survival analysis of ARPE-19 cells transfected with pHis/myc-HtrA1 or pHis/myc-HtrA1-12insSer.

MTT assay was performed on ARPE-19 cells transfected with pHis/myc-HtrA1, pHis/myc-HtrA1-12insSer or pcDNA6/myc-His© A vector. An excitation wavelength of 570 nm with reference 650 nm was measured by a spectrophotometer. The percentage of cell viability was expressed as OD_{570} of ARPE-19 cells transfected with pHis/myc-HtrA1 or pHis/myc-HtrA1-12insSer / OD_{570} of ARPE-19 cells transfected with empty vector. ARPE-19 cells transfected with pHis/myc-HtrA1 had a mean of 34% reduction of MTT signal while ARPE-19 cells transfected with pHis/myc-HtrA1-12insSer had a mean of 15.4% reduction of MTT signal, compared to that transfected with empty vector. Mean ± SD was presented.

119
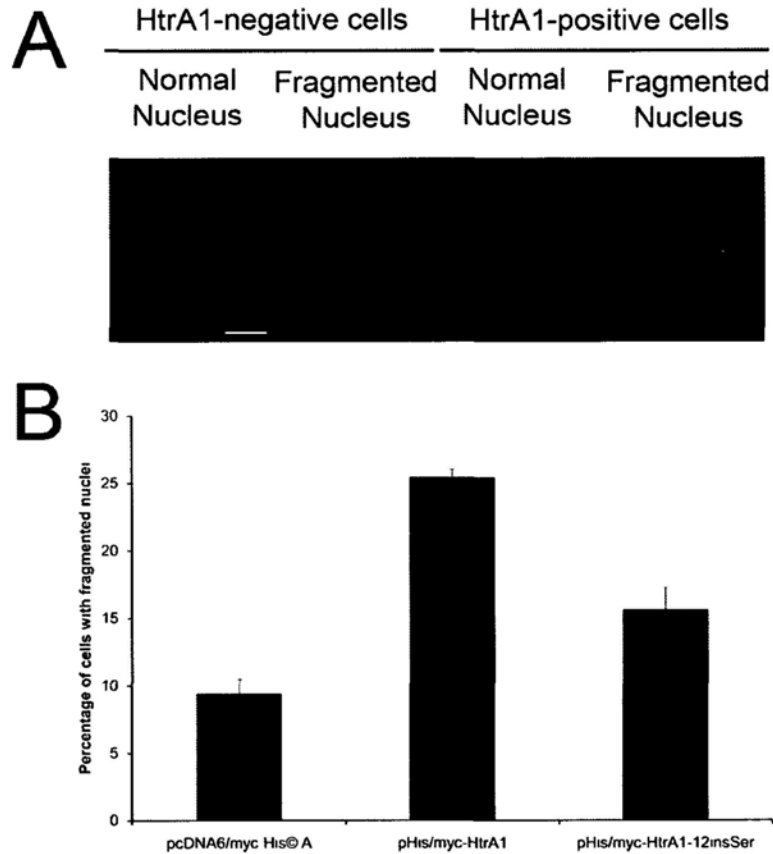
Figure 3.15: Cell apoptosis analysis of ARPE-19 cells transfected with pHis/myc-HtrA1 or pHis/myc-HtrA1-12insSer.

Cells undergoing terminal apoptosis were presented with fragmented nuclei. The apoptosis rates were compared among ARPE-19 cells transfected with pHis/myc-HtrA1, pHis/myc-HtrA1-12insSer or pcDNA6/myc-His© A vector. **(A)** Immunocytochemical analysis was used to label the transfected HtrA1 protein (in red fluorescence) and DAPI-stained nuclei (in blue), and to count the number of cells with fragmented nuclei. Scale bars: 10 μm. **(B)** The apoptosis rate was calculated as the number of transfected HtrA1-positive cells showing fragmented nuclei / the number of transfected HtrA1-positive cells. There was 25.4% of ARPE-19 cells transfected with pHis/myc-HtrA1 and 15.6% of ARPE-19 cells transfected with pHis/myc-HtrA1- 12insSer undergoing terminal apoptosis, compared to 9.4% of ARPE-19 cells transfected with pcDNA6/myc-His© A vector. Mean ± SD was presented.

120

Figure 3.16: Immunoblotting analysis of vitreous levels of HtrA1, VEGF and PEDF.

Equal amount (10 µg total protein) of the denatured vitreous humor samples were resolved on 12.5% SDS-polyacrylamide gel and electro-transferred to nitrocellulose membranes for probing sequentially with monoclonal antibodies against VEGF, HtrA1 and PEDF in the same blotting experiment. The signals were detected by the enhanced chemiluminescence. HtrA1, VEGF and PEDF were constitutively expressed in vitreous humors, but with different intensities. Fifteen of 55 vitreous humor samples were presented (grouped HtrA1 level, grouped VEGF level, and grouped PEDF level for same individual). '+': weak expression; '++': moderate expression; '+++': strong expression.

122
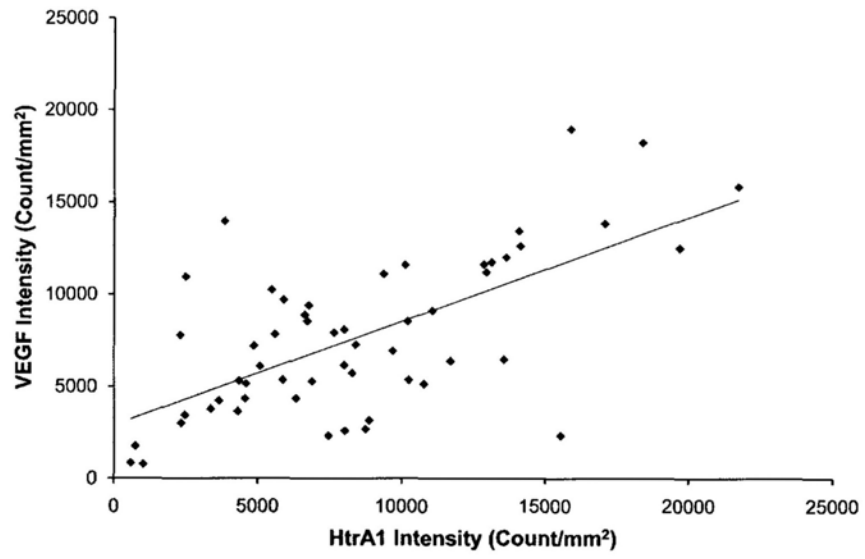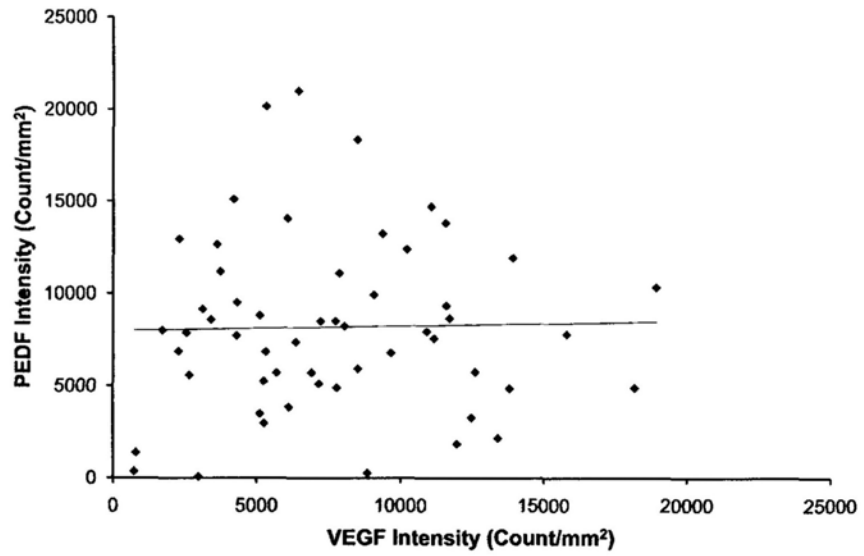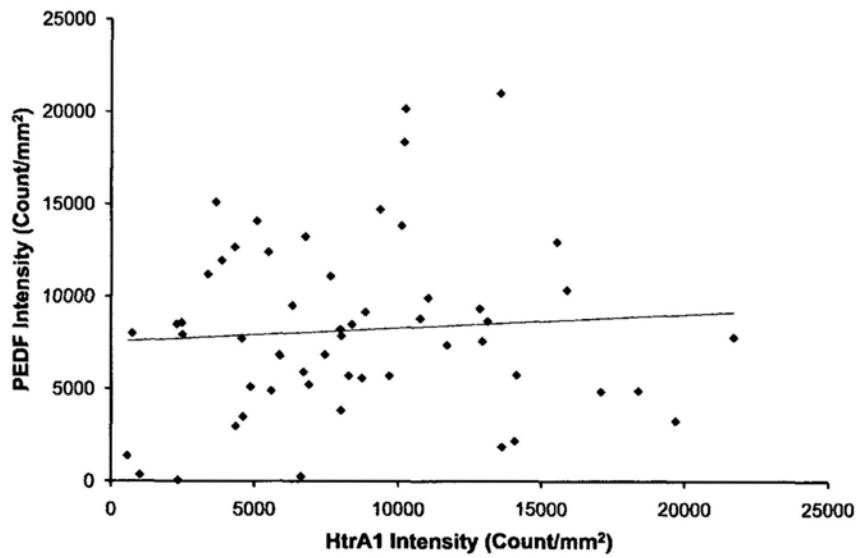
Figure 3.17: Correlation of vitreous levels of HtrA1, VEGF and PEDF.

The intensities of HtrA1, VEGF and PEDF for each sample in the same blotting experiment were quantified by Quantity One® Image Analysis software (BioRad) and correlated by Pearson's correlation coefficient test. **(A)** The vitreous level of HtrA1 was significantly associated with that of VEGF ($r = 0.650$, $p = 7.91 \times 10^{-8}$). There was no association for PEDF with VEGF **(B)** or HtrA1 **(C)** in human vitreous humor samples ($r = 0.023$, $p = 0.865$ and $r = 0.077$, $p = 0.575$, respectively).
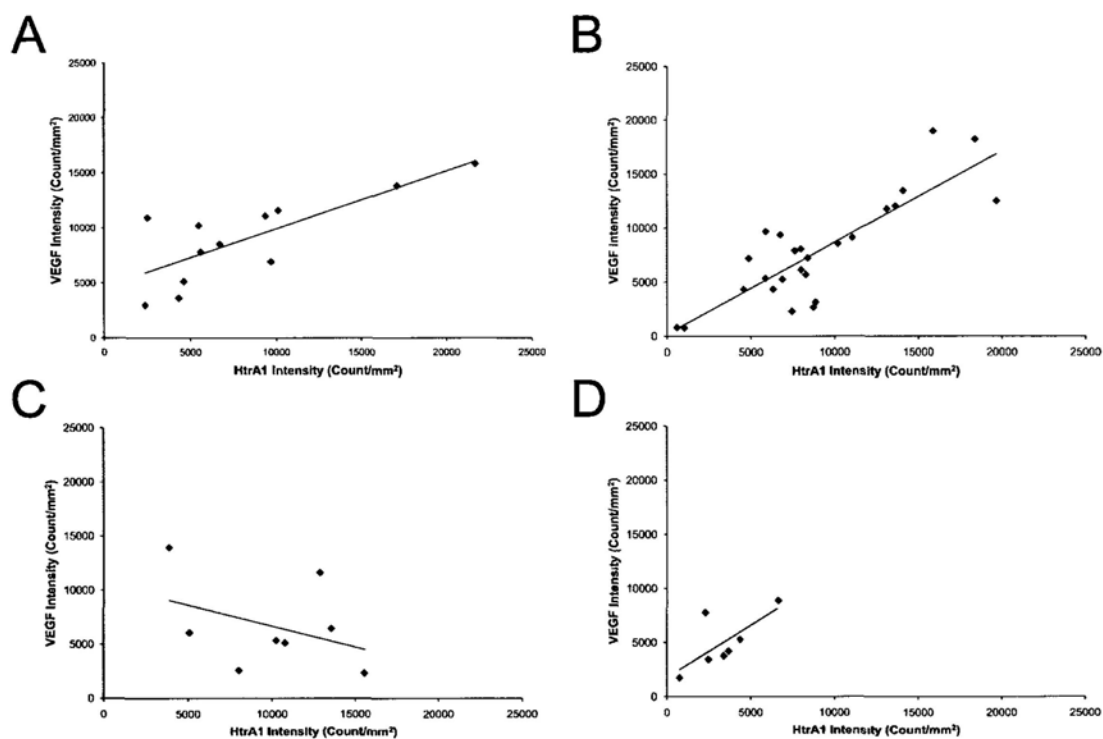
Figure 3.18: Correlation of vitreous levels of HtrA1 and VEGF in sub-clinical diagnosis.

The clinical diagnosis was categorized into 6 groups, including vascular diseases, retinal detachment, idiopathic macular hole, traumatic injury, ERM and IOL. The group with less than 6 patients (others: ERM and IOL) was excluded from the analysis. Vitreous HtrA1 levels were positively associated with vitreous VEGF levels in **(A)** retinal detachment (Pearson's correlation coefficient test; $r = 0.835$, $p = 2.14 \times 10^{-7}$) and mildly in **(B)** vascular diseases (Pearson's correlation coefficient test; $r = 0.778$, $p = 0.003$). However, no association was observed in **(C)** macular hole and **(D)** traumatic injuries (Pearson's correlation coefficient test; $r = -0.390$, $p = 0.340$ and $r = 0.706$, $p = 0.077$, respectively).
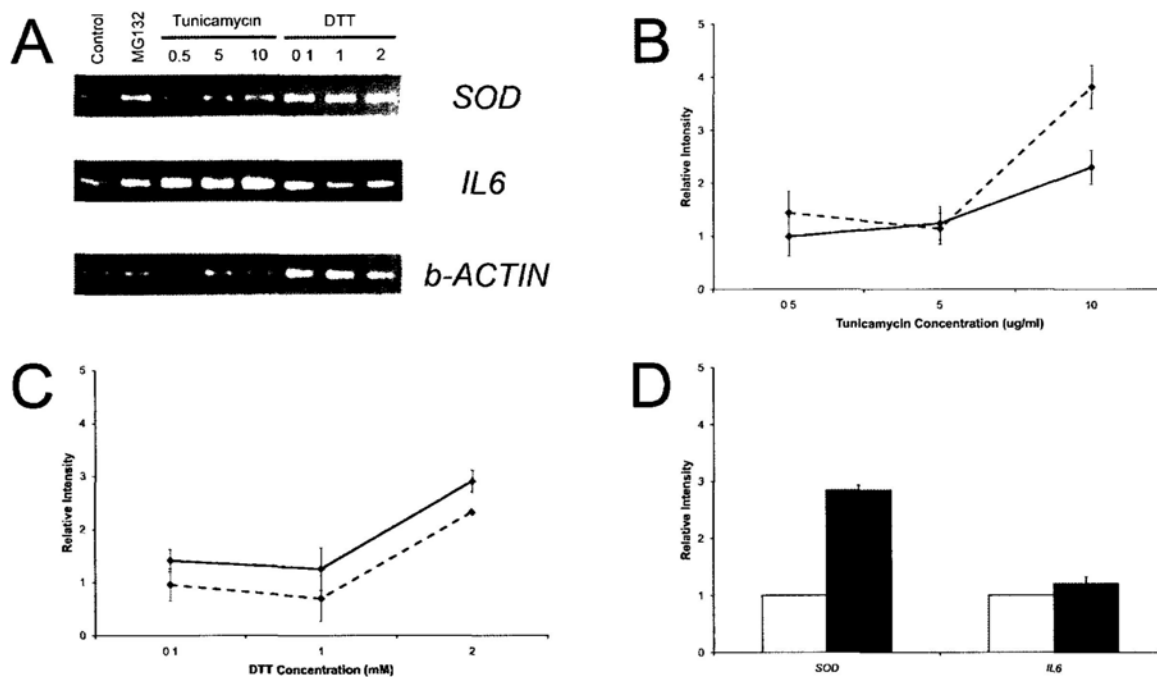
Figure 3.19: *SOD* and *IL6* expression analysis of human fetal RPE cells under cell stress response.

Confluent human fetal RPE cells were treated with tunicamycin (0.5, 5 and 10 μg/ml), DTT (0.1, 1 and 2 mM) and MG132 (10 μM) for 18 hours. Total RNA was collected and reverse-transcribed. **(A)** The gene expression levels of *SOD*, *IL6* and *β-ACTIN* were analyzed by semi-quantitative PCR. The intensities of gene expressions for the treated groups relative to that of control were presented. All 3 chemicals induced stress reponse as shown by upregulation of *SOD* **(B–D)**, whereas inflammation response could only be induced in tunicamycin and DTT treatments as shown by upregulation of IL6 **(B, C)**. **(B, C)** Solid line: relative intensities of SOD expression; Dotted line: relative intensities of IL6 expression. **(D)** White bar: relative intensities of gene expressions in control; Black bar: relative intensities of gene expressions in MG132 treatment.

125
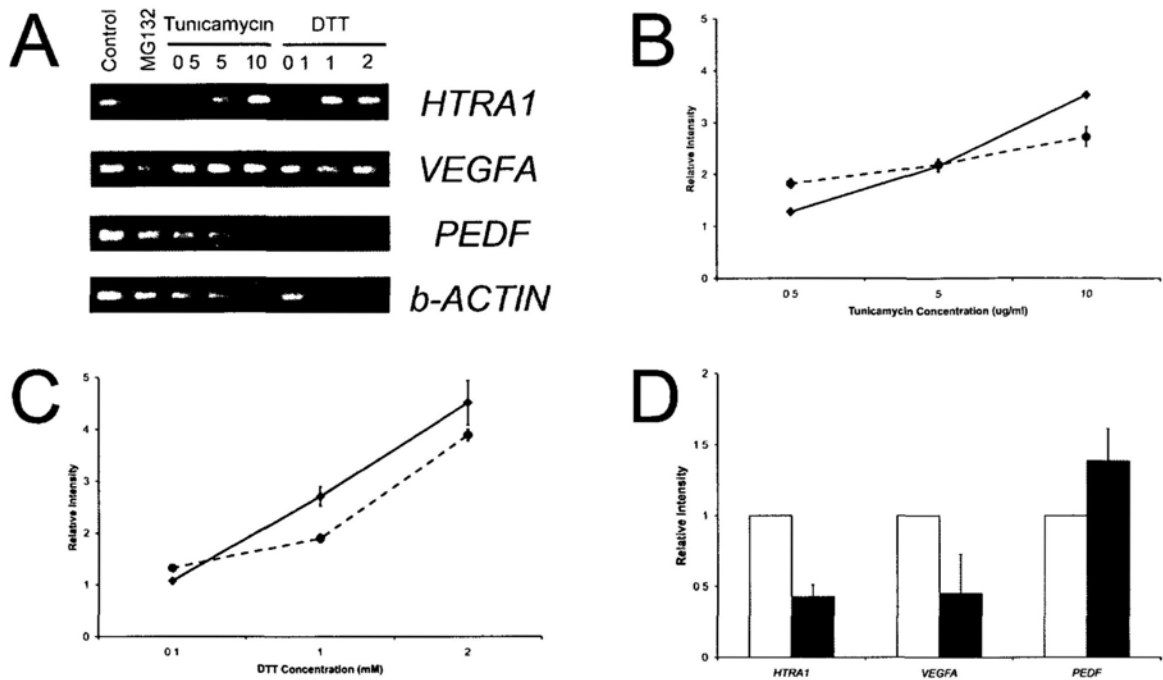
Figure 3.20: *HTRA1*, *VEGFA* and *PEDF* expression analysis of human fetal RPE cells under cell stress response.

(A) The gene expression levels of *HTRA1*, *VEGFA*, *PEDF* and *βACTIN* were analyzed by semi-quantitative PCR. The intensities of gene expressions for the treated groups relative to that of control were presented. The *HTRA1* and *VEGFA* expressions also showed a dose-dependent increase from 0.5 to 10 µg/ml tunicamycin and 0.1 to 2 mM DTT treatments **(B and C)**. For 10 µM MG132 treatment, *HTRA1* expression showed a time-dependent decrease and reached more than 2-fold reduction at 18 hours **(D)**. **(B, C)** Solid line: relative *HTRA1* expression intensities; dotted line: relative *VEGFA* expression intensities. **(D)** White bars: relative gene expressions in control; black bars: relative gene expressions in MG132 treatment. Mean ± SD was presented.
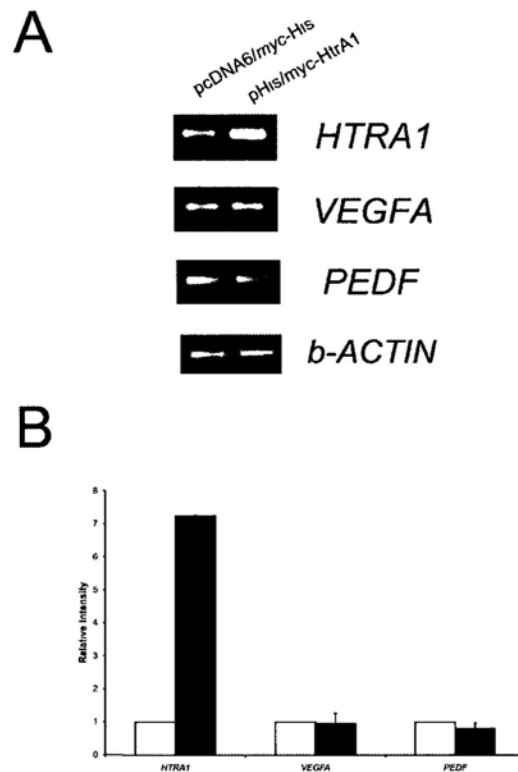
Figure 3.21: Gene expression analysis of human fetal RPE cells transfected with pHis/myc-HtrA1 construct.

Human fetal RPE cells were transfected with pHis/myc-HtrA1 and incubated for 24 hours before gene expression analysis. Total RNA was collected and reverse-transcribed. The gene expression levels of *HTRA1*, *VEGFA*, *PEDF* and *β-ACTIN* were analyzed by semi-quantitative PCR. Agarose gel-resolved PCR products were shown in **(A)** and the band intensities were shown in **(B)**. The HtrA1-transfected cells showed 7.2-fold elevated *HTRA1* expression compared to the empty vector control, suggesting HtrA1 overexpression. *VEGFA* (0.96-fold) and *PEDF* (0.81-fold) expressions in the HtrA1-transfected cells were not altered compared with that in the empty vector-transfected cells at 24 hours. **(B)** White bars: relative gene expression intensities for empty vector control; black bars: relative gene expression intensities for HtrA1-transfected cells. Mean ± SD was presented.

Figure 3.22: Gene expression analysis of vascular endothelial growth factor-treated human fetal RPE cells.

Human fetal RPE cells were treated with 10 ng/ml recombinant human VEGF for 24 hours before gene expression analysis. Total RNA was collected and reverse-transcribed. The gene expression levels of *HTRA1, VEGFA, PEDF* and *β-ACTIN* were analyzed by semi-quantitative PCR. Agarose gel-resolved PCR products were shown in **(A)** and the band intensities were shown in **(B)**. The expressions of *HTRA1* (0.94-fold), *VEGFA* (1.03-fold) and *PEDF* (1.12-fold) in VEGF-treated cells were not different from that in untreated control. **(B)** White bars: relative gene expression intensities for untreated control; black bars: relative gene expression intensities for VEGF-treated cells. Mean ± SD was presented.
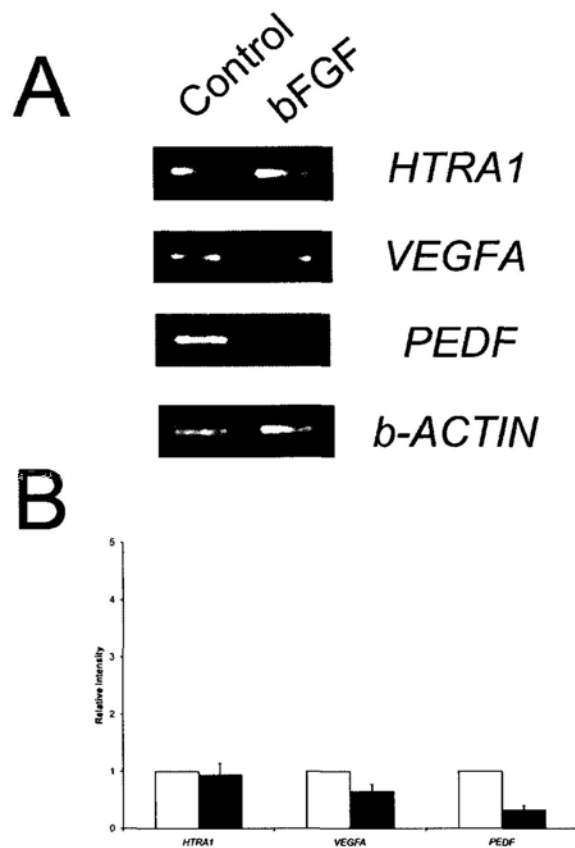
Figure 3.23: Gene expression analysis of basic fibroblast growth factor-treated human fetal RPE cells.

Human fetal RPE cells were treated with 10 ng/ml recombinant human bFGF for 24 hours before gene expression analysis. Total RNA was collected and reverse-transcribed. The gene expression levels of *HTRA1*, *VEGFA*, *PEDF* and *β-ACTIN* were analyzed by semi-quantitative PCR. Agarose gel-resolved PCR products were shown in **(A)** and the band intensities were shown in **(B)**. The expressions of *HTRA1* (0.93-fold) and *VEGFA* (0.64-fold) in bFGF-treated cells were not altered compared to that in untreated control. Rather, the *PEDF* expression level was reduced by 3 folds in the bFGF-treated cells compared with the untreated control. **(B)** White bars: relative gene expression intensities for untreated control; black bars: relative gene expression intensities for bFGF-treated cells. Mean ± SD was presented.
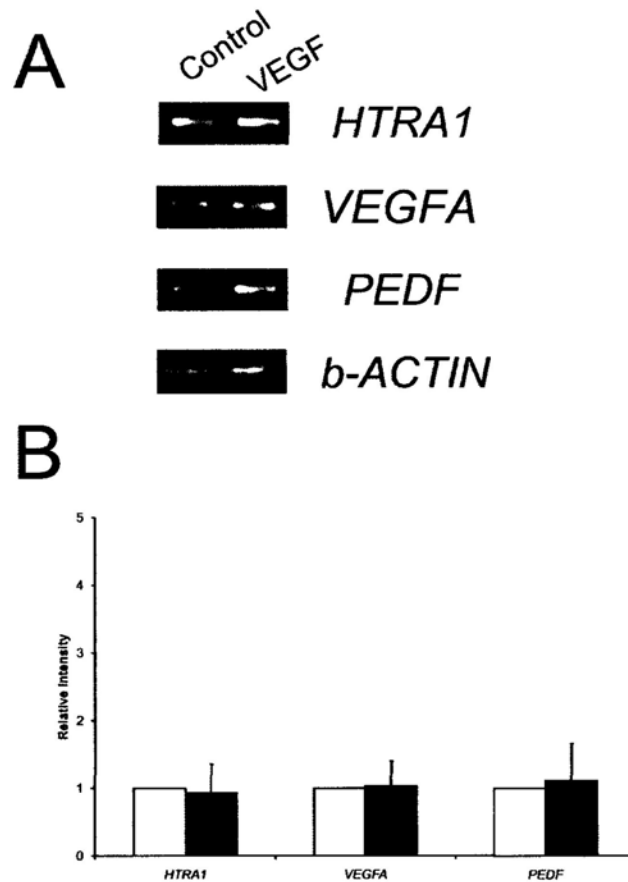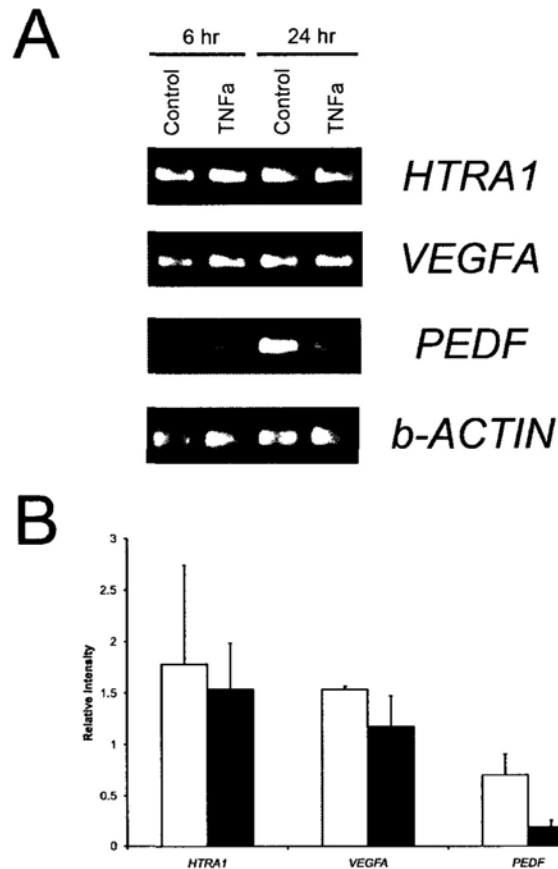
Figure 3.24: Gene expression analysis of tumor necrosis factor α-treated human fetal RPE cells.

Confluent human fetal RPE cells were treated with 10 ng/ml recombinant human TNFα for 6 or 24 hours. Total RNA was collected and reverse-transcribed. The gene expression levels of *HTRA1*, *VEGFA*, *PEDF* and *βACTIN* were analyzed by semi-quantitative PCR. Agarose gel-resolved PCR products were shown in **(A)** and the intensities of gene expressions for the treated groups relative to that of control were presented **(B)**. *PEDF* expression showed a time-dependent decrease and reached more than 5-fold reduction at 18 hours **(A and B)**. The changes of HTRA1 and VEGF expressions were not different in TNFα-treated cells compared to untreated control at 6 or 24 hours **(A and B)**. **(B)** White bars: relative gene expression intensities in 8-hour treatment; black bars: relative gene expression intensities in 18-hour treatment. Mean ± SD was presented.

130
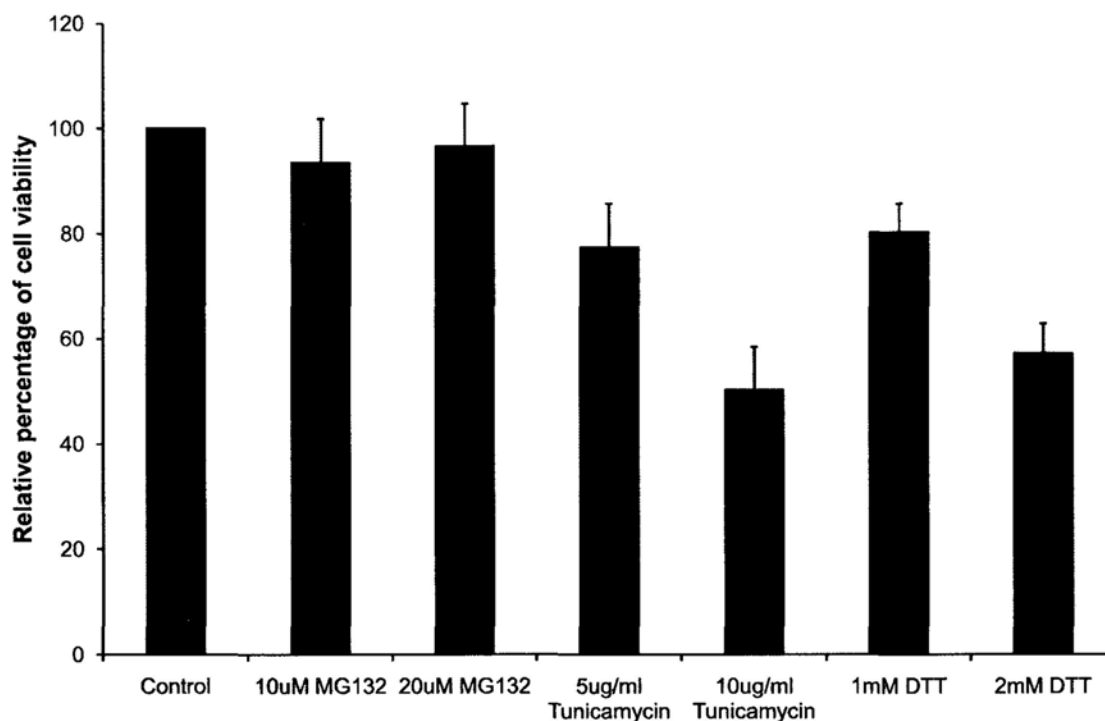
Figure 3.25: Cell survival analysis of human fetal RPE cells treated with cellular stress inducers.

MTT assay was performed on human fetal RPE cells treated with cellular stress inducers, tunicamycin, DTT and MG132. An excitation wavelength of 570 nm with reference 650 nm was measured by spectrophotometery. The percentage of cell viability was expressed as OD_{570} of treated-human fetal RPE cells / OD_{570} of untreated human fetal RPE cells. Human fetal RPE cells treated with 5 and 10 μg/ml of tunicamycin had a mean of 22.6% and 49.7% reduction of MTT signal, respectively, while human fetal RPE cells treated with 1 and 2 mM of DTT had a mean of 19.8% and 42.9% reduction of MTT signal, respectively, compared to the untreated control. In contrast, human fetal RPE cells treated with 10 and 20 μM of MG132 had only a mean of 6.5% and 3.4% reduction of MTT signal, respectively. Mean ± SD was presented.

Chapter 4: Discussion

4.1 *CFH* and age-related macular degeneration

Complement factor H (*CFH*), located on chromosome 1q31, is the first AMD-associated gene identified by GWAS (Klein RJ et al, 2005; Edwards AO et al, 2005; Haines JL et al, 2005). In this study, a different distribution pattern of *CFH* polymorphisms was found in Chinese when compared to other populations. The initial variant changing tyrosine 402 to histidine (Tyr402His; rs1061170, T>C) in *CFH* was suggested to be a possible risk factor in Caucasian populations. However, no association between Tyr402His and exudative AMD was observed in Hong Kong Chinese population. The discrepancy could be due to the differences in the minor allele frequency (C allele) in control subjects, which was about 38% in Caucasian (**Table 1.1**), but was 2.9% in Chinese (**Table 3.1**). Despite the lack of association of AMD with Tyr402His in Asian populations (**Table 1.1**), the contribution of Tyr402His to AMD pathogenesis could still be possible since Tyr402His change decreased the binding affinity for C-reactive protein (Yu J et al, 2007), which affected the negative control of CFH on the alternative complement pathway for innate immunity and inflammation (Donoso LA et al, 2006). In this study, a clear contribution of Tyr402His for the association with AMD could be observed if Tyr402His was considered together with other variants (**Table 3.2**). When Tyr402His was removed from the analysis, the percentage of *CFH* variant in exudative AMD patients would not be significantly different from that in control subjects (**Table 3.2**). This further supports a role of Tyr402His in AMD genetics, not only in Caucasian, but also in Chinese. Realistically, a balanced view could be portayed when the genotyping could be extended into a larger cohort, together with a deeper understanding of the role of *CFH* on AMD development.

Apart from Tyr402His, 2 completely linked SNPs (rs551397 and rs800292), located in intron 1 and exon 2 of *CFH*, were significantly associated with exudative AMD (p = 0.00056; **Table 3.1**). Coherent result could be found in a fine-scale LD mapping of AMD in the *CFH* gene region, which indicated a point location for a causal variant between exons 1 and 2 of the *CFH* gene (Ennis S et al, 2007). This provided strong evidence that *CFH* is an AMD-associated gene in Chinese population.

4.2 *HTRA1* and age-related macular degeneration

Chromosome 10q26 region is the second locus identified to be associated with exudative AMD by GWAS in the Hong Kong Chinese population (Dewan A et al, 2006). There are 3 genes located within this region, including pleckstrin homology domain containing family A (phosphoinositide binding specific) member 1 gene (*PLEKHA1*), *LOC387715* and *HTRA1*. The AMD-associated SNPs were the rs10490924 in *LOC387715* and rs11200638 in *HTRA1*, which are in complete LD. Therefore, *LOC387715* and *HTRA1* were suggested to be a potential disease-causing gene in this 10q26 region. However, there are debates arguing which gene would be the potential causative gene.

LOC387715 was initially suggested to be the disease-causing gene as rs10490924 (Ala69Ser) in *LOC387715* was demonstrated to be the most significantly associated SNP from a genetic study in a Caucasian population (Kanda A et al, 2007). Moreover, the LOC387715 protein with Ala69Ser substitution shows more association with the cytoskeleton as compared to the wildtype protein in COS7 cells (Wang G et al, 2009). Furthermore, a deletion-insertion (indel) polymorphism in *LOC387715* gene (c.372_815del443ins54) removes the polyadenylation signal of *LOC387715* transcript, which leads to rapid mRNA turnover (Fritsche LG et al, 2008). This variant is analogous to the loss of function of *LOC387715* gene, a potent contribution to the disease mechanism.

However, this indel polymorphism has no correlation with *LOC387715* mRNA levels in human retina and blood samples in independent studies (Wang G et al, 2010). In addition, haplotype analysis shows that the indel (c.372_815del443ins54) in *LOC387715* gene lies in the same strand of chromatid with the risk A allele of rs11200638 (Yang Z et al, 2010), indicating this indel is located on the risk haplotype. Furthermore, a nonsense mutation (Arg38X) in *LOC387715* was identified in the opposite strand of the indel (protective haplotype). This leads to loss of *LOC387715* mRNA as well (Yang Z et al, 2010). Since the variants in both risk and protective haplotypes results in the same effect of mRNA reduction, the *LOC387715* gene might not be the causative gene in this 10q26 region. Rather, the indel (c.372_815del443ins54) in *LOC387715* enhances the expression of *HTRA1* (Yang Z et al, 2010).

In this study, the association between rs11200638 and exudative AMD was studied with a larger cohort than the initial GWAS study (**Table 3.3**) with more exudative AMD patients (n = 163) and control subjects (n = 183). This risky SNP of *HTRA1* (rs11200638) appears to interact additively with rs800292 of *CFH* to increase the risk of exudative AMD by 23.3 folds, suggesting a high impart of the additive contributions of *HTRA1* and *CFH* in the development of exudative AMD. Moreover, rs11200638 of *HTRA1* also interacted additively with smoking (OR = 15.7), further suggesting the important role of the environmental risk factor in the multi-factorial AMD.

Three *HTRA1* variants, located in exon 1, were discovered (**Figure 3.1**). When all three variants were grouped, they are present more in control subjects than the exudative AMD patients (**Table 3.4**), indicating, in term of genetics, a protective effect. Among these 3 variants in *HTRA1*, 34delCinsTCCT alone was significantly associated with exudative AMD. To validate the importance of this variant, a total of 390 control subjects, twice as that of exudative AMD patients, were genotyped for 34delCinsTCCT. Eight percent of

control subjects was found to carry at least 1 allele of 34delCinsTCCT, which was much higher than 1.2% observed in exudative AMD patients (**Table 3.5**). Although the frequency of this variant suggested a protective effect, the haplotype of 34delCinsTCCT with rs11200638 has to be confirmed. Using allele-specific primer, the variant allele (delCinsTCCT) of 34delCinsTCCT was shown to share the same haplotype with the wildtype G allele of rs11200638 while the wildtype C allele of 34delCinsTCCT was in the same haplotype with the risk A allele of rs11200638 (**Figure 3.2**). This indicated that the variant allele was resided in the protective haplotype, but not in the risk haplotype with A allele of rs11200638. This further confirmed the protective effect of 34delCinsTCCT in control subjects. Therefore, it could be postulated that *HTRA1* gene can be a potential disease-causing gene in this AMD-associated 10q26 region.

Although the 34delCinsTCCT in *HTRA1* gene were validated to be protective genetically, there were 2 exudative AMD patients carrying this variant. One patient carried one allele of *CFH* Tyr402His variant and was a smoker, while the other patient carried one allele of *CFH*-associated Ile62Val SNP. This suggested that they carried the risk factor in *CFH* gene. Also this further indicated that AMD is a complex, polygenic and multi-factorial disease, and even carrying a protective factor, like 34delCinsTCCT in *HTRA1*, might not reduce the risk of AMD development.

4.3 The choice of retinal pigment epithelial cells

In AMD pathology, the occurrence of AMD involves RPE cells, endothelial cells in choroid, macrophages and acellular Bruch's membrane. RPE cells are damaged by the presence of excess drusen while vessels from the choroid penetrate through the Bruch's membrane and grow into the fovea (reviewed in de Jong PT, 2006). There are a few important observations on the HtrA1 associated with AMD. Firstly, HtrA1 mRNA and

protein were elevated in cells with AMD-associated risk A allele of rs11200638 than that with the wildtype G allele (Dewan A et al, 2006; Yang Z et al, 2006). Secondly, enhanced expression of HtrA1 attenuated ovarian cancer cell mobility and inhibited cell migration (Chein J et al, 2009b), while ectopic expression of HtrA1 attenuated trophoblast cell migration and invasion (Ajayi F et al, 2008). Furthermore, blood vessels started to invade into the cartilaginous condensations and ossification when HtrA1 expression was significantly upregulated (Tocharus J et al, 2004). All these results indicate that cells with high levels of HtrA1 will not participate in direct invasion or migration, suggesting that invading endothelial cells and macrophages do not express high levels of HtrA1. In addition, the cells expressing high levels of HtrA1 attract blood vessel invasion; therefore, RPE cells could be the one responsible for the elevated expression of HtrA1 in AMD. This hypothesis could be tested by the observation of elevated HtrA1 proteins in RPE cells from patients with AMD (Chan CC et al, 2007; Tuo J et al, 2008). Furthermore, endogenous *HTRA1* mRNA expression was detected in both ARPE-19 and primary human fetal RPE cells (**Figure 3.7** and **Figure 3.21**), indicating the presence of HtrA1 in the RPE, although HtrA1 protein in RPE cells was not detectable by immunoblotting (**Figure 3.8**). Therefore, RPE cells were chosen for the HtrA1 functional analysis in this study.

Recommended by American Type Culture Collection (Manassas, VA), ARPE-19 cells should be applied as a transfection host (Dunn KC et al, 1996). Therefore, *HTRA1* transfection studies were performed in ARPE-19 cells. For treatment purpose, it would be more suitable to use a primary RPE cell culture rather than ARPE-19 cell line (Geisen P et al, 2006). Therefore, previously established primary human fetal RPE cells (Choy KW et al, 2006) were selected as a platform to analyze the cell stress effect and angiogenic factor treatments on *HTRA1* and *VEGFA* expressions.

4.4 Localization of recombinant human HtrA1 protein

HtrA1 was initially suggested to be a secreted protein because of the presence of the signal peptide and extracellular protein (Hu SI et al, 1998). In this study, the secretory nature of HtrA1 protein was verified since the recombinant human HtrA1 protein tagged with *myc* and polyhistidine was detected in the medium from the HtrA1-transfected ARPE-19 cells by immunoprecipitation coupled with immunoblotting (**Figure 3.13**). Nevertheless, immunocytochemistry showed a haze of fluorescence signal outside the transfected cells (**Figure 3.10**), indicating a pattern of extracellular protein (Gilicze A et al, 2007; Ajayi F et al, 2008).

In addition to the extracellular HtrA1 protein, intracellular localization of HtrA1 was also reported (De Luca A et al, 2004a; Clawson GA et al, 2008; Chien J et al, 2009b). Coherently, in this study, a strong intracellular immunofluorescence signal was observed within the HtrA1-transfected ARPE-19 cells (**Figure 3.10**). The juxtanuclear localization pattern of recombinant HtrA1 in ARPE-19 cells was similar to the reported perinuclear staining for HtrA1 in a human cervical cancer CaSki cell line (Clawson GA et al, 2008). The prominent juxtanuclear fluorescence signal of HtrA1 suggested a Golgi-related localization. Dual immunofluorescence studies showed that the HtrA1 protein is associated with the Golgi apparatus since it co-localizes with the Golgi markers, giantin or TGN38 (**Figure 3.11A** and **Figure 3.11B**). As the trajectory of secretory proteins starts from ribosome, ER, Golgi apparatus to secretory vesicles, the co-localization of HtrA1 with Golgi should represent an intermediate stage. This result suggests that HtrA1 may be tightly associated with Golgi for its maturation and assembly, or its specific role in Golgi function. This may involve the PDZ domain of HtrA1, which was shown to bind GM130, a *cis*-Golgi matrix golgin subfamily protein (Murwantoko et al, 2004). Thus, HtrA1 may have dual functions as an extracellular protein (**Figure 3.13**) and Golgi-associated protein.

Recently, the proteolytic domain of HtrA1 was reported to bind to tubulin family of proteins (Chien J et al, 2009a) as HtrA1 was shown to co-localize with tubulins in ovarian cell lines (Chien J et al, 2009b). Surprisingly, in this study, the recombinant human HtrA1 does not co-localize with β-tubulin in transfected ARPE19 cells (**Figure 3.11F**). This difference could be due to different cell types used in the analysis. Apart from the microtubule-like localization, perinuclear and nuclear staining of endogenous HtrA1 was shown in human cervical cancer CaSki cells, embryonic kidney 293-T cells and hepatocyte cells (Clawson GA et al, 2008). Furthermore, HtrA1 was shown to localize in the cytosol of placental cells (De Luca A et al, 2004a). These reports further support HtrA1 in different cell types may have different subcellular localizations.

Unlike HtrA2, HtrA1 does not possess a mitochondrial localization signal. As expected, the HtrA1 protein does not co-localize with the mitochondrial marker, cytochrome C (**Figure 3.11E**).

4.5 HtrA1 variant protein

From sequencing analysis in this study, *HTRA1* gene was postulated to be a potential disease-causing gene in the AMD-associated 10q26 region because a protective variant (34delCinsTCCT) in *HTRA1* gene was discovered to be more prevalent in control subjects. This genetic observation requires further proteomic and functional analyses to confirm its relevance to AMD.

The *HTRA1* variant (34delCinsTCCT) results in an insertion of a serine residue at position 12th of the encoded HtrA1 protein (**Figure 3.6**) without altering the open reading frame and the critical arrangement of the leucine residues (shifted from position 12th to 13th). Immunoblotting analysis shows that the recombinant human HtrA1 variant protein obtained from transfection in ARPE-19 cells shares a similar molecular weight of about 53 kDa with

the wildtype HtrA1 protein (predicted size of 51 kDa; Hu SI et al, 1998). The immuno-detection of recombinant HtrA1 variant protein by commercial certified anti-HtrA1 antibody indicated that it has correct transcription and translation. Since the first 22 amino acids were suggested to be the signal peptide for secretion (Hu SI et al, 1998), the insertion of serine at position 12th might exert effect on the signal peptide. Bioinformatics analysis suggests that insertion of a serine residue in the leucine-rich signal peptide could reduce the overall hydrophobicity. This may alter the conformation and assembly of signal peptide (**Figure 3.3**).

This study shows that the HtrA1 variant exhibits differences in subcellular localization and secretion as compared to the wildtype protein. The wildtype and variant recombinant proteins were shown to share 90% similarity in subcellular localization. Both proteins had a predominant Golgi localization (**Figure 3.11A** and **Figure 3.11B**). However, more cells expressing HtrA1 variant protein (~ 8%) showed a partial co-localization with Golgi and ER as compared to the wildtype HtrA1-expressing cells (~ 2%) (**Figure 3.12**). Furthermore, the variant protein shows more significant co-localization with the ER marker, Bip, than the wildtype protein, suggesting that the serine insertion in the signal peptides enhances ER retention.

Could the differences between ER and Golgi association alter the secretory properties of the wildtype and variant proteins? Using anti-polyhistidine antibody, secreted His-tagged HtrA1 protein was immunoprecipitated from the culture medium of transfected ARPE-19 cells. **Figure 3.13** shows that the amount of secreted HtrA1 variant was much less than that of wildtype protein at 18 hours post-transfection, indicating the insertion of the serine residue may affect the secretion of recombinant HtrA1 variant (**Figure 3.13**). This may due to its retention in ER.

As proteins are modular in nature and function by independent domain, the changes in the signal peptide domain should not have influence on the proteolytic domain of HtrA1 protein. To validate this hypothesis, the ability of recombinant HtrA1 protein to digest β-casein was assessed (Grau S et al, 2006). Both recombinant wildtype and variant of HtrA1 were shown to digest β-casein (**Figure 3.9B**), suggesting that both proteins maintain their serine protease activities. In addition, the proteolytic rate, indicated by the rate of accumulated cleaved products, was similar between wildtype and variant (**Figure 3.9C**). This result suggests that the inserted serine in the signal peptide will not affect the activity of the proteolytic domain. However, whether the prolong ER retention and slower secretion rate with unaltered protease activity for the variant protein will affect the survival of the RPE cells is unknown.

Overexpression of *HTRA1* reduced the proliferative activity of metastatic LM cells and also their ability to invade extracellular matrix *in vitro* as well as retarded growth and metastases *in vivo* in nu/nu mice (Baldi A et al, 2002). Moreover, downregulation of *HTRA1* in SKOV3 ovarian cell line by RNA interference promoted the anchorage-independent growth while exogenous expression of HtrA1 in OV202 ovarian cell line induced a serine protease-dependent cell apoptosis (Chien J et al, 2004). These reports suggested that HtrA1 has a role in the regulation of cell growth in cancers, which depends on the active site of serine 328 residue in the catalytic triads (Chien J et al, 2004). In this study, overexpression of recombinant human wildtype HtrA1 in ARPE-19 cells reduced the cell viability by more than 30% compared to the empty vector (**Figure 3.14**). Furthermore, these cells had a 2.7-fold higher apoptotic rate than vector-only cells (**Figure 3.15**). These provided evidences that HtrA1 has a general effect on regulating cell growth in normal and tumor cells. Higher expression of HtrA1 could also trigger RPE cell death (**Figure 3.25**), which is a pathological observation in AMD (reviewed in de Jong PT, 2006). However, in this study,

ARPE-19 cells overexpressing recombinant HtrA1 variant had about 2-fold higher cell viability (**Figure 3.14**) and a lower apoptotic rate (**Figure 3.15**) than cells expressing wildtype protein. Thus, the variant has a protective role in RPE cell survival. Furthermore, while the variant protein is retained in the ER, the wildtype HtrA1 was more localized in the Golgi (**Figure 3.12** and **Figure 3.13**). It will be interesting to determinie whether the reduced viability and increased apoptosis is associated with Golgi-mediated cell death process (Walker A et al, 2004) and/or the extracellular role of secreted HtrA1 protein.

4.6 Vitreous levels of HtrA1 and VEGF

By the immunoblotting analysis using specific antibodies, HtrA1, VEGF and PEDF protein in human vitreous humor were detected (**Figure 3.16**). The intensity of HtrA1, VEGF and PEDF immunoreactive signal was measured by image analysis software and compared with each other in one experiment (same protein electrophoresis and blotting). Since the comparison between HtrA1, VEGF and PEDF was performed within individual vitreous samples, normalization with housekeeping protein was not required since equal amount of total protein of each sample was applied for immunoblot.

A significantly positive co-relationship between HtrA1 and VEGF expression in human vitreous humor was observed (**Figure 3.17A** and **Table 3.7**). This is similar to the observations in arthritis (HtrA1-associated disease; Hu SI et al, 1998; Grau S et al, 2006), rheumatoid and osteoarthritis where elevated synovial fluid levels of HtrA1 were found (Grau S et al, 2006). Interestingly, synovial fluid containing significant levels of VEGF were detected in patients with rheumatoid arthritis (Lee SS et al, 2001). Thus, both HtrA1 and VEGF are probably upregulated in rheumatoid arthritis condition. It will be interstingto discover whether similar trend of HtrA1 and VEGF expressions can be found in Alzheimer's disease. Nevertheless, HtrA1, which colocalizes with β-amyloid deposits in

141

human brain samples, was upregulated in patients with Alzheimer's disease (Grau S et al, 2005). And, VEGF behaves similarly (Tarkowski E et al, 2002; Yang SP et al, 2004). This observation suggests the association of HtrA1 and VEGF is not only unique in human vitreous humors, but also occurring in other system.

4.7 Vitreous levels of HtrA1 and rs11200638 genotype

Individuals carrying AA genotype of rs11200638 had higher HtrA1 expression in both mRNA and protein level in the eyes and leukocytes compared to that with GG genotype (Yang Z et al, 2006; Tuo J et al, 2008). However, no association between vitreous HtrA1 level and rs11200638 genotype was found (**Table 3.8**). One possible explanation was that the effect of vascular and inflammatory disease conditions regulating HtrA1 expression might counteract with the effect of rs11200638 genotype on HtrA1 expression. Since the recruited patients possessed different clinical situations, the calculation of the association between vitreous HtrA1 levels and rs11200638 genotype was not adjusted by the clinical diagnosis. Even if the clinical diagnosis was adjusted, there would not be enough power to detect the association (type II error) or the results could be false negative (type I error) as the number of patients was low. Therefore, the comparison of vitreous HtrA1 levels among different rs11200638 genotypes based on same clinical diagnosis was not feasible, and only a general trend of association could be obtained.

4.8 Cell stress, inflammation and age-related macular degeneration

Over the lifetime, RPE is exposed to high levels of oxidative and photo-oxidative damage due to intense light exposure, high metabolic activity and oxygen consumption (Beatty S et al, 2000). Moreover, the age-related thickening of Bruch's membrane and accumulation of drusen impair the choroidal-RPE hemodynamics and lead to potential

hypoxic conditions (Ambati J et al, 2003). Furthermore, age-related accumulation of RPE lipofuscin in lysosomes prevents healthy autophagy of old mitochondria, leading to an increased oxidative stress because of mitochondrial production of hydrogen peroxide (Terman A et al, 2007). In addition, the primary components of RPE lipofuscin, the autofluorescent pigment N-retinylidene-N- retinylethanolamine (A2E), could create light-induced oxidative stress and bleach the cell membrane (Delori FC et al, 2001; Sparrow JR and Boulton M, 2005). Collectively, oxidative stress could inactivate chaperones, promote aberrant disulphide bond formation, promote stabilization of undesirable intermediates and inhibit degradation of misfolded proteins, which together impair the unfolded protein response and induce the ER stress (Marciniak SJ and Ron D, 2006; Banhegyi G et al, 2007). Misfolded protein-induced ER stress in the RPE and/or choroid could be a primary pathogenic mechanism leading to chronic oxidative stress, complement deregulation and AMD (Sauer T et al, 2008; Libby RT and Gould DB, 2010).

AMD has long been suggested to be associated with inflammation as higher serum C-reaction protein levels was found in patients with advanced AMD than those without AMD (Seddon JM et al, 2004), and mouse knockout model of inflammatory chemokine Ccl-2 develops the phenotypes of AMD (Ambati J et al, 2003). In this study, the association of inflammation with AMD was further supported by the association of *CFH* gene with exudative AMD in Hong Kong Chinese cohort (**Table 3.1**). Moreover, a positive association between vitreous HtrA1 and VEGF levels was found in retinal detachment (**Figure 3.18**), which is related to the inflammatory and stress responses (Zacks DN et al, 2006; Hollborn M et al, 2008). Complement factors, C3a and C5a, upregulate VEGF in RPE cells (Nozaki M et al, 2006). Furthermore, VEGF immunoreactivity is greater in inflammatory active CNV than inactive one (Grossniklaus HE et al, 2002). In addition, *HTRA1* is genetically associated with geographic atrophy (Cameron DJ et al, 2007) and

HtrA1 protein is detectable in the drusen (Yang Z et al, 2006; Tuo J et al, 2008). These further suggest HtrA1 and VEGF could be associated with inflammation, a pathogenic condition in AMD.

In this study, tunicamycin, DTT and MG132 were applied to induce cell stress. Tunicamycin is a glucosamine-containing nucleoside antibiotic generated by *Streptomyces*, and is an inhibitor of N-linked glycosylation by the formation of *N*-glycosidic protein-carbohydrate linkages (Mahoney WC and Duksin D, 1979). Tunicamycin specifically inhibits dolichol pyrophosphate-mediated glycosylation of asparaginyl residues of glycoproteins (Olden K et al, 1979), leading to the presence of the unfolded protein and the induction of the ER stress (Lee AS, 2001; Patil C and Walter P, 2001). DTT is a reducing agent (Cleland WW, 1964), which prevents intramolecular and intermolecular disulfide bonds formation between cysteine residues of proteins (Ruegg UT and Rudinger J, 1977). Similar to tunicamycin, DTT induces unfolded protein response, resulting in the ER stress (Lemin AJ et al, 2007). MG132 is a substrate analogue and a potent transition-state inhibitor primarily for the chymotrypsin-like activity of the proteasome (Rock KL et al, 1994; Lee DH and Goldberg AL, 1996), which is responsible for 80 – 90% protein breakdown occurred in most cultured mammalian cells under optimal nutritional conditions (Lee DH and Goldberg AL, 1998). MG132-inhibited proteasome cannot perform protein degradation, which leads to an accumulation of undigested protein in the ER and this aggravated the ER stress (Szokalska A et al, 2009). In addition, proteasomal inhibition by MG132 also causes oxidative stress (Goldbaum O et al, 2006).

Expectedly, all the 3 chemicals induced cell stress, as shown by upregulation of *SOD* (**Figure 3.19**). Moreover, inflammatory response, indicated by *IL-6* upregulation (Leung KW et al, 2009), was also induced by tunicamycin and DTT (**Figure 3.19**). Cell stress induction by tunicamycin and DTT in a dose-dependent manner leads to upregulated

144

HTRA1 and *VEGFA* expressions in human fetal RPE cells (**Figure 3.20**). The upregulation of VEGF by tunicamycin or DTT treatments has been reported in ARPE-19 cell line (Abcouwer SF et al, 2002; Roybal CN et al, 2004; Koyama Y et al, 2008). This suggested that HtrA1 and VEGF may be regulated in the same manner upon cell stress and inflammation.

HtrA family belongs to the group of stress-related protein since DeP/HtrA in *E. coli* is required for abnormal protein removal and survival in high temperature (Strauch KL and Beckwith J, 1988; Lipinska B et al, 1988). Similarly, the human HtrA member, HtrA2, is upregulated in response to stress induced by heat shock and tunicamycin in mammalian cells (Gray CW et al, 2000). Moreover, Syrian hamster HtrA1 mRNA and protein are elevated in response to estrogen-induced oxidative stress (Zurawa-Janicka D et al, 2008). From this study, it is confirmed that human HtrA1 may be related to stress and inflammatory responses.

Cell viability of human fetal RPE cells was dose-dependently reduced under tunicamycin and DTT treatments (**Figure 3.25**). Analogous to the reduction in cell viability and increases in cell apoptosis in HtrA1-overexpressed ARPE-19 cells (**Figure 3.14** and **Figure 3.15**), the elevated *HTRA1* expression in the treatment of tunicamycin or DTT could be related to the decreased cell viability in human fetal RPE cells (**Figure 3.25**). It could be possible that stress-induced HtrA1 upregulation would trigger RPE cell death, a pathogenic mechanism in AMD (de Jong PT, 2006). This HtrA1-induced RPE cell death might be a disease-causing mechanism for AMD pathogenesis since damage to the RPE and a chronic aberrant inflammatory response may lead to geographic atrophy and/or the expression of VEGF (reviewed in D'Amico DJ, 1994; de Jong PT, 2006; Jager RD et al, 2008).

4.9 MG132 and HtrA1

Unexpectedly, downregulation of *HTRA1* and *VEGFA* expressions was observed in human fetal RPE cells under the treatment of MG132 (**Figure 3.20D**). It has been shown that MG132 could downregulate the expression of VEGF in cancers (Shibata A et al, 2002; Matsuo Y et al, 2010). Nevertheless, the downregulation might not be entirely due to the cellular stress response mediated regulation of HtrA1 and/or VEGF expression.

Proteasome, cathepsins and calpains are the direct targets of MG132 (Rock KL et al, 1994; Lee DH and Goldberg AL, 1996; Lee DH and Goldberg AL, 1998). Although there is no reported on the correlation of HtrA1 with cathepsins and calpains, cathepsins are potential candidate for AMD (Rakoczy PE et al, 2002; Im E and Kazlauskas A, 2007). Activation of zinc chelator-induced calpain has been shown to damage human RPE cells (Tamada Y et al, 2007). However, further analyses are needed to investigate whether HtrA1 has a role in AMD mediated by cathepsins and calpains. Proteasome has a vital role in controlling protein turnover, which is crucial in regulating growth and metabolism. The proteasome inhibitor MG132 might inhibit the degradation of these proteins, hence, affecting the related signaling pathways. Proteins degraded by proteasome include NFκB (p105), IκB, YY1, activating transcription factor 2, hypoxia-inducible factor 1, inducible cAMP early repressor, cyclins, cyclin-dependent kinase inhibitors, c-jun, c-fos, c-mos, E2A protein, p53, receptor-associated protein kinases, DNA topoisomerase and ornithine decarboxylase (reviewed in Lee DH and Goldberg AL, 1998). Among these proteins, NFκB may be important as the NFκB-dependent signaling pathway could regulate HtrA1 since the human papillomavirus type 16 E7 protein, which enhances NFκB activity (Eichten A et al, 2004), upregulates *HTRA1* (Clawson GA et al, 2008). There are few postulated roles of NFκB in AMD. Firstly, advanced glycation end products, which accumulate in RPE cells of AMD (Ishibashi T et al, 1998), activate NFκB and alter the gene expression involved in

146

cellular stress, resulting in apoptosis (Basta G et al, 2002; Howes KA et al, 2004). Secondly, intake of omega-3 long-chain polyunsaturated fatty acids, which alters prostaglandin synthesis, inhibits NFκB signaling (Komatsu W et al, 2003; Kaarniranta K and Salminen A, 2009). This results in protection against the prevalent advanced AMD (Klein R et al, 1991; Klein R et al, 1992; Cho E et al, 2001; Seddon JM et al, 2001). Therefore, HtrA1 could be biologically associated with AMD through NFκB-related mechanism.

However, *HTRA1* expression in human fetal RPE cells were not influenced by addition of TNFα (**Figure 3.24**), which trigger NFκB activation by causing phosphorylation of IκB (Li X et al, 1999). This agrees with the absence of NFκB binding site in the *HTRA1* promoter (Transcription Element Search System (TESS); http://www.cbil.upenn.edu/ cgi-bin/tess/tess). Despite the absence of direct regulation by NFκB, HtrA1 could be indirectly correlated with NFκB because NFκB regulates the expression of many genes involved in immune and inflammatory responses (Kopp EB and Ghosh S, 1995). They include pro-inflammatory cytokines, chemokines, enzymes that generate mediators of inflammation, immune receptors, and adhesion molecules that play a key part in the initial recruitment of leukocytes to sites of inflammation (reviewed in Barnes PJ and Karin M, 1997). Moreover, NFκB frequently functions together with other transcription factors that are also involved in the regulation of inflammatory and immune genes (Stein B and Baldwin AS, 1993; Stein B et al, 1993). Therefore, HtrA1 could be indirectly related to NFκB through other inflammatory pathways as *HTRA1* is an inflammation-associated gene (Cameron DJ et al, 2007).

Beside NFκB, the downregulation of *HTRA1* by MG132 could also be mediated by other candidates, one of which could be the serum response factor (SRF). *HTRA1* promoter has SRF transcription factor binding sites (Dewan A et al, 2006) for transcription activation (Chai J and Tarnawski AS, 2002). MG132 inhibits the DNA binding activity of SRF

(Sandbo N et al, 2005). Repression of SRF activity might have a negative effect on *HTRA1* expression. However, downregulation of *HTRA1* by MG132 could be a complex situation modulated by several mechanisms.

4.10 Mutual interaction of HtrA1 and VEGF

Until now, there is no report indicating the relationship of HtrA1 and VEGF. In this study, an association between HtrA1 and VEGF was observed in vitreous humors (**Figure 3.17A**) and human fetal RPE cells (**Figure 3.20**). However, neither overexpression of recombinant human HtrA1 nor exogenous addition of recombinant human VEGF altered the expression of *VEGFA* or *HTRA1*, respectively, in human fetal RPE cells (**Figure 3.21** and **Figure 3.22**). This suggests that they might not be mutually regulating each other. Their interaction could be indirectly related, which might be relevant to HtrA1-related molecules, such as Tgfβ, bFGF and IGF-I.

Firstly, HtrA1 binds to various Tgfβ family proteins, such as Tgfβ1, Tgfβ2, Bmp4, Gdf5 and activin, through its proteolytic domain, and subsequently inhibit Bmp4, Bmp2 and Tgfβ1 signaling (Oka C et al, 2004; Tocharus J et al, 2004). In RPE of maculae with AMD, expression of both VEGF and Tgfβ were significantly enhanced (Kliffen M et al, 1997). Moreover, Tgfβ2 stimulated the expression and secretion of VEGF in human RPE cells (Bian ZM et al, 2007). These reports suggested that HtrA1 might negatively regulate Tgfβ proteins, but Tgfβ positively regulates VEGF. Thus, HtrA1 may not interact with VEGF through TGFβ signaling.

Secondly, FGF signaling is necessary and sufficient for *HTRA1* expression in chick facial and forelimb mesenchyme (Ferrer-Vaquer A et al, 2008) although HtrA1 does not bind to FGF-2 (Oka C et al, 2004). Similarly, FGF signaling is sufficient but not required for *HtrA1* transcription in *Xenopus* embryos (Hou S et al, 2007). In photocoagulated human

RPE cells, expression of both VEGF and bFGF were increased (Ogata N et al, 2001). Moreover, bFGF increased the L-type calcium channel activity of RPE cells, resulting in an increase of VEGFA secretion from RPE cells (Rosenthal R et al, 2005). This implies that FGF signaling might positively regulate both HtrA1 and VEGF. However, in this study, both *HTRA1* and *VEGFA* expression was not altered in response to exogenous addition of recombinant human bFGF in human fetal RPE cells (**Figure 3.23**).

Thirdly, HtrA1 modulates IGF signaling by cleaving the IGFBP-5 (Hou J et al, 2005). Inhibition of HtrA1 proteolytic activity inhibited IGFBP-5 proteolysis, allowing IGF-1-stimulated DNA and protein synthesis (Hou J et al, 2005). Normal RPE cells produce IGFBP-2, 3, 4, 5, 6 (Mukherjee S et al, 2009). Moreover, IGF-1 induced VEGF expression and secretion in human RPE cells (Punglia RS et al, 1997; Slomiany MG and Rosenzweig SA, 2004). It could be possible that HtrA1 could possibly regulate VEGF in a positive manner through the cleavage of IGFBP-5 and subsequent induction by IGF-1.

Chapter 5: Conclusion and future prospects

This research study identified several AMD-associated variants in the *CFH* and *HTRA1* genes. A *HTRA1* variant (34delCinsTCCT) showed a protective effect according to results of both genetic and expression studies, suggesting that *HTRA1* on chromosome 10q26 is a potential disease-causing gene for exudative AMD. This study provided an excellent example in disease-causing gene identification through variant hunting and characterization. Further variant screening could be extended to a larger cohort, such as hundreds and thousands of patients, so that more variants might be discovered to substantiate the effect of disease-causing genes. Moreover, *CFH* variants, which were not studied in this thesis, could be investigated in the prospective experiments to understand their biological association with AMD involving the complement pathway.

The latter part of this thesis reported a positive association of HtrA1 and VEGF in human vitreous humor, especially in patients with retinal detachment. This association was consistently found in primary human fetal RPE cell culture undergoing cell stress or inflammation. Further studies could aim to explore the *in vivo* and *in vitro* interaction of HtrA1 with AMD-associated molecules other than VEGF. These include PEDF and complement factors. In addition, the signaling pathways involved in the direct regulation of *HTRA1* and *VEGFA* could also be a focus in the future analysis.

The current study revealed a possible mechanism for HtrA1 on AMD development through the induction of RPE cell death by a high expression level of HtrA1. The direct *in vivo* role of HtrA1 in AMD pathogenesis should be followed. Furthermore, therapeutic treatments that target the HtrA1 regulatory pathways could be considered as a research area in the future. Finally, this thesis demonstrated the fundamental and critical strategies in identifying the underlying mechanisms of disease-susceptible gene, and established a foundation for disease realization and pathogenesis.

Reference

Abcouwer SF, Marjon PL, Loper RK, Vander Jagt DL. Response of VEGF expression to amino acid deprivation and inducers of endoplasmic reticulum stress. Invest Ophthalmol Vis Sci 2002; 43:2791-2798.

Adam Z, Adamska I, Nakabayashi K, Ostersetzer O, Haussuhl K, Manuell A, Zheng B, Vallon O, Rodermel SR, Shinozaki K, Clarke AK. Chloroplast and mitochondrial proteases in Arabidopsis. A proposed nomenclature. Plant Physiol 2001; 125:1912-1918.

Ades SE, Connolly LE, Alba BM, Gross CA. The Escherichia coli σ(E)-dependent extracytoplasmic stress response is controlled by the regulated proteolysis of an anti-s factor. Genes Dev 1999; 13:2449-2461.

Adler R, Belecky-Adams TL. The role of bone morphogenetic proteins in the differentiation of the ventral optic cup. Development 2002; 129:3161-3171.

Ajayi F, Kongoasa N, Gaffey T, Asmann YW, Watson WJ, Baldi A, Lala P, Shridhar V, Brost B, Chien J. Elevated expression of serine protease HtrA1 in preeclampsia and its role in trophoblast cell migration and invasion. Am J Obstet Gynecol 2008; 199:557.e1-557.e10.

Alba BM, Zhong HJ, Pelayo JC, Gross CA. degS (hhoB) is an essential Escherichia coli gene whose indispensable function is to provide σ(E) activity. Mol Microbiol 2001; 40:1323-1333.

Albarosa R, Colombo BM, Roz L, Magnani I, Pollo B, Cirenei N, Giani C, Conti AM, DiDonato S, Finocchiaro G. Deletion mapping of gliomas suggest the presence of two small regions for candidate tumor-suppressor genes in a 17-cM interval on chromosome 10q. Am J Hum Genet 1996; 58:1260-1267.

Altaweel M, Ip M. Macular hole: improved understanding of pathogenesis, staging, and management based on optical coherence tomography. Semin Ophthalmol 2003; 18:58-66.

Ambati J, Ambati BK, Yoo SH, Ianchulev S, Adamis AP. Age-related macular degeneration: etiology, pathogenesis, and therapeutic strategies. Surv Ophthalmol 2003; 48:257-293.

Ambati J, Anand A, Fernandez S, Sakurai E, Lynn BC, Kuziel WA, Rollins BJ, Ambati BK. An animal model of age-related macular degeneration in senescent Ccl-2- or Ccr-2-deficient mice. Nat Med 2003; 9:1390-1397.

An E, Sen S, Park SK, Gordiah-Dressman H, Hathout Y. Identification of novel substrates for the serine protease HTRA1 in the human RPE secretome. Invest Ophthalmol Vis Sci 2010. In press.

Anderson DH, Mullins RF, Hageman GS, Johnson LV. A role for local inflammation in the formation of drusen in the aging eye. Am J Ophthalmol 2002; 134:411-431.

Baffi J, Byrnes G, Chan CC, Csaky KG. Choroidal neovascularization in the rat induced by adenovirus mediated expression of vascular endothelial growth factor. Invest Ophthalmol Vis Sci 2000; 41:3582-3589.

Bakay M, Zhao P, Chen J, Hoffman EP. A web-accessible complete transcriptome of normal human and DMD muscle. Neuromuscul Disord. 2002; 12:S125-141.

Bakker D, Vader CE, Roosendaal B, Mooi FR, Oudega B, de Graaf FK. Structure and function of periplasmic chaperone-like proteins involved in the biosynthesis of K88 and K99 fimbriae in enterotoxigenic Escherichia coli. Mol Microbiol 1991; 5:875-886.

Balasubramanian V, Sterling P. Receptive fields and functional architecture in the retina. J Physiol 2009; 587:2753-2767.

Baldi A, De Luca A, Morini M, Battista T, Felsani A, Baldi F, Catricala C, Amantea A, Noonan DM, Albini A, Natali PG, Lombardi D, Paggi MG. The HtrA1 serine protease

152

is down-regulated during human melanoma progression and represses growth of metastatic melanoma cells. Oncogene 2002; 21:6684-6688.

Baldi A, Mottolese M, Vincenzi B, Campioni M, Mellone P, Di Marino M, di Crescenzo VG, Visca P, Menegozzo S, Spugnini EP, Citro G, Ceribelli A, Mirri A, Chien J, Shridhar V, Ehrmann M, Santini M, Facciolo F. The serine protease HtrA1 is a novel prognostic factor for human mesothelioma. Pharmacogenomics 2008; 9:1069-1077.

Bánhegyi G, Benedetti A, Csala M, Mandl J. Stress on redox. FEBS Lett 2007; 581:3634-3640.

Barnes PJ, Karin M. Nuclear factor-kappaB: a pivotal transcription factor in chronic inflammatory diseases. N Engl J Med 1997; 336:1066-1071.

Bass S, Gu Q, Christen A. Multicopy suppressors of prc mutant Escherichia coli include two HtrA (DegP) protease homologs (HhoAB), DksA, and a truncated R1pA. J Bacteriol 1996; 178:1154-1161.

Basta G, Lazzerini G, Massaro M, Simoncini T, Tanganelli P, Fu C, Kislinger T, Stern DM, Schmidt AM, De Caterina R. Advanced glycation end products activate endothelium through signal-transduction receptor RAGE: a mechanism for amplification of inflammatory responses. Circulation 2002; 105:816-822.

Baum L, Chan WM, Li WY, Lam DS, Wang PB, Pang CP. ABCA4 sequence variants in Chinese patients with age-related macular degeneration or Stargardt's disease. Ophthalmologica 2003; 217:111-114.

Beatty S, Koh H, Phil M, Henson D, Boulton M. The role of oxidative stress in the pathogenesis of age-related macular degeneration. Surv Ophthalmol 2000; 45:115-134.

Bian ZM, Elner SG, Elner VM. Regulation of VEGF mRNA expression and protein secretion by TGF-beta2 in human retinal pigment epithelial cells. Exp Eye Res 2007; 84:812-822.

Bird AC, Marshall J. Retinal pigment epithelial detachments in the elderly. Trans Ophthalmol Soc UK 1986; 105:674-682.

Bird AC, Bressler NM, Bressler SB, Chisholm IH, Coscas G, Davis MD, de Jong PT, Klaver CC, Klein BE, Klein R, et al. An international classification and grading system for age-related maculopathy and age-related macular degeneration. The International ARM Epidemiological Study Group. Surv Ophthalmol 1995; 39:367-374.

Biswas S, Biswas I. Role of HtrA in surface protein expression and biofilm formation by Streptococcus mutans. Infect Immun 2005; 73:6923-6934.

Bloomfield SA, Dacheux RF. Rod vision: Pathways and processing in mammalian retina. Prog Retin Eye Res 2001; 20:351-384.

Bodmer W, Bonilla C. Common and rare variants in multifactorial susceptibility to common diseases. Nat Genet 2008; 40:695-701.

Bok D, Young RW. Phagocytic properties of the retinal pigment epithelium. In: Zinn KM, Marmor MF. The retinal pigment epithelium. Cambridge, MA: Harvard University Press, 1979:148-174.

Bowden MA, Di Nezza-Cossens LA, Jobling T, Salamonsen LA, Nie GY. Serine proteases HTRA1 and HTRA3 are down-regulated with increasing grades of human endometrial cancer. Gynecol Oncol 2006; 103:253-260.

Bowden MA, Li Y, Liu YX, Findlay JK, Salamonsen LA, Nie G. HTRA3 expression in non-pregnant rhesus monkey ovary and endometrium, and at the maternal-fetal interface during early pregnancy. Reprod Biol Endocrinol 2008; 6:22.

Bowden M, Drummond AE, Salamonsen LA, Findlay JK, Nie G. Evolutionary conservation of mammalian HTRA3 and its developmental regulation in the rat ovary. J Exp Zool B Mol Dev Evol 2009; 312:701-713.

Cameron DJ, Yang Z, Gibbs D, Chen H, Kaminoh Y, Jorgensen A, Zeng J, Luo L, Brinton E,

Brinton G, Brand JM, Bernstein PS, Zabriskie NA, Tang S, Constantine R, Tong Z, Zhang K. HTRA1 variant confers similar risks to geographic atrophy and neovascular age-related macular degeneration. Cell Cycle 2007; 6:1122-1125.

Canfield AE, Hadfield KD, Rock CF, Wylie EC, Wilkinson FL. HtrA1: a novel regulator of physiological and pathological matrix mineralization? Biochem Soc Trans 2007; 35:669-671.

Cavard C, Lazdunski C, Howard SP. The acylated precursor form of the colicin A lysis protein is a natural substrate of the DegP protease. J Bacteriol 1989; 171:6316-6322.

Chai J, Tarnawski AS. Serum response factor: discovery, biochemistry, biological roles and implications for tissue injury healing. J Physiol Pharmacol 2002; 53:147-157.

Chamberland A, Wang E, Jones AR, Collins-Racie LA, LaVallie ER, Huang Y, Liu L, Morris EA, Flannery CR, Yang Z. Identification of a novel HtrA1-susceptible cleavage site in human aggrecan. J Biol Chem 2009; 284:27352-27359.

Chan CC, Shen D, Zhou M, Ross RJ, Ding X, Zhang K, Green R, Tuo J. Human HtrA1 in the archived eyes with age-related macular degeneration. Trans Am Ophthalmol Soc 2007; 105:92-98.

Chan WM, Lai TY, Chan KP, Li H, Liu DT, Lam DS, Pang CP. Changes in aqeous vascular endothelial growth factor and pigment epithelial-derived factor levels following intravitreal bevacizumab injections for choroidal neovascularization secondary to age-related macular degeneration or pathologic myopia. Retina 2008; 28:1308-1313.

Chance B, Erecińska M, Lee CP. Localization of cytochromes in intact and fragmented mitochondrial membranes. Proc Natl Acad Sci U S A 1970; 66:928-935.

Chen H, Yang Z, Gibbs D, Yang X, Hau V, Zhao P, Ma X, Zeng J, Luo L, Pearson E, Constantine R, Kaminoh Y, Harmon J, Tong Z, Stratton CA, Cameron DJ, Tang S, Zhang K. Association of HTRA1 polymorphism and bilaterality in advanced

age-related macular degeneration. Vision Res 2008; 48:690-694.

Chen SJ, Cheng CY, Peng KL, Li AF, Hsu WM, Liu JH, Chou P. Prevalence and associated risk factors of age-related macular degeneration in an elderly Chinese population in Taiwan: the Shihpai Eye Study. Invest Ophthalmol Vis Sci 2008; 49:3126-3133.

Chen W, Xu W, Tao Q, Liu J, Li X, Gan X, Hu H, Lu Y. Meta-analysis of the association of the HTRA1 polymorphisms with the risk of age-related macular degeneration. Exp Eye Res 2009; 89:292-300.

Chien J, Staub J, Hu SI, Erickson-Johnson MR, Couch FJ, Smith DI, Crowl RM, Kaufmann SH, Shridhar V. A candidate tumor suppressor HtrA1 is downregulated in ovarian cancer. Oncogene 2004; 23:1636-1644.

Chien J, Aletti G, Baldi A, Catalano V, Muretto P, Keeney GL, Kalli KR, Staub J, Ehrmann M, Cliby WA, Lee YK, Bible KC, Hartmann LC, Kaufmann SH, Shridhar V. Serine protease HtrA1 modulates chemotherapy-induced cytotoxicity. J Clin Invest 2006; 116:1994-2004.

Chien J, He X, Shridhar V. Identification of tubulins as substrates of serine protease HtrA1 by mixture-based oriented peptide library screening. J Cell Biochem 2009a; 107:253-263.

Chien J, Ota T, Aletti G, Shridhar R, Boccellino M, Quagliuolo L, Baldi A, Shridhar V. Serine protease HtrA1 associates with microtubules and inhibits cell migration. Mol Cell Biol 2009b; 29:4177-4187.

Cho E, Hung S, Willett WC, Spiegelman D, Rimm EB, Seddon JM, Colditz GA, Hankinson SE. Prospective study of dietary fat and the risk of age-related macular degeneration. Am J Clin Nutr 2001; 73:209-218.

Chong NH, Keonin J, Luthert PJ, Frennesson CI, Weingeist DM, Wolf RL, Mullins RF, Hageman GS. Decreased thickness and integrity of the macular elastic layer of Bruch's

membrane correspond to the distribution of lesions associated with age-related macular degeneration. Am J Pathol 2005; 166:241-251.

Choy KW, Wang CC, Ogura A, Lau TK, Rogers MS, Ikeo K, Gojobori T, Lam DS, Pang CP. Genomic annotation of 15,809 ESTs identified from pooled early gestation human eyes. Physiol Genomics 2006; 25:9-15.

Clausen T, Southan C, Ehrmann M. The HtrA family of proteases: Implications for protein composition and cell fate. Mol Cell 2002; 10:443-455.

Clawson GA, Bui V, Xin P, Wang N, Pan W. Intracellular localization of the tumor suppressor HtrA1/Prss11 and its association with HPV16 E6 and E7 proteins. J Cell Biochem 2008; 105:81-88.

Cleland WW. Dithiothreitol, a new protective reagent for SH groups. Biochemistry 1964; 3:480-482.

Clouet J, Grimandi G, Pot-Vaucel M, Masson M, Fellah HB, Guigand L, Cherel Y, Bord E, Rannou F, Weiss P, Guicheux J, Vinatier C. Identification of phenotypic discriminating markers for intervertebral disc cells and articular chondrocytes. Rheumatology (Oxford) 2009; 48:1447-1450.

Coats G. The pathology of macular holes. Roy London Hosp Rep 1907; 17:69-96.

Cole JN, Aquilina JA, Hains PG, Henningham A, Sriprakash KS, Caparon MG, Nizet V, Kotb M, Cordwell SJ, Djordjevic SP, Walker MJ. Role of group A Streptococcus HtrA in the maturation of SpeB protease. Proteomics 2007; 7:4488-4498.

Congdon N, O'Colmain B, Klaver CC, Klein R, Munoz B, Friedman DS, Kempen J, Taylor HR, Mitchell P, Eye Diseases Prevalence Research Group. Cause and prevalence of visual impairment among adults in the United States. Arch Ophthalmol 2004; 122:477-485.

Cousins SW, Espinosa-Heidmann DG, Csaky KG, Monocyte activation in patients with

age-related macular degeneration: a biomarker of risk for choroidal neovascularization? Arch Ophthalmol 2004; 122:1013-1018.

Crabb JW, Miyagi M, Gu X, Shadrach K, West KA, Sakaguchi H, Kamei M, Hasan A, Yan L, Rayborn ME, Salomon RG, Hollyfield JG. Drusen proteome analysis: an approach to the etiology of age-related macular degeneration. Proc Natl Acad Sci USA 2002; 99:14682-14687.

de Jong PT. Age-related macular degeneration. N Engl J Med 2006; 355:1474-1485.

De Luca A, De Falco M, Severino A, Campioni M, Santini D, Baldi F, Paggi MG, Baldi A. Distribution of the serine protease HtrA1 in normal human tissues. J Histochem Cytochem 2003; 51:1279-1284.

De Luca A, De Falco M, Fedele V, Cobellis L, Mastrogiacomo A, Laforgia V, Tuduce IL, Campioni M, Giraldi D, Paggi MG, Baldi A. The serine protease HtrA1 is upregulated in the human placenta during pregnancy. J Histochem Cytochem 2004a; 52:885-892.

De Luca A, De Falco M, De Luca L, Penta R, Shridhar V, Baldi F, Campioni M, Paggi MG, Baldi A. Pattern of expression of HtrA1 during mouse development. J Histochem Cytochem 2004b; 52:1609-1617.

Delori FC, Goger DG, Dorey CK. Age-related accumulation and spatial distribution of lipofuscin in RPE of normal subjects. Invest Ophthalmol Vis Sci 2001; 42:1855-1866.

Despriet DD, Klaver CC, Witteman JC, Bergen AA, Kardys I, de Maat MP, Boekhoorn SS, Vingerling JR, Hofman A, Oostra BA, Uitterlinden AG, Stijnen T, van Duijn CM, de Jong PT. Complement factor H polymorphism, complement activators, and risk of age-related macular degeneration. JAMA 2006; 296:301-309.

Dewan A, Liu M, Hartman S, Zhang SS, Liu DT, Zhao C, Tam PO, Chan WM, Lam DS, Snyder M, Barnstable C, Pang CP, Hoh J. HTRA1 promoter polymorphism in wet age-related macular degeneration. Science 2006; 314:989-992.

Donati G, Kapetanios AD, Pournaras CJ. Principles of treatment of choroidal neovascularization with photodynamic therapy in age-related macular degeneration. Semin Ophthalmol 1999; 14:2-10.

Donoso LA, Kim D, Frost A, Callahan A, Hageman G. The role of inflammation in the pathogenesis of age-related macular degeneration. Surv Ophthalmol 2006; 51:137-152.

Dunn KC, Aotaki-Keen AE, Putkey FR, Hjelmeland LM. ARPE-19, a human retinal pigment epithelial cell line with differentiated properties. Exp Eye Res 1996; 62:155-169.

Edwards AO, Ritter R 3rd, Abel KJ, Manning A, Panhuysen C, Farrer LA. Complement factor H polymorphism and age-related macular degeneration. Science 2005; 308:421-424.

Eichten A, Rud DS, Grace M, Piboonniyom S, Zacny V, Munger K. Molecular pathways executing the trophic sentinel response in HPV-16 E7-expressing normal human diploid fibroblasts upon growth factor deprivation. Virology 2004; 319:81-93.

Elbein AD. Inhibitors of the biosynthesis and processing of N-linked oligosaccharides. CRC Crit Rev Biochem 1984; 16:21-49.

Ennis S, Goverdhan S, Cree A, Hoh J, Collins A, Lotery A. Fine-scale linkage disequilibrium mapping of age-related macular degeneration in the complement factor H gene region. Br J Ophthalmol 2007; 91:966-970.

Espenshade PJ, Li WP, Yabe D. Sterols block binding of COPII proteins to SCAP, thereby controlling SCAP sorting in ER. Proc Natl Acad Sci U S A 2002; 99:11694-11699.

Esposito V, Campioni M, De Luca A, Spugnini EP, Baldi F, Cassandro R, Mancini A, Vincenzi B, Groeger A, Caputi M, Baldi A. Analysis of HtrA1 serine protease expression in human lung cancer. Anticancer Res 2006; 26:3455-3459.

Eyetech Study Group. Anti-vascular endothelial growth factor therapy for subfoveal

choroidal neovascularization secondary to age-related macular degeneration: phase II study results. Ophthalmology 2003; 110:979-986.

Fahrenkrog B, Sauder U, Aebi U. The S. cerevisiae HtrA-like protein Nma111p is a nuclear serine protease that mediates yeast apoptosis. J Cell Sci 2004; 117:115-126.

Farn J, Roberts M. Effect of inactivation of the HtrA-like serine protease DegQ on the virulence of Salmonella enterica serovar Typhimurium in mice. Infect Immun 2004; 72:7357-7359.

Ferrara N. Role of vascular endothelial growth factor in physiologic and pathologic angiogenesis: therapeutic implications. Semin Oncol 2002; 29:10-14.

Ferrer-Vaquer A, Maurey P, Werzowa J, Firnberg N, Leibbrandt A, Neubuser A. Expression and regulation of HTRA1 during chick and early mouse development. Dev Dyn 2008; 237:1893-1900.

Field GD, Chichilnisky EJ. Information processing in the primate retina: circuitry and coding. Annu Rev Neurosci 2007; 30:1-30.

Fisher SA, Abecasis GR, Yashar BM, Zareparsi S, Swaroop A, Iyengar SK, Klein BE, Klein R, Lee KE, Majewski J, Schultz DW, Klein ML, Seddon JM, Santangelo SL, Weeks DE, Conley YP, Mah TS, Schmidt S, Haines JL, Pericak-Vance MA, Gorin MB, Schulz HL, Pardi F, Lewis CM, Weber BH. Meta-analysis of genome scans of age-related macular degeneration. Hum Mol Genet 2005; 14:2257-2264.

Folgueira MA, Carraro DM, Brentani H, da Costa Patrao DF, Barbosa EM, Netto MM, Caldeira JR, Katayama ML, Soares FA, Oliveira CT, Reis LF, Kaiano JH, Camargo LP, Vencio RZ, Snitcovsky IM, Makdissi FB, e Silva PJ, Goes JC, Brentani MM. Gene expression profile associated with response to doxorubicin-based therapy in breast cancer. Clin Cancer Res 2005; 11:7434-7443.

Folkman J. Angiogenesis in cancer, vascular, rheumatoid, and other diseases. Nat Med 1995;

1:27-31.

Friedman DS, O'Colmain BJ, Munoz B, Tomany SC, McCarty C, de Jong PT, Nemesure B, Mitchell P, Kempen J, Eye Diseases Prevalence Research Group. Prevalence of age-related macular degeneration in the United States. Arch Ophthalmol 2004; 122:564-572.

Fritsche LG, Loenhardt T, Janssen A, Fisher SA, Rivera A, Keilhauer CN, Weber BH. Age-related macular degeneration is associated with an unstable ARMS2 (LOC387715) mRNA. Nat Genet 2008; 40:892-896.

Galli-Resta L, Leone P, Bottari D, Ensini M, Rigosi E, Novelli E. The genesis of retinal architecture: an emerging role for mechanical interactions? Prog Retin Eye Res 2008; 27:260-283.

Gariano RF, Gardner TW. Retinal angiogenesis in development and disease. Nature 2005; 438:960-966.

Geisen P, McColm JR, King BM, Hartnett ME. Characterization of barrier properties and inducible VEGF expression of several types of retinal pigment epithelium in medium-term culture. Curr Eye Res 2006; 31:739-748.

Gilicze A, Kohalmi B, Pocza P, Keszei M, Jaeger J, Gorbe E, Papp Z, Toth S, Falus A, Wiener Z. HtrA1 is a novel mast cell serine protease of mice and men. Mol Immunol 2007; 44:2961-2968.

Glickstein M. Organization of the visual pathways. Evidence is discussed concerning parallel pathways from the eye to the brain. Science 1969: 164:917-926.

Gold B, Merriam JE, Zernant J, Hancox LS, Taiber AJ, Gehrs K, Cramer K, Neel J, Bergeron J, Barile GR, Smith RT; AMD Genetics Clinical Study Group, Hageman GS, Dean M, Allikmets R. Variation in factor B (BF) and complement component 2 (C2)

genes is associated with age-related macular degeneration. Nat Genet 2006; 38:458-462.

Goldbaum O, Vollmer G, Richter-Landsberg C. Proteasome inhibition by MG-132 induces apoptotic cell death and mitochondrial dysfunction in cultured rat brain oligodendrocytes but not in astrocytes. Glia 2006; 53:891-901.

Gomi M, Sonoyama M, Mitaku S. High performance system for signal peptide prediction: SOSUIsignal. Chem-Bio Info J 2004; 4:142-147.

Gragoudas ES, Adamis AP, Cunningham ET Jr, Feinsod M, Guyer DR; VEGF Inhibition Study in Ocular Neovascularization Clinical Trial Group. Pegaptanib for neovascular age-related macular degeneration. N Engl J Med 2004; 351:2805-2816.

Grau S, Baldi A, Bussani R, Tian X, Stefanescu R, Przybylski M, Richards P, Jones SA, Shridhar V, Clausen T, Ehrmann M. Implications of the serine protease HtrA1 in amyloid precursor protein processing. Proc Natl Acad Sci USA 2005; 102:6021-6026.

Grau S, Richards PJ, Kerr B, Hughes C, Caterson B, Williams AS, Junker U, Jones SA, Clausen T, Ehrmann M. The role of human HtrA1 in arthritic disease. J Biol Chem 2006; 281:6124-6129.

Gray CW, Ward RV, Karran E, Turconi S, Rowles A, Viglienghi D, Southan C, Barton A, Fantom KG, West A, Savopoulos J, Hassan NJ, Clinkenbeard H, Hanning C, Amegadzie B, Davis JB, Dingwall C, Livi GP, Creasy CL. Characterization of human HtrA2, a novel serine protease involved in the mammalian cellular stress response. Eur J Biochem 2000; 267:5699-5710.

Grossniklaus HE, Ling JX, Wallace TM, Dithmar S, Lawson DH, Cohen C, Elner VM, Elner SG, Sternberg P Jr. Macrophage and retinal pigment epithelium expression of angiogenic cytokines in choroidal neovascularization. Mol Vis 2002; 8:119-126.

Grossniklaus HE, Green WR. Choroidal neovascularization. Am J Ophthalmol 2004;

137:496-503.

Haddad S, Chen CA, Santangelo SL, Seddon JM. The genetics of age-related macular degeneration: a review of progress to date. Surv Ophthalmol 2006; 51:316-363.

Hadfield KD, Rock CF, Inkson CA, Dallas SL, Sudre L, Wallis GA, Boot-Handford RP, Canfield AE. HtrA1 inhibits mineral deposition by osteoblasts: Requirement for the protease and PDZ domains. J Biol Chem 2008; 283:5928-5938.

Hageman GS, Luthert PJ, Victor Chong NH, Johnson LV, Anderson DH, Mullins RF. An integrated hypothesis that considers drusen as biomarkers of immune-mediated processes at the RPE-Bruch's membrane interface in aging and age-related macular degeneration. Prog Retin Eye Res 2001; 20:705-732.

Haines JL, Hauser MA, Schmidt S, Scott WK, Olson LM, Gallins P, Spencer KL, Kwan SY, Noureddine M, Gilbert JR, Schnetz-Boutaud N, Agarwal A, Postel EA, Pericak-Vance MA. Complement factor H variant increases the risk of age-related macular degeneration. Science 2005; 308:419-421.

Han C, Nam MK, Park HJ, Seong YM, Kang S, Rhim H. Tunicamycin-induced ER stress upregulated the expression of mitochondrial HtrA2 and promotes apoptosis through the cytosolic release of HtrA2. J Microbiol Biotechnol 2008; 18:1197-1202.

Hara K, Shiga A, Fukutake T, Nozaki H, Miyashita A, Yokoseki A, Kawata H, Koyama A, Arima K, Takahashi T, Ikeda M, Shiota H, Tamura M, Shimoe Y, Hirayama M, Arisato T, Yanagawa S, Tanaka A, Nakano I, Ikeda S, Yoshida Y, Yamamoto T, Ikeuchi T, Kuwano R, Nishizawa M, Tsuji S, Onodera O. Association of HTRA1 mutations and familial ischemic cerebral small-vessel disease. New Engl J Med 2009; 360:1729-1739.

Harris BZ, Lim WA. Mechanism and role of PDZ domains in signaling complex assembly. J Cell Sci 2001; 114:3219-3231.

Hartong DT, Berson E, Dryja TP. Retinitis pigmentosa. Lancet 2006; 368:1795-1809.

Haußuhl K, Andersson B, Adamska I. A chloroplast DegP2 protease performs the primary cleavage of the photodamaged D1 protein in plant photosystem II. EMBO J 2001; 20:713-722.

Haupert CL, McCuen BW 2nd, Jaffe GJ, Steuer ER, Cox TA, Toth CA, Fekrat S, Postel EA. Pars plana vitrectomy, subretinal injection of tissue plasminogen activator, and fluid-gas exchange for displacement of thick submacular hemorrhage in age-related macular degeneration. Am J Ophthalmol 2001; 131:208-215.

Hauske P, Meltzer M, Ottmann C, Krojer T, Clausen T, Ehrmann M, Kaiser M. Selectivity profiling of DegP substrates and inhibitors. Bioorg Med Chem 2009; 17:2920-2924.

Hawkins BS, Bressler NM, Miskala PH, Bressler SB, Holekamp NM, Marsh MJ, Redford M, Schwartz SD, Sternberg P Jr, Thomas MA, Wilson DJ; Submacular Surgery Trials (SST) Research Group. Surgery for subfoveal choroidal neovascularization in age-related macular degeneration: ophthalmic findings: SST report no. 11. Ophthalmology 2004; 111:1967-1980.

He S, Dong W, Deng Q, Weng S, Sun W. Seeing more clearly: recent advances in understanding retinal circuitry. Science 302:408-411.

He X, Ota T, Liu P, Su C, Chien J, Shridhar V. Downregulation of HtrA1 promotes resistance to anoikis and peritoneal dissemination of ovarian cancer cells. Cancer Res 2010; 70:3109-3118.

Ho AC, Suyer DR, Fine SL. Macular hole. Surv Ophthalmol 1998; 42:393-416.

Hollborn M, Francke M, iandiev I, Buhner E, Foja C, Kohen L, Reichenbach A, Wiedemann P, Bringmann A, Uhlmann S. Early activation of inflammation- and immune response-related genes after experimental detachment of the porcine retina. Invest Ophthalmol Vis Sci 2008; 49:1262-1273.

Hou J, Clemmons DR, Smeekens S. Expression and characterization of a serine protease

that preferentially cleaves insulin-like growth factor binding protein-5. J Cell Biochem 2005; 94:470-484.

Hou S, Maccarana M, Min T, Strate I, Pera E. The secreted serine protease xHtrA1 stimulates long-range FGF signaling in the early Xenopus embryo. Dev Cell 2007; 13:226-241.

Howes KA, Liu Y, Dunaief JL, Milam A, Frederick JM, Marks A, Baehr W. Receptor for advanced glycation end products and age-related macular degeneration. Invest Ophthalmol Vis Sci 2004; 45:3713-3720.

Hu SI, Carozza M, Klein M, Nantermet P, Luk D, Crowl RM. Human HtrA1, an evolutionary conserved serine protease identified as a differentially expressed gene product in osteoarthritic cartilage. J Biol Chem 1998; 273:34406-34412.

Huesgen PF, Schuhmann H, Adamska I. The family of Deg proteases in cynobacteria and chloroplasts of high plants. Physiol Plant 2005; 123:413-420.

Huesgen PF, Schuhmann H, Adamska I. Proteolysis in plant mitochondria and chloroplasts. In A. Hemantaranjan (Ed.), Advances in Plant Physiology. Jodhpur: Scientific Publishers (India). 2006; pp. 255-294.

Huesgen PF, Scholz P, Adamska I. The serine protease HhoA from Synechocystis sp. strain PCC 6803: substrate specificity and formation of a hexameric complex are regulated by the PDZ domain. J Bacteriol 2007; 189:6611-6618.

Huesgen PF, Schuhmann H, Adamska I. Deg/HtrA proteases as components of a network for photosystem II quality control in chloroplasts and cynobacteria. Res Microbiol 2009; 160:726-732.

Hung AY, Sheng M. PDZ domains: structural modules for protein complex assembly. J Biol Chem 2002; 277:5699-5702.

Hutchinson J, Tay W. Symmetrical central choroido-retinal disease occurring in senile

persons. R Lond Ophthalmic Hosp Rep J Ophthalmic Med Surg 1874; 8:231-244.

Im E, Kazlauskas A. The role of cathepsins in ocular physiology and pathology. Exp Eye Res 2007; 84:383-388.

Ishibashi T, Murata T, Hangai M, Nagai R, Horiuchi S, Lopez PF, Hinton DR, Ryan SJ. Advanced glycation end products in age-related macular degeneration. Arch Ophthalmol 1998; 116:1629-1632.

Jacobs GH. Primate color vision: a comparative perspective. Vis Neurosci 2008; 25:619-633.

Jager RD, Mieler WF, Miller JW. Age-related macular degeneration. N Engl J Med 2008; 358:2606-2617.

Jomaa A, Iwanczyk J, Tran J, Ortega J. Characterization of the autocleavage process of the Escherichia coli HtrA protein: Implications for its physiological role. J Bacteriol 2009; 191:1924-1932.

Jamsa E, Simonen M, Makarow M. Selective retention of secretory proteins in the yeast endoplasmic reticulum by treatment of cells with a reducing agent. Yeast 1994; 10:355-370.

Jones CH, Dexter P, Evans AK, Liu C, Hultgren SJ, Hruby DE. Escherichia coli DegP protease cleaves between paired hydrophobic residues in a natural substrate: the PapA pilin. J Bacterial 2002; 184:5762-5771.

Kaarniranta K, Salminen A. NF-κB signaling as a putative target for omega-3 metabolites in the prevention of age-related macular degeneration. Exp Gerontol 2009; 44:685-688.

Kall L, Krogh A, Sonnhammer EL. A combined transmembrane topology and signal peptide prediction method. J Mol Biol 2004; 338:1027-1036.

Kanda A, Chen W, Othman M, Branham KE, Brooks M, Khanna R, He S, Lyons R, Abecasis GR, Swaroop A. A variant of mitochondrial protein LOC387715/ARMS2, not

HTRA1, is strongly associated with age-related macular degeneration. Proc Natl Acad Sci USA 2007; 104:16227-16232.

Kapri-Pardes E, Naveh L, Adam Z. The thylakoid lumen protease Deg1 is involved in the repair of photosystem II from photoinhibition in Arabidopsis. Plant Cell 2007; 19:1039-1047.

Kashiwagi A, DiGirolamo CM, Kanda Y, Niikura Y, Esmon CT, Hansen TR, Shioda T, Pru JK. The postimplanatation embryo differentially regulates endometrial gene expression and decidualization. Endocrionology 2007; 148:4173-4184.

Kato MV, Sato H, Tsukada T, Ikawa Y, Aizawa S, Nagayoshi M. A follistatin-like gene, mac25, may act as a growth suppressor of osteosarcoma cells. Oncogene 1996; 12:1361-1364.

Kato MV. A secreted tumor-suppressor, mac25, with activin-binding activity. Mol Med 2000; 6:126-135.

Katta S, Kaur I, Chakrabarti S. The molecular genetic basis of age-related macular degeneration: an overview. J Genet 2009; 88:425-449.

Keck PJ, Hauser SD, Krivi G, Sanzo K, Warren T, Feder J, Connolly DT. Vascular permeability factor, an endothelial cell mitogen related to PDGF. Science 1989; 246:1309-1312.

Kijlstra A, La Heij E, Hendrikse F. Immunological factors in the pathogenesis and treatment of age-related macular degeneration. Ocul Immunol Inflamm 2005; 13:3-11.

Kim DY, Kim KK. Structure and function of HtrA family proteins, the key players in protein quality control. J Biochem Mol Biol 2005; 38:266-274.

Kim KI, Park SC, Kang SH, Cheong GW, Chung CH. Selective degradation of unfolded proteins by the self-compartmentalizing HtrA protease, a periplasmic heat shock protein in Escherichia coli. J Mol Biol 1999; 294:1363-1374.

Klein R, Davis MD, Magli YL, Segal P, Klein BE, Hubbard L. The Wisconsin age-related maculopathy grading system. Ophthalmology 1991; 98:1128-1134.

Klein R, Meuer SM, Moss SE, Klein BE. Detection of drusen and early signs of age-related maculopathy using a nonmydriatic camera and a standard fundus camera. Ophthalmology 1992; 99:1686-1692.

Klein R, Klein BE, Tomany SC, Meuer SM, Huang GH. Ten-year incidence and progression of age-related maculopathy: the Beaver Dam eye study. Ophthalmology 2002; 109:1767-1779.

Klein RJ, Zeiss C, Chew EY, Tsai JY, Sackler RS, Haynes C, Henning AK, SanGiovanni JP, Mane SM, Mayne ST, Bracken MB, Ferris FL, Ott J, Barnstable C, Hoh J. Complement factor H polymorphism in age-related macular degeneration. Science 2005; 308:385-389.

Kliffen M, Sharma HS, Mooy CM, Kerkvliet S, de Jong PT. Increased expression of angiogenic growth factors in age-related maculopathy. Br J Ophthalmol 1997; 81:154-162.

Komatsu W, Ishihara K, Murata M, Saito H, Shinohara K. Docosahexaenoic acid suppresses nitric oxide production and inducible nitric oxide synthase expression in interferon-gamma plus lipopolysaccharide-stimulated murine macrophages by inhibiting the oxidative stress. Free Radic Biol Med 2003; 34:1006-1016.

Kopp EB, Ghosh S. NF-kappa B and rel proteins in innate immunity. Adv Immunol 1995; 58:1-27.

Koyama Y, Matsuzaki S, Gomi F, Yamada K, Katayama T, Sato K, Kumada T, Fukuda A, Matsuda S, Tano Y, Tohyama M. Induction of amyloid beta accumulation by ER calcium disruption and resultant upregulation of angiogenic factors in ARPE19 cells. Invest Ophthalmol Vis Sci 2008; 49:2376-2383.

Krieglstein K, Strelau J, Schober A, Sullivan A, Unsicker K. TGF-beta and the regulation of neuron survival and death. J Physiol Paris 2002; 96:25-30.

Krojer T, Garrido-Franco M, Huber R, Ehrmann M, Clausen T. Crystal structure of DegP (HtrA) reveals a new protease-chaperone machine. Nature 2002; 416:455-459.

Launay S, Maubert E, Lebeurrier N, Tennstaedt A, Campioni M, Docagne F, Gabriel C, Dauphinot L, Potier MC, Ehrmann M, Baldi A, Vivien D. HtrA1-dependent proteolysis of TGF-β controls both neuronal maturation and developmental survival. Cell Death Differ 2008; 15:1408-1416.

Lee AH, Iwakoshi NN, Anderson KC, Glimcher LH. Proteasome inhibitors disrupt the unfolded protein response in myeloma cells. Proc Natl Acad Sci USA 2003; 100:9946-9951.

Lee AS. The glucose-regulated proteins: stress induction and clinical applications. Trends Biochem Sci 2001; 26:504-510.

Lee DH, Goldberg AL. Selective inhibitors of the proteasome-dependent and vacuolar pathways of protein degradation in Saccharomyces cerevisiae. J Biol Chem 1996; 271:27280-27284.

Lee DH, Goldberg AL. Proteasome inhibitors: valuable new tools for cell biologists. Trends Cell Biol 1998; 8:397-403.

Lee SS, Joo YS, Kim WU, Min DJ, Min JK, Park SH, Cho CS, Kim HY. Vascular endothelial growth factor levels in the serum and synovial fluid of patients with rheumatoid arthritis. Clin Exp Rheumatol 2001; 19:321-324.

Leung KW, Barnstable CJ, Tombran-Tink J. Bacterial endotoxin activates retinal pigment epithelial cells and induces their degeneration through IL-6 and IL-8 autocrine signaling. Mol Immunol 2009; 46:1374-1386.

Li J, Wang JJ, Yu Q, Wang M, Zhang SX. Endoplasmic reticulum stress is implicated in

retinal inflammation and diabetic retinopathy. FEBS Lett 2009; 583:1521-1527.

Li X, Fang Y, Zhao X, Jiang X, Duong T, Kain SR. Characterization of NFkappaB activation by detection of green fluorescent protein-tagged IkappaB degradation in living cells. J Biol Chem 1999; 274:21244-21250.

Li Y, Xu L, Wang YX, You QS, Yang H, Jonas JB. Prevalence of age-related maculopathy in the adult population in China: the Beijing eye study. Am J Ophthalmol 2008; 146:329.

Libby RT, Gould DB. Endoplasmic reticulum stress as a primary pathogenic mechanism leading to age-related macular degeneration. Adv Exp Med Biol 2010; 664:403-409.

Linstedt AD, Hauri HP. Giantin, a novel conserved Golgi membrane protein containing a cytoplasmic domain of at least 350 kDa. Mol Biol Cell 1993; 4:679-693.

Lipinska B, Sharma S, Georgopoulos C. Sequence analysis and regulation of the htrA gene of Escherichia coli: a sigma 32-independent mechanism of heat-inducible transcription. Nucleic Acids Res 1988; 16:10053-10067.

Lipinska B, Zylicz M, Georgopoulos C. The HtrA (DegP) protein, essential for Escherichia coli survival at high temperatures, is an endopeptidase. J Bacteriol 1990; 172:1791-1797.

Lotery AJ, Munier FL, Fishman GA, Weleber RG, Jacobson SG, Affatigato LM, Nichols BE, Schorderet DF, Sheffield VC, Stone EM. Allelic variation in the VMD2 gene in best disease and age-related macular degeneration. Invest Ophthalmol Vis Sci 2000; 41:1291-6.

Lyall F. Mechanisms regulating cytotrophoblast invasion in normal pregnancy and preeclampsia. Aust N Z J Obstet Gynaecol 2006; 46:266-273.

Lyon WR, Caparon MG. Role for serine protease HtrA (DegP) of Streptococcus pyogenes in the biogenesis of virulence factors SpeB and the hemolysin streptolysin S. Infect

Immun 2004; 72:1618-1625.

Magnusson KP, Duan S, Sigurdsson H, Petursson H, Yang Z, Zhao Y, Bernstein PS, Ge J, Jonasson F, Stefansson E, Helgadottir G, Zabriskie NA, Jonsson T, Björnsson A, Thorlacius T, Jonsson PV, Thorleifsson G, Kong A, Stefansson H, Zhang K, Stefansson K, Gulcher JR. CFH Y402H confers similar risk of soft drusen and both forms of advanced AMD. PLoS Med 2006; 3:e5.

Mahoney WC, Duksin D. Biological activities of the two major components of tunicamycin. J Biol Chem 1979; 254:6572-6576.

Manolio TA, Collins FS. The HapMap and genome-wide association studies in diagnosis and therapy. Annu Rev Med 2009; 60:443-456.

Marciniak SJ, Ron D. Endoplasmic reticulum stress signaling in disease. Physiol Rev 2006; 86:1133-1149.

Marneros AG, She H, Zambarakji H, Hashizume H, Connolly EJ, Kim I, Gragoudas ES, Miller JW, Olsen BR. Endogenous endostatin inhibits choroidal neovascularization. FASEB J 2007; 21:3809-3818.

Martins LM, Turk BE, Cowling V, Borg A, Jarrell ET, Cantley LC, Downward J. Binding specificity and regulation of the serine protease and PDZ domains of HtrA2/Omi. J Biol Chem 2002; 278:49417-49427.

Marzioni D, Quaranta A, Lorenzi T, Morroni M, Crescimanno C, De Nictolis M, Toti P, Muzzonigro G, Baldi A, De Luca A, Castellucci M. Expression pattern alterations of the serine protease HtrA1 in normal human placental tissues and in gestational trophoblastic diseases. Histol Histopathol 2009; 24:1213-1222.

Matsuo Y, Sawai H, Ochi N, Yasuda A, Sakamoto M, Takahashi H, Funahashi H, Takeyama H, Guha S. Proteasome inhibitor MG132 inhibits angiogenesis in pancreatic cancer by blocking NF-kappaB activity. Dig Dis Sci 2010; 55:1167-1176.

171

McDonnell PJ, Fine SL, Hillis AI. Clinical features of idiopathic macular cysts and holes. Am J Ophthalmol 1982; 93:777-786.

McMaster MT, Zhou Y, Fisher SJ. Abnormal placentation and the syndrome of preeclampsia. Semin Nephrol 2004; 24:540-547.

Meyers SM. A twin study on age-related macular degeneration. Trans Am Ophthalmol Soc 1994; 92:775-843.

Montesanti A, Deignan K, Hensey C. Cloning and characterization of Xenopus laevis Smac/DIABLO. Gene 2007; 392:187-195.

Morgan CM, Schatz H. Involutional macular thinning: A pre-macular hole condition. Ophthalmology 1986; 93:153-161.

Mruthyunjaya P, Stinnett SS, Toth CA. Change in visual function after macular translocation with 360 degrees retinectomy for neovascular age-related macular degeneration. Ophthalmology 2004; 111:1715-1724.

Mukherjee S, King JL, Guidry C. Phenotype-associated changes in retinal pigment epithelial cell expression of insulin-like growth factor binding proteins. Invest Ophthalmol Vis Sci 2009; 50:5449-5455.

Murwantoko, Yano M, Ueta Y, Murasaki A, Kanda H, Oka C, Kawaichi M. Binding of proteins to the PDZ domain regulated proteolytic activity of HtrA1 serine protease. Biochem J 2004; 381:895-904.

Nagineni CN, Samuel W, Nagineni S, Pardhasaradhi K, Wiggert B, Detrick B, Hooks JJ. Transforming growth factor-beta induces expression of vascular endothelial growth factor in human retinal pigment epithelial cells: involvement of mitogen-activated protein kinases. J Cell Physiol 2003; 197:453-462.

Nakata K, Crabb JW, Hollyfield JG. Crystallin distribution in Bruch's membrane-choroid complex from age-related macular degeneration and age-matched donor eyes. Exp Eye

Res 2005; 80:821-86.

Narkiewicz J, Klasa-Mazurkiewicz D, Zurawa-Janicka D, Skorko-Glonek J, Emerich J, Lipinska B. Changes in mRNA and protein levels of human HtrA1, HtrA2 and HtrA3 in ovarian cancer. Clin Biochem 2008; 41:561-569.

Narkiewicz J, Lapinska-Szumczyk S, Zurawa-Janicka D, Skorko-Glonek J, Emerich J, Lipinska B. Expression of human HtrA1, HtrA2, HtrA3 and TGF-1 genes in primary endometrial cancer. Oncol Rep 2009; 21:1529-1537.

Nie GY, Hampton A, Li Y, Findlay JK, Salamonsen LA. Identification and cloning of two isoforms of human high-temperature requirement factor A3 (HtrA3), characterization of its genomic structure and comparison of its tissue distribution with HtrA1 and HtrA2. Biochem J 2003; 371:38-48.

Nie GY, Li Y, Salamonsen LA. Serine protease HtrA1 is developmentally regulated in trophoblast and uterine decidual cells during placental formation in the mouse. Dev Dyn 2005; 233:1102-1109.

Nie GY, Hale K, Li Y, Manuelpillai U, Wallace EM, Salamonsen LA. Distinct expression and localization of serine protease HtrA1 in human endometrium and first-trimester placenta. Dev Dyn 2006; 235:3448-3455.

Nishijima K, Ng YS, Zhong L, Bradley J, Schubert W, Jo N, Akita J, Sameulsson SJ, Robinsin GS, Adamis AP, Shima DT. Vascular endothelial growth factor-A is a survival factor for retinal neurons and a critical neuroprotectant during the adaptive response to ischemic injury. Am J Pathol 2007; 171:53-67.

Nishizawa H, Pryor-Koishi K, Kato T, Kowa H, Kurahashi H, Udagawa Y, Microarray analysis of differentially expressed fetal genes in placental tissue derived from early and late onset severe preeclampsia. Placenta 2007; 28:487-497.

Nozaki M, Raisler BJ, Sakurai E, Sarma JV, Barnum SR, Lambris JD, Chen Y, Zhang K,

Ambati BK, Baffi JZ, Ambati J. Drusen complement components C3a and C5a promote choroidal neovascularization. Proc Natl Acad Sci U S A 2006; 103:2328-2333.

Ogata N, Ando A, Uyama M, Matsumura M. Expression of cytokines and transcription factors in photocoagulated human retinal pigment epithelial cells. Graefes Arch Clin Exp Ophthalmol 2001; 239:87-95.

Ohno-Matsui K, Morita I, Tombran-Tink J, Mrazek D, Onodera M, Uetama T, Hayano M, Murota SI, Mochizuki M. Novel mechanism for age-related macular degeneration: an equilibrium shift between the angiogenesis factors VEGF and PEDF. J Cell Physiol 2001; 189:323-333.

Oka C, Tsujimoto R, Kajikawa M, Koshiba-Takeuchi K, Ina J, Yano M, Tsuchiya A, Ueta Y, Soma A, Kanda H, Matsumoto M, Kawaichi M. HtrA1 serine protease inhibits signaling mediated by Tgfβ family proteins. Development 2004; 131:1041-1053.

Olden K, Pratt RM, Jaworski C, Yamada KM. Evidence for role of glycoprotein carbohydrates in membrane transport: specific inhibition by tunicamycin. Proc Natl Acad Sci USA 1979; 76:791-795.

Padmanabhan N, Fichtner L, Dickmanns A, Ficner R, Schulz JB, Braus GH. The yeast HtrA orthologue Ynm3 is a protease with chaperone activity that aids survival under heat stress. Mol Biol Cell 2009; 20:68-77.

Pallen M, Wren B. The HtrA family of serine proteases. Mol Microbiol 1997; 26:209-221.

Park HJ, Kim SS, Seong YM, Kim KH, Goo HG, Yoon EJ, Min do S, Kang S, Rhim H. Beta-amyloid precursor protein is a direct cleavage target of HtrA2 serine protease. Implications for the physiological function of HtrA2 in the mitochondria. J Biol Chem 2006; 281:34277-34287.

Pascolini D, Mariotti SP, Pokharel GP, Pararajasegaram R, Etya'ale D, Negrel AD, Resnikoff S. 2002 global update of available data on visual impairment: a compilation

of population-based prevalence studies. Ophthalmic Epidemiol 2004; 11:67-115.

Patel N, Adewoyin T, Chong NV. Age-related macular degeneration: a perspective on genetic studies. Eye 2008; 22:768-776.

Patil C, Walter P. Intracellular signaling from the endoplasmic reticulum to the nucleus: the unfolded protein response in yeast and mammals. Curr Opin Cell Biol 2001; 13:349-355.

Polur I, Lee PL, Servais JM, Xu L, Li Y. Role of HTRA1, a serine protease, in the progression of articular cartilage degeneration. Histol Histopathol 2010; 25:599-608.

Poquet I, Saint V, Seznec E, Simoes N, Bolotin A, Gruss A. HtrA is the unique surface housekeeping protease in Lactococcus lactis and is required for natural protein processing. Mol Microbiol 2000; 35:1042-1051.

Punglia RS, Lu M, Hsu J, Kuroki M, Tolentino MJ, Keough K, Levy AP, Levy NS, Goldberg MA, D'Amato RJ, Adamis AP. Regulation of vascular endothelial growth factor expression by insulin-like growth factor I. Diabetes 1997; 46:1619-1626.

Rakoczy PE, Zhang D, Robertson T, Barnett NL, Papadimitriou J, Constable IJ, Lai CM. Progressive age-related changes similar to age-related macular degeneration in a transgenic mouse model. Am J Pathol 2002; 161:1515-1524.

Ramrattan RS, van der Schaft TL, Mooy CM, de Bruijn WC, Mulder PG, de Jong PT. Morphometric analysis of Bruch's membrane, the choriocapillaris, and the choroid in aging. Invest Ophthalmol Vis Sci 1994; 35:2857-2864.

Redman CW, Sargent IL. Latest advances in understanding preeclampsia. Science 2005; 308:1592-1594.

Ritter E, Elgeti M, Barti FJ. Activity switches of rhodopsin. Photochem Photobiol 2008; 84:911-920.

Rock KL, Gramm C, Rothstein L, Clark K, Stein R, Dick L, Hwang D, Goldberg AL.

Inhibitors of the proteasome block the degradation of most cell proteins and the generation of peptides presented on MHC class I molecules. Cell 1994; 78:761-771.

Rosenfeld PJ, Brown DM, Heier JS, Boyer DS, Kaiser PK, Chung CY, Kim RY; MARINA Study Group. Ranibizumab for neovascular age-related macular degeneration. N Engl J Med 2006; 355:1419-1431.

Rosenthal R, Malek G, Salomon N, Peill-Meininghaus M, Coeppicus L, Wohlleben H, Wimmers S, Bowes Rickman C, Strauss O. The fibroblast growth factor receptors, FGFR-1 and FGFR-2, mediate two independent signalling pathways in human retinal pigment epithelial cells. Biochem Biophys Res Commun 2005; 337:241-247.

Roybal CN, Yang S, Sun CW, Hurtado D, Vander Jagt DL, Townes TM, Abcouwer SF. Homocysteine increases the expression of vascular endothelial growth factor by a mechanism involving endoplasmic reticulum stress and transcription factor ATF4. J Biol Chem 2004; 279:14844-14852.

Rudnew A. Ueber die Entstehung, der sogenannten Glaskoerper der Choroides des menschlichen Auges und uber das Wesen der Hyalinen Degeneration der Gefasse derselben. Arch Pathol Anat Physiol Klin Med 1871; 53:455-465.

Ruegg UT, Rudinger J. Cleavage of disulfide bonds in proteins. Methods Enzymol 1977; 47:111.

Runyon ST, Zhang Y, Appleton BA, Sazinsky SL, Wu P, Pan B, Wiesmann C, Skelton NJ, Sidhu SS. Structural and functional analysis of the PDZ domains of human HtrA1 and HtrA3. Prot Sci 2007; 16:2454-2471.

Sakamoto W. Protein degradation machineries in plastids. Annu Rev Plant Biol 2006; 57:599-621.

Sandbo N, Qin Y, Taurin S, Hogarth DK, Kreutz B, Dulin NO. Regulation of serum response factor-dependent gene expression by proteasome inhibitors. Mol Pharmacol

2005; 67:789-797.

Sarks SH, Arnold JJ, Killingsworth MC, Sarks JP. Early drusen formation in the normal and aging eye and their relation to age related maculopathy: a clinicopathological study. Br J Ophthalmol 1999; 83:358-368.

Sauer T, Patel M, Chan CC, Tuo J. Unfolding the Therapeutic Potential of Chemical Chaperones for Age-related Macular Degeneration. Expert Rev Ophthalmol 2008; 3:29-42.

Schork NJ, Murray SS, Frazer KA, Topol EJ. Common vs. rare allele hypotheses for complex diseases. Curr Opin Genet Dev 2009; 19:212-219.

Schulte D, Bumsted-O'Brien KM. Molecular mechanisms of vertebrate retina development: Implication for ganglion cell and photoreceptor patterning. Brain Res 2008; 1192:151-164.

Seddon JM, Rosner B, Sperduto RD, Yannuzzi L, Haller JA, Blair NP, Willett W. Dietary fat and risk for advanced age-related macular degeneration. Arch Ophthalmol 2001; 119:1191-1199.

Seddon JM, Santangelo SL, Book K, Chong S, Cote J. A genomewide scan for age-related macular degeneration provides evidence for linkage to several chromosomal regions. Am J Hum Genet 2003; 73:780-790.

Seddon JM, Gensler G, Milton RC, Klein ML, Rifai N. Association between C-reactive protein and age-related macular degeneration. JAMA 2004; 291:704-710.

Serra R, Johnson M, Filvaroff EH, LaBorde J, Sheehan DM, Derynck R, Moses HL. Expression of a truncated, kinase-defective TGF-beta type II receptor in mouse skeletal tissue promotes terminal chondrocyte differentiation and osteoarthritis. J Cell Biol 1997; 139:541-552.

Sheng M, Sala C. PDZ domains and the organization of supra-molecular complexes. Ann

Rev Neurosci 2001; 24:1-29.

Shibata A, Nagaya T, Imai T, Funahashi H, Nakao A, Seo H. Inhibition of NF-kappaB activity decreases the VEGF mRNA expression in MDA-MB-231 breast cancer cells. Breast Cancer Res Treat 2002; 73:237-243.

Skorko-Glonek J, Krzewski K, Lipinska B, Bertoli E, Tanfani F. Comparison of the structure of wild-type HtrA heat shock protease and mutant HtrA proteins. A Fourier transform infrared spectroscopic study. J Biol Chem 1995; 270:11140-11146.

Slomiany MG, Rosenzweig SA. Autocrine effects of IGF-I-induced VEGF and IGFBP-3 secretion in retinal pigment epithelial cell line ARPE-19. Am J Physiol Cell Physiol 2004; 287:C746-753.

Sobral RA, Honda ST, Katayama ML, Brentani H, Brentani MM, Patrao DF, Folgueira MA. Tumor slices as a model to evaluate doxorubicin in vitro treatment and expression of trios of genes PRSS11, MTSS1, CLPTM1 and PRSS11, MTSS1, SMYD2 in canine mammary gland cancer. Acta Veterinaria Scandinavica 2008; 50:27.

Sokolenko A, Pojidaeva E, Zinchenko V, Panichkin V, Glaser VM, Herrmann RG, Shestakov SV. The gene complement for proteolysis in the cyanobacterium Synechocystis sp. PCC 6803 and Arabidopsis thaliana chloroplasts. Curr Genet 2002; 41:291-310.

Spaide RF, Laud K, Fine HF, Klancnik JM Jr, Meyerle CB, Yannuzzi LA, Sorenson J, Slakter J, Fisher YL, Cooney MJ. Intravitreal bevacizumab treatment of choroidal neovascularization secondary to age-related macular degeneration. Retina 2006; 26:383-390.

Sparrow JR, Boulton M. RPE lipofuscin and its role in retinal pathobiology. Exp Eye Res 2005; 80:595-606.

Spiess C, Beil A, Ehrmann M. A temperature-dependent switch from chaperone to protease

178

in a widely conserved heat shock protein. Cell 1999; 97:229-347.

Spilsbury K, Garrett KL, Shen WY, Constable IJ, Rakoczy PE. Overexpression of vascular endothelial growth factor (VEGF) in the retinal pigment epithelium leads to the development of choroidal neovascularization. Am J Pathol 2000; 157:135-144.

Spugnini EP, Cardillo I, Verdina A, Crispi S, Saviozzi S, Calogero R, Nebbioso A, Altucci L, Cortese G, Galati R, Chien J, Shridhar V, Vincenzi B, Citro G, Cognetti F, Sacchi A, Baldi A. Piroxicam and cisplatin in a mouse model of peritoneal mesothelioma. Clin Cancer Res 2006; 12:6133-6143.

Srinivasula SM, Gupta S, Datta P, Zhang Z, Hegde R, Cheong N, Fernandes-Alnemri T, Alnemri ES. Inhibitor of apoptosis proteins are substrates for the mitochondrial serine protease Omi/HtrA2. J Biol Chem 2003; 278:31469-31472.

Stankewich MC, Tse WT, Peters LL, Ching Y, John KM, Stabach PR, Devarajan P, Morrow JS, Lux SE. A widely expressed betaIII spectrin associated with Golgi and cytoplasmic vesicles. Proc Natl Acad Sci USA 1998; 95:14158–14163.

Starita C, Hussain AA, Pagliarini S, Marshall J. Hydrodynamics of ageing Bruch's membrane: implications for maular disease. Exp Eye Res 1996; 62:565-572.

Stein B, Baldwin AS Jr. Distinct mechanisms for regulation of the interleukin-8 gene involve synergism and cooperativity between C/EBP and NF-kappa B. Mol Cell Biol 1993; 13:7191-7198.

Stein B, Baldwin AS Jr, Ballard DW, Greene WC, Angel P, Herrlich P. Cross-coupling of the NF-kappa B p65 and Fos/Jun transcription factors produces potentiated biological function. EMBO J 1993; 12:3879-3891.

Stone EM, Braun TA, Russell SR, Kuehn MH, Lotery AJ, Moore PA, Eastman CG, Casavant TL, Sheffield VC. Missense variations in the fibulin 5 gene and age-related macular degeneration. N Engl J Med 2004; 351:346-353.

Strauch KL, Beckwith J. An Escherichia coli mutation preventing degradation of abnormal periplasmic proteins. Proc Natl Acad Sci USA 1988; 85:1576-1580.

Strauss KM, Martins LM, Plun-Favreau H, Marx FP, Kautzmann S, Berg D, Gasser T, Wszolek Z, Müller T, Bornemann A, Wolburg H, Downward J, Riess O, Schulz JB, Krüger R. Loss of function mutations in the gene encoding Omi/HtrA2 in Parkinson's disease. Hum Mol Genet 2005; 14:2099-2111.

Streeten BW. The sudanophilic granules of the human retinal pigment epithelium. Arch Ophthalmol 1961; 66:391-398.

Sun X, Peng L, Guo J, Chi W, Ma J, Lu C, Zhang L. Formation of DEG5 and DEG8 complexes and their involvement in the degradation of photodamaged photosystem II reaction center D1 protein in Arabidopsis. Plant Cell 2007a; 19:1347-1361.

Sun X, Wang L, Zhang L. Involvement of DEG5 and DEG8 proteases in the turnover of the photosystem II reaction center D1 protein under heat stress in Arabidopsis thaliana. Chin Sci Bull 2007b; 52:1742-1745.

Swamy KH, Chung CH, Goldberg AL. Isolation and characterization of protease do from Escherichia coli, a large serine protease containing multiple subunits. Arch Biochem Biophys 1983; 224:543-554.

Szokalska A, Makowski M, Nowis D, Wilczynski GM, Kujawa M, Wójcik C, Mlynarczuk-Bialy I, Salwa P, Bil J, Janowska S, Agostinis P, Verfaillie T, Bugajski M, Gietka J, Issat T, Glodkowska E, Mrówka P, Stoklosa T, Hamblin MR, Mróz P, Jakóbisiak M, Golab J. Proteasome inhibition potentiates antitumor effects of photodynamic therapy in mice through induction of endoplasmic reticulum stress and unfolded protein response. Cancer Res 2009; 69:4235-4243.

Tam PO, Ng TK, Liu DT, Chan WM, Chiang SW, Chen LJ, DeWan A, Hoh J, Lam DS, Pang CP. HTRA1 variants in exudative age-related macular degeneration and

interactions with smoking and CFH. Invest Ophthalmol Vis Sci 2008; 49:2357-65.

Tamada Y, Walkup RD, Shearer TR, Azuma M. Contribution of calpain to cellular damage in human retinal pigment epithelial cells cultured with zinc chelator. Curr Eye Res 2007; 32:565-573.

Tarkowski E, Issa R, Sjogren M, Wallin A, Blennow K, Tarkowski A, Kumar P. Increased intrathecal levels of the angiogenic factors VEGF and TGF-beta in Alzheimer's disease and vascular dementia. Neurobiol Aging 2002; 23:237-243.

Terman A, Gustafsson B, Brunk UT. Autophagy, organelles and ageing. J Pathol 2007; 211:134-143.

Thakkinstian A, Han P, McEvoy M, Smith W, Hoh J, Magnusson K, Zhang K, Attia J. Systematic review and meta-analysis of the association between complement factor H Y402H polymorphisms and age-related macular degeneration. Hum Mol Genet 2006; 15:2784-2790.

Tocharus J, Tsuchiya A, Kajikawa M, Ueta Y, Oka C, Kawaichi M. Developmentally regulated expression of mouse HtrA3 and its role as an inhibitor of TGF-beta signaling. Dev Growth Differ 2004; 46:257-274.

Tong F, Black PN, Bivins L, Quackenbush S, Ctrnacta V, DiRusso CC. Direct interaction of Saccharomyces cerevisiae Faa1p with the Omi/HtrA protease orthologue Ynm3p alters lipid homeostasis. Mol Genet Genomics 2006; 275:330-343.

Tong JP, Chan WM, Liu DT, Lai TY, Choy KW, Pang CP, Lam DS. Aqueous humor levels of vascular endothelial growth factor and pigment epithelium-derived factor in polypoidal choroidal vasculopathy and choroidal neovascularization. Am J Ophthalmol 2006; 141:456-462.

Tong JP, Lam DS, Chan WM, Choy KW, Chan KP, Pang CP. Effects of triamcinolone on the expression of VEGF and PEDF in human retinal pigment epithelial and human

umbilical vein endothelial cells. Mol Vis 2006; 12:1490-1495.

Tsuchiya A, Yano M, Tocharus J, Kojima H, Fukumoto M, Kawaichi M, Oka C. Expression of mouse HtrA1 serine protease in normal bone and cartilage and its upregulation in joint cartilage damaged by experimental arthritis. Bone 2005; 37:323-336.

Tuo J, Ross RJ, Reed GF, Yan Q, Wang JJ, Bojanowski CM, Chew EY, Feng X, Olsen TW, Ferris FL 3rd, Mitchell P, Chan CC. The HtrA1 promoter polymorphism, smoking, and age-related macular degeneration in multiple case-control samples. Ophthalomology 2008; 115:1891-1898.

Umeda S, Suzuki MT, Okamoto H, Ono F, Mizota A, Terao K, Yoshikawa Y, Tanaka Y, Iwata T. Molecular composition of drusen and possible involvement of anti-retinal autoimmunity in two different forms of macular degeneration in cynomolgus monkey (Macaca fascicularis). FASEB J 2005; 19:1683-1685.

van Essen DC, Anderson CH, Felleman DJ. Information processing in the primate visual system: an integrated systems perspective. Science 1992; 255:419:423.

van Newkirk MR. The Hong Kong vision study: a pilot assessment of visual impairment in adults. Trans Am Ophthalmol Soc 1997; 95:715-49

Vande Walle L, Lamkanfi M, Vandenabeele P. The mitochondrial serine protease HtrA2/Omi: an overview. Cell Death Differ 2008; 15:453-460.

Waller PR, Sauer RT. Characterization of degQ and degS, Escherichia coli genes encoding homologs of the DegP protease. J Bacteriol 1996; 178:1146-1153.

Walsh NP, Alba BM, Bose B, Gross CA, Sauer RT. OMP peptide signals initiate the envelope-stress response by activating DegS protease via relief of inhibition mediated by its PDZ domain. Cell 2003; 113:61-71.

Walker A, Ward C, Sheldrake TA, Dransfield I, Rossi AG, Pryde JG, Haslett C. Golgi fragmentation during Fas-mediated apoptosis is associated with the rapid loss of

GM130. Biochem Biophys Res Commun 2004; 316:6-11.

Wang G, Spencer KL, Court BL, Olson LM, Scott WK, Haines JL, Pericak-Vance MA. Localization of age-related macular degeneration-associated ARM2 in cytosol, not mitochondria. Invest Ophthalmol Vis Sci 2009; 50:3084-3090.

Wang G, Spencer KL, Scott WK, Whitehead P, Court BL, Ayala-Haedo J, Mayo P, Schwartz SG, Kovach JL, Gallins P, Polk M, Agarwal A, Postel EA, Haines JL, Pericak-Vance MA. Analysis of the indel at the ARMS2 3'UTR in age-related macular degeneration. Hum Genet 2010; 127:595-602.

Wang X, Jobin C, Allen JB, Roberts WL, Jaffe GJ. Supression of NF-κB-dependent proinflammatory gene expression in human RPE cells by a proteasome inhibitor. Invest Ophthalmol Vis Sci 1999; 40:477-486.

Wang X, Wang G, Wang Y. Intravitreous vascular endothelial growth factor and hypoxia-inducible factor 1a in patients with proliferative diabetic retinopathy. Am J Ophthalmol 2009; 148:883-889.

Wu J, Liu W, Bemis A, Wang E, Qiu Y, Morris EA, Flannery CR, Yang Z. Comparative proteomic characterization of articular cartilage tissue from normal donors and patients with osteoarthritis. Arthritis Rheum 2007; 56:3675-3684.

Yang QH, Church-Hajduk R, Ren J, Newton ML, Du C. Omi/HtrA2 catalytic cleavage of inhibitor of apoptosis (IAP) irreversibly inactivates IAPs and facilitates caspase activity in apoptosis. Genes Dev 2003; 17:1487-1496.

Yang SP, Bae DG, Kang HJ, Gwag BJ, Gho YS, Chae CB. Co-accumulation of vascular endothelial growth factor with beta-amyloid in the brain of patients with Alzheimer's disease. Neurobiol Aging 2004; 25:283-290.

Yang X, Chen L, Xu X, Li C, Huang C, Deng CX. TGF-beta/Smad3 signals repress chondrocyte hypertrophic differentiation and are required for maintain articular

cartilage. J Cell Biol 2001; 153:35-46.

Yang Z, Camp NJ, Sun H, Tong Z, Gibbs D, Cameron DJ, Chen H, Zhao Y, Pearson E, Li X, Chien J, Dewan A, Harmon J, Bernstein PS, Shridhar V, Zabriskie NA, Hoh J, Howes K, Zhang K. A variant of the HTRA1 gene increases susceptibility to age-related macular degeneration. Science 2006; 314:992-993.

Yang Z, Tong Z, Chen Y, Zeng J, Lu F, Sun X, Zhao C, Wang K, Davey L, Chen H, London N, Muramatsu D, Salasar F, Carmona R, Kasuga D, Wang X, Bedell M, Dixie M, Zhao P, Yang R, Gibbs D, Liu X, Li Y, Li C, Li Y, Campochiaro B, Constantine R, Zack DJ, Campochiaro P, Fu Y, Li DY, Katsanis N, Zhang K. Genetic and functional dissection of HTRA1 and LOC387715 in age-related macular degeneration. PLoS Genet 2010; 6:e1000836.

Yates JR, Sepp T, Matharu BK, Khan JC, Thurlby DA, Shahid H, Clayton DG, Hayward C, Morgan J, Wright AF, Armbrecht AM, Dhillon B, Deary IJ, Redmond E, Bird AC, Moore AT; Genetic Factors in AMD Study Group. Complement C3 variant and the risk of age-related macular degeneration. N Engl J Med 2007; 357:553-561.

Yu J, Wiita P, Kawaguchi R, Honda J, Jorgensen A, Zhang K, Fischetti VA, Sun H. Biochemical analysis of a common human polymorphism associated with age-related macular degeneration. Biochemistry 2007; 46:8451-8461.

Zacks DN, Han Y, Zeng Y, Swaroop A. Activation of signaling pathways and stress-response genes in an experimental model of retinal detachment. Invest Ophthalmol Vis Sci 2006; 47:1691-1695.

Zarbin MA. Current concepts in the pathogenesis of age-related macular degeneration. Arch Ophthalmol 2004; 122:598-614.

Zhang SX, Wang JJ, Gao G, Parke K, Ma JX. Pigment epithelium-derived factor downregulates vascular endothelial growth factor (VEGF) expression and inhibits

VEGF-VEGF receptor 2 binding in diabetic retinopathy. J Mol Endocrinol 2006; 37:1-12.

Zumbrunn J, Trueb B. Primary structure of a putative serine protease specific for IGF-binding proteins. FEBS Lett 1996; 398:187-192.

Zurawa-Janicka D, Kobiela J, Stefaniak T, Wozniak A, Narkiewicz J, Wozniak M, Limon J, Lipinska B. Changes in expression of serine proteases HtrA1 and htrA2 during estrogen-induced oxidative stress and nephrocarcinogenesis in male Syrian hamster. Acta Biochim Pol 2008; 55:9-19.